Bastien Emmanuel Dénarié

# Real-time 3-D echocardiography: challenges of parallel transmission and acquisition

Thesis for the degree of Philosophiae Doctor

Trondheim, November 2013

Norwegian University of Science and Technology
Faculty of Medicine
MI-Lab, Department of Circulation and Medical Imaging

**NTNU – Trondheim**
Norwegian University of
Science and Technology

**NTNU**
Norwegian University of Science and Technology

Thesis for the degree of Philosophiae Doctor

Faculty of Medicine
Department of Circulation and Medical Imaging
MI-Lab



ISBN 978-82-326-0132-5 (printed version)
ISBN 978-82-326-0133-2 (electronic version)
ISSN 1503-8181

Doctoral theses at NTNU, 2014:104

Printed by NTNU-trykk

# Sanntid 3-D ekkokardiografi: utfordringer med parallelle sending og mottak

Ultralydavbildning er en veletablert, non-invasiv og relativt billig metode for å evaluere hjertefunksjon. Ved å gi høyoppløselige avbildningsvolum i sanntid, kan 3-D ekkokardiografi potentielt forbedre og automatisere kliniske diagnoser. Men begrensninger i lydhastighet hindrer fortsatt opptak av store volum med tilstrekkelig bildefrekvens til å vurdere den komplekse dynamikken i et bankende hjerte. For å øke bildefrekvens, har parallellisering av både sending og mottak blitt foreslått. I denne avhandlingen inngår fire publikasjoner som adresserer utfordringene med Multi-Linje Transmisjon (MLT) og Syntetisk Transmit Aperture (STA) for å avbilde hjertet i sanntid 3-D når det kreves en optimal bildekvalitet.

Når flere fokuserte ultralydpulser blir sendt i parallell kan det dannes bildeartifakter fra interaksjoner mellom de samtidige strålene. Dette er også kjent som MLT krysstale. Krysstalen fremtrer som ekstra støy i bildet, særlig på steder hvor kantbølger fra en stråle overlapper med hovedloben til en annen stråle, både på sending og mottak. For å isolere de parallelle strålene, foreslår vi å kombinere MLT med harmonisk avbildning, der sidelobe nivået på sending er lavere ved enn vanlig fundamentalavbildning. Resultatet viser her 10 til 15 dB reduksjoner av sendingskrysstale både *in vitro* og *in vivo*. Stråleisolering kan også oppnås ved anvendelse av 3-D-disposisjoner. Ved plassere strålene langs 45-graders-diagonalen til transduceren, ble det oppnådd reduksjoner på opp til 30 dB for både sendings- og mottaks- krysstale i simuleringer og vanntankmålinger. Dette gir en potensiell økning av bildefrekvens med en faktor fem uten synlig dårligere bilder.

Ved bruk av parallelle mottaksstråler og STA, vil koherent kombinasjon av data fra suksessive transmisjoner kunne gjenopprette romlige oppløsning og kontrast, samtidig som en vedlikeholder en høy bildefrekvens. Resultatet av denne kombinasjonen er imidlertid ikke lenger garantert dersom avbildet vev beveger seg hurtig; slik som er tilfellet for myokard eller blod. Påvirkningen av bevegelse er i denne avhandlingen studert for følgende STA-applikasjoner som kombinerer data fra to eller flere transmisjoner: Syntetisk Transmit Strålerforming, både i 2-D og 3-D, og for Koherent Planebølge Kombinering. Ved betydelig aksialbevegelse ble det observert lateralt bildeskift og forringelse av syntetisk transmit fokus, noe som igjen resulterte i tap av kontrast og SNR. Bevegelseskompensasjonsalgoritmer basert på krysskorrelasjon ble innført for å korrigere for den aksiale bevegelseskomponenten. Slike algoritmer er robuste, beregningsmessig billige og deres nødvendighet er demonstrert gjennom både simuleringer og *in vivo* eksperimenter.

Bastien Dénarié
MI-Lab, Institutt for sirkulasjon og bildediagnostikk, NTNU
Hovedveileder: Tore Grüner Bjåstad, Medveileder: Hans Torp

*Ovennevnte avhandling er funnet verdig til å forsvares offentlig for graden Philosophiae Doctor (Ph.D.) i Medisinsk Teknologi. Disputas finner sted i Auditoriet (KBA), Kvinne-barnsenteret, tirsdag 25. mars 2014 kl. 12.15.*

# Abstract

Ultrasound imaging is a well-established, noninvasive and relatively low cost method for assessing the cardiac function. By providing dense image volumes in real-time, three-dimensional echocardiography could improve and automatize the diagnostic by professionals. But the limited speed of sound still prevents the acquisition of large fields of view at frame rates sufficient to assess the complex dynamics of a beating heart. To increase the frame rate, parallelizations of both the transmission and reception processes is being proposed. In this thesis, the challenges of Multi-Line Transmission (MLT) and two Synthetic Transmit Aperture (STA) techniques for imaging the heart in real-time 3-D when an optimal image quality is required are addressed across four scientific publications.

When transmitting multiple focused ultrasound pulses in parallel, interactions between the simultaneous beams are prone to generate artifacts, *aka.* MLT cross-talks. Cross-talks appear as additional clutter in the image, notably at every location where the edge waves of one beam overlap with the main-lobe of another beam, both on transmission and reception. To isolate the parallel beams, we propose to combine MLT with the low transmit side-lobe levels of second harmonic imaging. 10 to 15 dB reductions of transmit cross-talks are observed both *in vitro* and *in vivo*. Beam isolation may also be achieved using 3-D dispositions. When aligning the beams along the transducer transverse diagonal, reductions of up to 30 dB of both transmit and receive cross-talks are observed in simulations backed-up by water tank measurements. This allow a potential increase of the frame rate by a factor five without visible image degradation.

Using parallel receive beams with STA focusing, the coherent combination of data acquired over successive transmit events allow to recover the spatial resolution and contrast while maintaining higher frame rates. However, the success of this combination is no longer guaranteed in presence of rapid displacements such as observed in the myocardium or the blood. The influence of motion is studied for STA applications combining two or many transmit events: Synthetic Transmit Beamformation, both in 2-D and 3-D, and Coherent Plane Wave Compounding. In presence of significant axial motion, lateral image shifts and deteriorations of the focusing capability are observed, resulting in losses of contrast and SNR. Motion compensation algorithms based on cross-correlation are introduced to correct for the axial motion component. Such algorithms are robust, computationally inexpensive and their necessity is demonstrated through both simulations and *in vivo* experiments.

# Preface

The present thesis is submitted in partial fulfillment of the requirements for the degree of *Philosophiae Doctor* (Ph.D.) at the Faculty of Medicine of the Norwegian University of Science and Technology (NTNU). The research was funded by *Medical Imaging Lab* (MI-Lab) and was carried out under the supervision of PhD Tore G. Bjåstad and Professor Hans Torp in the Department of Circulation and Medical Imaging, NTNU.

**Acknowledgments**

Several people have contributed to this thesis in some way or another, and deserve my gratitude. First of all, I wish to thank my main supervisor Tore for his support and guidance. He has always been very interested and involved in my work, spending an invaluable amount of time reviewing my work and providing fruitful ideas. For co-supervising me, Hans also deserves my respect for being a profound source of knowledge in the ultrasound world and always provide innovative approaches to my problems. I would like to thank the Faculty of Medicine, MI-Lab and the Department of Circulation and Medical Imaging at NTNU for giving me the opportunity to conduct this thesis. All my co-authors deserve my gratitude for their involvement, especially Fabrice, Ling and Lasse for providing new insights and help me improving my work.

I am also very thankful to many people at GE Vingmed Ultrasound, among them Anders, Håvard, Per, Jan-Gustav and Geir. Spending several months working with them provided me an invaluable insight on ultrasound imaging technology as well as a strong motivation for getting through this thesis. Kjell Kristoffersen should also be mentioned for giving an experienced feedback on even the most unrealistic ideas.

Sincere thanks go to all my colleagues at ISB for maintaining a friendly atmosphere at the department. In particular, I would like to thank my fellow (post-)doctoral students Birger, Daniel, Gabriel, Ingvild, Jochen, Jon-Petter, Jørgen, Saeed, Sigurd, Solveig and Tonje for fruitful discussions and a lot of fun.

Finally, I wish to thank Emilie for her love, her invaluable patience and encouragements during all these years.

# Table of Contents

# Chapter 1

# Introduction

Bastien Emmanuel Dénarié
MI-Lab, Dept. Circulation and Medical Imaging, NTNU

Line-by-line acquisition is a central principle in medical ultrasound. In order to build an image, the desired field of view is first divided in a given number of directions known as image lines. Each of these lines are then filled up by emitting an ultrasound pulse focused along this direction and by listening to the echoes propagating back to the surface of the transducer from reflectors located along the image line direction. This acquisition process is tedious, as it requires to wait for the propagation of the ultrasound pulse back and forth in the body for each single image line.

To understand the line-by-line approach, we have to look back a few decades. When the first ultrasound imaging scanners were developed, the probe consisted of a physically concave transducer with a single fixed focus [1]. B-mode images were then acquired by manually sliding the probe above the object of interest until transducers placed on rotating motors automatized the process [2]. Ultimately, such convex transducers were replaced by an array of smaller piezoelectric transducers. [3] The focus depth could now be controlled electronically by applying a set of individual delays to each element of the transducer array. On transmit, the focal depth could be selected to improve the image quality around a preferred range. On reception, series of delay curves could be applied such that the pulse propagation was followed at all depths, introducing a dynamic focusing capability. In addition, the set of delays applied to the probe elements could be adjusted to steer the ultrasound beams in any direction, removing the need for motors in 2-D imaging [4, 5].

However, the line-by-line acquisition paradigm had to be adapted with the arrival of 3-D imaging. Scanning a three-dimensional volume requires squaring the number of image lines, and hence impose a quadratic reduction on the achievable frame rate. Imaging the complex kinematics of organs such as the beating heart requires an elevated frame rate which is far from achievable on large imaging volumes using the classical line-by-line approach. Indeed, considering the speed of sound in biological tissues to be around 1540 m/s, about 200 µs are required to acquire a single image line with a 15 cm depth. This is approximately 5000 lines per second which may be used to form either 50 frames per second using 100 lines to cover a reasonably large sector, or 1 volume every 2 seconds if you would acquire an equivalent three-dimensional volume using $100 \times 100$ image lines. The contraction of the human heart presents temporal frequencies as high as 200 Hz [6]. While a correct qualitative assessment of most cardiac pathologies may be obtained with 25 frames per second, new clinical

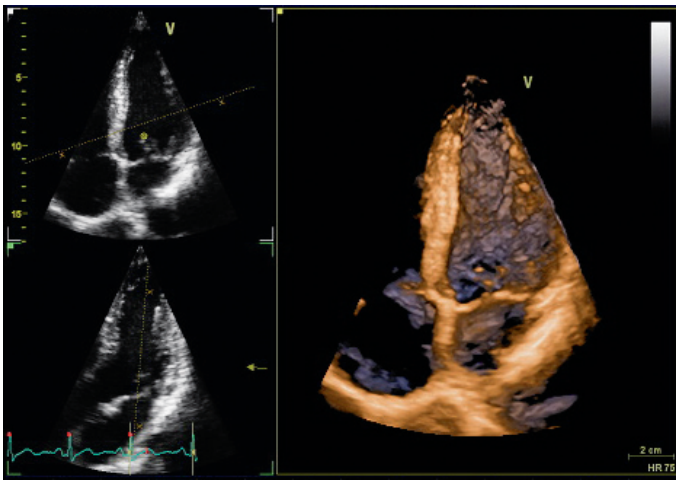

Figure 1.1: Example of a 3-D trans-thoracic apical view of the left ventricle. The $45 \times 45$ deg volume was acquired using a state-of-the-art cardiac ultrasound scanner at 6 frames per second. Courtesy of GE Vingmed Ultrasound.

methods based on strain estimations require very high frame rates [7]. For 3-D cardiac imaging, this is very far from what can be achieved with a line-by-line approach. As an illustration, the 3-D apical view of Fig. 1.1 with a limited imaging angle of $45 \times 45$ deg was acquired at a frame rate of 6 fps.

To achieve higher frame rates, it is necessary to acquire a larger portion of the field of view for each transmit event. Technically, this was made possible by extensive advances in semiconductor technology: receive beamforming has been digitalized and parallelized, allowing the formation of a plurality of image lines per transmission [8, 9].

These image lines could be a plurality of adjacent lines surrounding the transmit beam direction. In that case, broad transmit pulses can be used to illuminate the desired field of view with fewer illuminations. However, a sparser transmit lateral sampling also results in a net image degradation: not only is the contrast reduced due to increased side-lobes in the transmitted pressure wave, but the resolution and lateral shift invariance of the image are also degraded. Strong focusing, both on transmission and reception, is especially important when imaging the heart, where multiple factors tends to make the task of imaging more arduous: the access points are often occluded by the ribs, shadowing from the lungs degrades the images severely, reverberations and aberrations of the ultrasonic wave fronts caused by fatty subcutaneous tissues tends to destroy the focusing capabilities of the system [10]. In order to recover the focusing capability while using broad illuminations, it has been proposed to use a technique called Synthetic Transmit Aperture (STA) imaging, originally developed for radar detection systems [11]. By coherently combining the data acquired from successive and spatially overlapping ultrasound pulse emissions, one may retrospectively recreate a transmit focus along each line of the final image.

Another approach to increase the frame rate is by simultaneously transmitting several focused ultrasound pulses steered in laterally spaced directions [12, 13]. With this technique called Multi-Line Transmission (MLT), a number of image lines equal to the number of parallel transmit pulses may be beamformed simultaneously. Using MLT, one may potentially keep thin and strongly focused transmit beams while the frame rate is increased by a fold equal to the number of parallel pulses in each transmission.

But while both the MLT and STA techniques tend to alienate the line-by-line acquisition principle, they also come with the cost of many undesired and under-investigated compromises. In presence of motion, the coherent combination of data acquired over successive transmissions may result in an erroneous behavior for the STA techniques. When a superposition of several pressure fields propagate simultaneously, interactions between the energy of the parallel beams will introduce severe artifacts in the images acquired using the MLT technique.

As of today, none of these techniques have been successfully adapted to 3-D echocardiography such that it is possible to acquire a large volume covering the entire heart with a high frame rate and no losses in term of image quality compared to todays high-end 2-D images. The topic of this thesis is to study how far from the conventional line-by-line acquisition one may deviate without sacrificing the image quality and thus the potential for an efficient clinical diagnostic. In this work, I explore the challenges related to two of the most promising approaches to higher frame rates in ultrasound imaging: cross-talks reduction with Multi-Line Transmission, and motion compensation techniques with Synthetic Transmit Aperture imaging.

This thesis is organized as follows. First, an overview of the two techniques which may both be considered as cornerstones for this research is presented: the parallel transmission of a plurality of focused beams and the synthetic reconstruction of the transmit focus from data acquired with parallel beamformation over several transmits. Then the aims and research questions of this thesis are highlighted, and summaries of each publication are presented before they are discussed. This discussion includes a conclusion about all the aspects of the presented work, as well ideas for future research activities. The four papers that constitute this thesis follow as individual chapters.

## 1.1 Parallel transmission of focused ultrasound beams

### 1.1.1 Principle and implementation

Multi-Line Transmission (MLT) is a technique where a plurality of focused pulses steered along laterally separated directions are emitted simultaneously. On receive, parallel beamforming is used to generate image lines along all the transmit directions, resulting in a increase in frame rate proportional to the number of parallel transmit beams. The major drawback of the MLT technique is inter-beam interferences, also known as cross-talks, which create artifacts in the image. The more the beams are focused, the lower these interferences will be. This makes MLT a good candidate for increasing the frame rate in cardiac ultrasound without having to use broad beams:

the focus in transmit ensures a deep penetration, a high sensitivity and allows for the use of second harmonic imaging.

The first documented implementation of MLT dates from 1987 [12] where two beams were transmitted simultaneously using two different sets of transducer elements for the transmission of the beams (the odd and even elements). While illustrative, this approach suffers from high side-lobe levels and grating lobes generated by the large pitch in the independent sets of elements. The excitation signals can also be summed together over all the elements of the transducer using the superposition principle, resulting in the parallel transmission of a higher number of beams [13]. However, this requires a more complex transmit circuitry combined with the capability to receive along several directions, something that has restrained the study of MLT over the last decades.

### 1.1.2 Limitations

Physically, ultrasound pulses are pressure waves propagating through the body. As they propagate, damages to the tissues may occur, either due to temperature increase when a too high level of energy is concentrated in one location, or induced by cavitational effects. In order to avoid that, guidelines have been established restricting the intensities and amplitude of the ultrasound pulses that may be used for imaging [14]. When using parallel transmit beams, it may be expected that the intensity level of each individual pulse has to be lowered to comply with the safety limits. For a conventional cardiac B-mode imaging application (1 to 2 periods pulse centered around 1.5 to 3 MHz transmitted with a 2.5 cm $\times$ 1.5 cm aperture), the voltage applied to the transducer is already limited by these safety guidelines on the Mechanical Index (MI) and the temperature of the probe surface, and not by the technical limitations of the power supply. When implementing an MLT application, if the parallel transmit directions are sufficiently spaced laterally, the superposition of several pulses should only occur in the near-field, where the pressure levels are relatively low. Therefore, the limitation on the MI should not be a bigger problem compared with a single transmit beam scenario. Furthermore, it is possible to contain the superposition of several pulses in the near-field to a maximum of two pulses at each spatial location by superposing the transmit excitations appropriately. This can be done either by introducing a slight time delay between the transmits [15] or by inverting the polarity of the overlapping pulse excitations. Therefore, while the bio-effects have to be considered with care when implementing multi-line transmission, they might not be the biggest limitation to the technique.

The implementation of MLT on an ultrasound scanner requires complex transmit electronics: we may consider to implement it having a number of transmit pulsers equal to the number parallel beams coupled with a summation of the excitation signals [13], or by providing a single arbitrary wavefront generator per transducer element [16]. In addition, the MLT technique will face some challenges for 3-D imaging, where the thousands of elements on the transducer surface are coupled together in small sets of sub-apertures sharing a single main focusing delay. This approach is no longer valid when using parallel beams, neither in transmission or reception, because sub-apertures

as they are designed today cannot cope with a superposition of pulses focused in several widely separated directions.

The MLT technique also possesses two intrinsic problems which may result in image artifacts. The first of them is similar to the stitching artifact observed when imaging 3-D volumes over several heart cycles using the ECG information: the acquisition of the field of view is divided in sub-sectors that are acquired at the same time in successive cardiac cycles and stitched; and if the scanning is done conventionally by acquiring the sub-sector from left to right, a large time gap at the border between these sub-sectors may give spatial discontinuities in case of tissue motion. To prevent this time gap to cause artifacts in the image, alternative scan sequencing schemes were presented where the beams at both borders of each sub-volumes are acquired successively until the center of each zone [17].

The second and probably most important problem related to MLT is the interaction between the simultaneous beams, and will be discussed in-depth in the two first papers of this thesis. Using parallel transmit beams, some energy contained in the side-lobes of a transmit beam for a given direction may align with the main-lobe of a receive beam corresponding to another imaging direction. The phenomenon is also present the other way around: the side-lobes of one receive direction may be sensitive to the energy from the main-lobe of another transmit direction. These phenomenons, respectively denominated transmit and receive cross-talks, were already observed with the first MLT applications and described as "butterfly" patterns appearing in the image [18]. Several techniques to reduce this artifacts have been proposed and are listed in the next paragraph. The cross-talk artifacts appear as an additional clutter around the areas where scattering is present, and as a shadow of the surrounding tissues in the areas such as cysts and cavities where small amounts of signals should be present. These cross-talk artifacts are probably the main reason why MLT has not focused the interest of ultrasound scanner manufacturers.

### 1.1.3 Beam isolation techniques combined with MLT

Different approaches have been proposed and investigated in order to limit the cross-talks between simultaneously transmitted beams. They are listed here:

- The simultaneous transmit beams can be isolated from each other spatially by maximizing the angle between them [19] or choosing an angle separation corresponding to a minimum in the side-lobes of the transmitted beams [20]. The latter technique is sensitive to aberrations caused by inhomogeneities in the body wall, which may change the locations of the side lobes.

- Different frequencies within the frequency band of the transducer may be used to transmit two or more simultaneous pulses [19, 20]. On receive, frequency filtering is applied to extract the components from each direction. Different frequencies will of course result in different penetrations, but also different spatial resolutions, and the system must implement spatial filtering to homogenize the image rendering. This approach is however not possible to combine with conventional harmonic imaging, where the entire transducer bandwidth is used

for one transmit frequency. It has been proposed to use orthogonal frequency division multiplexing [21, 22] to transmit longer pulses which may be better separated in the frequency spectrum. If the bandwidth of the transducer is broad enough, separated second harmonic signals may be received for each of the beams. However, this approach results in a severe loss in axial resolution.

- The parallel transmit beams produce replicates of the signal present in the other transmit directions, and may therefore be suppressed by combining the signal from the lines in different transmit directions in an appropriate way. A least-square minimization test was proposed [18] for estimating coefficients that could be used in a linear combination of the beams received after parallel emissions. This approach is heavy, relies on good estimates, and has shown to perform worse on beams with large steering angle.

- Coded transmissions have also been proposed as a way to isolate the beams [20, 23]. Different pseudo-random binary sequences (typically Golay codes) can be used as a codes for each of the pulses excitations. If the excitation codes are chosen orthogonal, the pulses may be decoded independently from each other on receive using heavy filtering (typically match filters or correlations). This technique requires a transducer with a high bandwidth, such that the real pulses correspond to the excitation code. While interesting, this approach is very limited in cardiac applications as it is not compatible with second harmonic imaging, where the non-linearities will transform the coded excitation.

- Both transmit and receive apodization applied to the transducer surface may be used to reduce the level of side-lobes in the system. They will result in a reduction in the transmit and receive cross-talks respectively. Different apodization windows have been evaluated [24], but it is important to note the presence of a two trade-off between the quantity of energy transmitted (or the lateral resolution for the two-way beams) and the level of side-lobes.

- Another approach to reduce cross-talk artifacts is to use inversion of polarity coupled with a merging of the signals acquired over several transmits, a technique similar to what is achieved for pulse-inversion harmonic imaging [25]. For example, if two beams are transmitted simultaneously, the pulse polarity of one of these two beams may be reversed on the next transmission such that two receive directions lines may be obtained with both the sum and the subtraction of the lines obtained after each transmission. This principle may be extended to a larger number of parallel transmit directions, and it is also possible to avoid reducing the frame rate by summing the receive lines of successive transmit beams laterally overlapping. The major drawback of this technique is that it is sensible to motion in the field of view since data acquired after successive emissions are merged together. In addition, the transducer must be able to produce pulses with positive and negative polarities being perfectly symmetric. This symmetry can be destroyed by non-linear propagation, and the technique is therefore not suitable for harmonic imaging.

- More recently, a new beamforming technique differing from the conventional delay-and-sum approach has been proposed [15]. By applying spatial decoding combined with a temporal modulation of the emitted pulses, one may better define the way the echoes from overlapping parallel beams propagate back and forth to each transducer element. The results are promising, but the success of the technique relies on a perfectly linear propagation and a relatively large aperture, and no fair comparison against high-end cardiac images has been conducted yet.

Despite all these proposed methods, the levels of cross-talks observed in the scientific studies are still significant. For cardiac imaging, trading the frame rate at the cost of such strong artifacts may not be beneficial for establishing correct diagnostics. Echocardiography is probably the most challenging ultrasound imaging application, as the imaging strategy must be robust against aberrations, have a large penetration, have a small footprint in order to image between the ribs, be compatible with harmonic imaging, and not being affected by the severe motion of the myocardium. All these conditions make the task of isolating the parallel transmissions very difficult, and the reduction of the cross-talk artifacts will only be achieved by a combination of isolation methods such as proposed above.

## 1.2 Parallel beamforming and Synthetic Transmit Aperture techniques

### 1.2.1 Parallel beamforming and synthesized transmit

Multi-Line Acquisition (MLA) is often used to designate the technique where a plurality of beams covering a small sub-volume around the transmit direction are beamformed in parallel. This principle was introduced in the late 1970's by combining the output of receive electronic boards working in parallel in the scanner, and was designed as a way to achieve frame rates required in 3-D cardiac imaging [8, 26]. As of today, most of the commercial scanners provide the support for 4 to 16 MLA, with a beamforming implemented in hardware, while some research platforms allow for storing the channel data and perform an unlimited number of MLA in software processing.

The number of parallel receive beams required for a given imaging application may differ based on the desired lateral resolution. Basically, the best achievable lateral resolution of a given ultrasound system is defined by its two-way beam width at focal depth using conventional focusing on both reception and transmission [27]. According to the Fraunhofer approximation for a rectangular aperture, the beam width in the focal plane is equal to $\lambda \cdot F_{\#}$, where $F_{\#}$ is the $f$-number in transmission ($F^t_{\#}$) or reception ($F^r_{\#}$), and $\lambda$ is the wavelength corresponding to the pulse center frequency. The lateral bandwidth of the pulse-echo can then found using the convolution of the transmit and receive beam profiles to be equal to $\lambda \cdot F^{tr}_{\#} = \lambda \left(1/F^t_{\#} + 1/F^r_{\#}\right)^{-1}$. The Nyquist sampling requirement for beam density is of one image line per beam width.

Using the Fraunhofer approximation, the transmit lateral sampling frequency can be written as [28]:

$$f_s^t = \frac{1}{p^t} \frac{1}{\lambda \cdot F_\#^t} \tag{1.1}$$

where $p^t$ is the oversampling factor ($p^t \leq 1$). The two-way sampling frequency follows with its corresponding two-way oversampling factor $p^{tr}$ ($p^{tr} \leq 1$):

$$f_s^{tr} = \frac{1}{p^{tr}} \frac{1}{\lambda \cdot F_\#^{tr}} \tag{1.2}$$

The number of necessary parallel beams is now found as the ratio between $f_s^{tr}$ and $f_s^t$:

$$N_{pb} = \frac{p^{tr}}{p^t} \left( 1 + \frac{F_\#^t}{F_\#^r} \right) \tag{1.3}$$

If one want to use broader transmit beams to cover larger sub-volumes, and thus achieve a higher acquisition rate, one must compensate the high $F_\#^t$ using a plurality of parallel receive beams. The higher number of MLA will not however recover the loss in two-way lateral resolution as the lateral transmit bandwidth is decreased.

In addition, the misalignment of the transmit and receive directions is prone to generate degradation in the lateral shift invariance, due to warping and skewing effects, most often referred in the literature as MLA- or block-artifacts [28]. To cope with this problem while maintaining a low transmit sampling, it has been proposed to synthesize a transmit beam in the direction corresponding to each receive line, based on the spatial overlap between the transmit pressure fields. Out of several proposed methods [28, 29], the Synthetic Transmit Beamformation (STB) technique has probably proven to be the most adapted to cardiac ultrasound imaging. STB is based on lateral interpolation between data acquired from adjacent transmissions, and may be applied either before or after receive beamforming. It has proven to be effective in removing the MLA artifacts and is robust against aberrations [28, 30, 31].

### 1.2.2 Synthetic Transmit Aperture (STA) techniques

While the STB technique synthesizes the transmit focus direction using the spatial overlap between the transmit pressure fields of two adjacent transmit directions, it can not be used to control the focal point of the synthesized transmit beam, nor the depth of focus. By delaying and summing the data received from several overlapping transmit beams, one may also be able to synthesize the transmit focus in every single image location. This is the core idea of the Synthetic Transmit Aperture (STA) techniques.

Synthetic transmit aperture imaging takes its root from radar technologies, and has proven as an efficient method for ultrasound imaging in cases where strong constraints on the number of channels were present [11]. Taking advantage of the superposition theorem, the transmit focus may be synthesized in every location by delaying and summing a plurality of datasets (before or after conventional beamforming) acquired

from successive transmissions. The quality of the resulting focus depends on several factors, among which the most important are the number of overlapping transmissions and the lateral bandwidth of the transmitted sound fields in k-space [32–34].

Over the last decade, several applications of STA have been demonstrated for ultrasound imaging.

- The original STA application used single element excitations, but is now applied using virtual point sources generated with small subsets of transducer elements in order to increase the energy forwarded into the tissue and therefore increase the SNR [11]. This technique is targeted towards high resolution imaging with broad transducers and hundreds of excitations per frame, where high frame rates are not a necessity.

- Coherent plane wave imaging (PWI) is another application of STA beamforming. By transmitting a succession of plane waves steered in different directions, one may recreate the transmit focus while covering substantially the entire field of view at each plane wave illumination [35, 36]. PWI is well suited for linear array transducers and may allow for very high frame rates, but the amount of energy transfered in the body is limited and second harmonic imaging can thus not be applied.

- A straightforward expansion of PWI to cardiac imaging with phased array transducers is the use of coherent compounding with diverging transmit beams, i.e. with a focus located behind the transducer surface, also known as diverging wave imaging (DWI) [37, 38]. This application of STA ensures very high frame rate while covering a wide sector view. However, the current applications were shown to present a low lateral resolution due to high levels of side lobes in the transmit focusing synthesis, and the energy dispersion prevents the generation of second harmonic signal [39].

- Several research groups investigated STA with limited diffraction beams, which are beams that avoids diffraction and keeps a rather stable transverse beam pattern while propagating [40–42]. Such beams should theoretically combine the potential for high frame rate imaging with an increased SNR, since the energy would remain concentrated in the transmit direction, but the energy levels remains low for second harmonic generation.

- Finally, an interesting application of STA for cardiac imaging is the use of focused beams [43–46]. Focused beams are typically narrow and well separated around focal depth, but overlapping both in the near-field and the far-field of the transducer. Coherent compounding in these overlap regions can be used to recreate the transmit focus. This technique, also known as retrospective transmit beamformation (RTB) or dynamic transmit focusing, provides several advantages specific to cardiac imaging: the number and disposition of the transmit beams may remain unchanged compared to conventional B-mode, the focused pulses will generate a sufficient level of second harmonics, and the computing power necessary to achieve this STA technique remains reasonable.

RTB can be considered as a more advanced version of the STB technique where a plurality of beams are compounded to synthesize both the transmit focus direction and focal depth.

By allowing both high frame rate and dynamic focus on transmit and receive, STA applications have opened the door to new multi-modality applications in ultrasound imaging. For example, the same acquisition sequence which is used for generating B-mode images may also be used over one or several frames to generate color flow images, pulsed-wave Doppler spectra, or even elastography measurements [11, 47–49].

If the vast majority of the STA techniques remains limited to the research scanners, simple applications of STA are emerging in the industry. The latest high-end scanners released this year dispose of a dynamic transmit focus based on STA (RTB) with a restricted number of adjacent focused transmit beams [50–52].

### 1.2.3 Limitations using parallel beamforming

Parallel beamformation can help increasing the frame rate in ultrasound imaging by reducing the number of transmissions required to sample a given field of view. But in order to maintain a high spatial resolution, the lateral extent of the emitted wave-field must remain limited. To do so, one must either keep a low $f$-number on transmission or one must use synthetic transmit aperture imaging techniques to retrospectively recreate a narrow transmit beam profile. In the case of very high frame rate applications where broad illuminations combined with parallel receive beamforming are desired, the STA techniques become a necessary complement.

Although STA imaging may allow the spatial resolution to be similar or even improved compared to single line focused ultrasound, it does not ensures a good sensitivity in the sense that neither the SNR, the penetration or the contrast are ensured to be comparable to what is achieved in conventional ultrasound imaging. The sensitivity is actually directly related to the characteristics of the emitted pulses: the frequency band and focus depth give an indication of how attenuated a pulse will be, the peak intensity is an indicator of the non-linear effects build-up during the propagation, and the aperture size and pulse duration describe the amount of energy transmitted. We can thus improve the sensitivity by maximizing the acoustic output, but one must consider the limitations of an ultrasound system, both technical and biological. One must have a powerful signal generator to drive a big amount of energy through the piezo-electric transducer, and this may lead to over-heating of the probe surface. We must also avoid damages to the tissues caused by cavitational effects or over-heating. In practice, one must adjust the acoustic output such that both the peak and the temporal average intensities remain under given thresholds. As of today, such safety guides are regulated by the the United States Food and Drug Administration (FDA) [14], and take the form of upper limits on given indexes: the mechanical index (MI $\leq 1.9$), the derated spatial-peak-temporal-average intensity ($I_{spta} \leq 720\,\mathrm{mW/cm^2}$), and the derated spatial-peak-pulse-average intensity ($I_{sppa} \leq 190\,\mathrm{W/cm^2}$).

In order to achieve a high sensitivity with a STA imaging application, one must not only consider the energy of each emitted pulse, but also maximize the number of

data-sets which are coherently compounded. Indeed, during the synthesis, the signals corresponding to effective targets will sum in phase, while noise will sum incoherently. As a result, the SNR will be improved by a factor $\sqrt{n}$, where $n$ is the number of emissions that are coherently compounded [53]. But these two constraints imply a trade-off: to maximize the number of combined beams, one must ensure high spatial overlaps between the transmitted pulses, and hence use broad beam transmissions where the energy is likely to spread out and the intensity will be reduced.

The spatial resolution achieved with STA imaging is dependent on the characteristics of the successive transmissions. As for conventional focused ultrasound imaging, the axial resolution is proportional to the pulse bandwidth (a larger bandwidth means a shorter pulse and thus a higher axial resolution). Thermal noise is also directly proportional with the pulse bandwidth. In order to increase the SNR with STA, one may want to maximize the transmitted energy by increasing the pulse amplitude. But in most imaging applications, the pulse amplitude is already limited by the MI and one may be tempted to increase the energy per pulse by increasing the pulse duration. Unfortunately, this will also result in a poorer axial resolution. As an alternative, it has been proposed to use linear frequency modulated (FM) excitations (also known as chirps) combined with a match filtering on reception, to increase the energy level without sacrificing the axial resolution [23]. The lateral resolution is only defined by the capability of the STA process to synthesize a narrow synthetic transmit beam profile, a capability which is itself defined by the diversity of the transmit wavefronts combined at each location. For example, the capability of coherent plane wave compounding to reproduce a focused transmit beam (i.e. the synthetic $f$-number in transmission) is directly related to the steering angle span of the combined plane wave emissions [36].

Finally, one of the major problems encountered with parallel beamforming and STA imaging, and which will be covered in details in this thesis, is the presence of motion in the imaged medium. The synthetic transmit aperture technique is based on the superposition theorem and its success relies entirely on the hypothesis that the targets in the field of view stand still. The presence of motion is prone to generate a misalignment between the signals coherently summed in the STB and STA techniques. This will result in a destruction of the transmit focus synthesis. In ultrasound imaging, tissue motion is mainly produced by the cardiovascular system, respiration or by the sonographer while scanning. Large velocity ranges are especially observed in the myocardium and in the blood. The sensitivity to motion in the field of view is a major drawback for STA imaging where motion generates artifacts such as spatial shifts, distortions, as well as loss of contrast and spatial resolutions. Several approaches to reduce motion artifacts have been investigated for the classical STA approach with point source insonifications [54–56], but there is a need for further research on efficient methods which provide both an efficient correction and a low computational cost to be used in real-time applications.

## 1.3 Motivation and aims of study

The main motivation of this study was the need for achieving real-time 3-D imaging of the full heart with an image quality comparable to state the art 2-D echocardiography. While three-dimensional imaging is a common modality on most of the commercially available high-end ultrasound scanners, their implementation still relies on broad focused ultrasound beams combined with parallel beamforming of a limited number of image lines. As a result, 3-D images of the heart suffer of a lower quality in terms of both spatial resolution and sensitivity, while the frame rate is slow and ECG-based stitching is required. Parallel transmission of a plurality of ultrasound beams as well as synthetic transmit aperture techniques are two potential candidates for improving both the image quality and the frame rate of 3-D cardiac imaging.

A requirement for higher frame rates in ultrasound imaging is to increase the portion of the image acquired with every transmission. Transmitting broader beams has been proposed, but cardiac applications require both a deep penetration and the generation of second harmonic components, two conditions that can only be met using strongly focused beams. Another approach is to simultaneously transmit several ultrasound pulses focused in non adjacent locations. Such parallel transmissions have not been the center of interest of the scientific community, mainly due to the severe cross-talk artifacts resulting from the interaction between the wave fields. While commercial patents describe techniques to minimize such artifacts, they do not provide any insight on the real performances of such methods, and the absence of any commercial application more than twenty years after the first publications enlightens the need for more academic work.

While it is important to insonify more of the imaged object for each transmission event, maintaining the image uniformity and resolution achieved by both the transmit and receive focus in each point is equally important. With the recent generalization of parallel receive beamforming techniques, the attention of the scientific community is big on the different applications of synthetic transmit aperture. No longer limited to using single elements as point sources on transmit, but generalized for using focused, plane, diverging or limited diffraction beams, the synthetic transmit aperture applications provide an efficient way to maximize the use of the full lateral span of the transmitted beams without losing the system capability for two-way focusing. However, the synthetic transmit aperture techniques are all based on combining low-resolution image lines obtained over several emissions, and hence rely on coherent summation. Cardiac tissue motion is prone to introduce a misalignment in this summation, and there is a need for research on what effect this will have on the final image and how we can try to efficiently correct for it.

The aims of this thesis are to:

**Aim 1:** Describe and understand the mechanisms of cross-talk artifacts when using parallel transmit beams.

**Aim 2:** Investigate how such cross-talk artifacts may be reduced in cardiac imaging applications.

**Aim 3:** Study the effects of motion for two different synthetic transmit aperture techniques: Synthetic Transmit Beams and Coherent Plane Wave Compounding.

**Aim 4:** Address motion artifacts using simple and robust algorithms suitable for real-time implementation.

## 1.4 Summary of presented work

**Paper no. 1:**
**Multi-Line Transmission in Medical Imaging Using the Second Harmonic Signal**

This paper investigated the fundamental source of cross-talk artifacts using parallel transmit beams. The edge waves from the pulses transmitted in different directions add to the signal focused on receive in the direction of interest, and vice versa, resulting on two main types of artifacts, namely the transmit and receive cross-talks. While the intensity of receive cross-talk may be modulated by processing of the received signals, such as apodization windows, the transmit cross-talk are directly related to the intensity of the edge waves of the transmitted pressure field. When an ultrasound pulse propagates, the nonlinear propagation process results in the build up of a signal around the second harmonic of the transmitted frequency. As the nonlinear build up is proportional to the square amplitude of the linear wave, the second harmonic beam presents a sharper profile with most of the energy concentrated in the main-lobe and attenuated side-lobes. This sharpness provides both an improved contrast and a higher spatial resolution, while the low amount of harmonics generated in the near-field will result in a reduced level of clutter from multiple reflections. Using filtering of the received signal around this second harmonic to improve the image quality has become the standard modality in cardiac imaging. The hypothesis behind this study was that the reduced side-lobe levels in the second harmonic profile will result in a reduction of the transmit cross-talk artifacts using parallel transmit beams. Simulations supported by both *in vitro* and *in vivo* measurements confirmed that the hypothesis is valid, while its impact is limited to systems providing a high sensitivity. The observed artifacts appear as stains around the main echo of a point target, and their intensity is reduced for the second harmonic signal. The paper also highlighted the limitations of the Multi-Line Transmission technique in the very near field where the pulses overlap and the perturbation level increases.

*The work was a joint effort with PhD candidate Fabrice Prieur. Fabrice Prieur conducted the theoretical work, simulations and most of the writing. The author's main responsibilities were the design, realization and analysis of* in vitro *and* in vivo *measurements.*

*This paper will be published in IEEE Transactions on Ultrasonics, Ferroelectrics,*

*and Frequency Control, vol. 60, December 2013.*

**Paper no. 2:**
**Multi-Line Transmission in 3-D with Reduced Cross-Talk Artifacts: a Proof of Concept Study**

This paper proposed a new approach to Multi-Line Transmission when imaging a 3-D volume with a cardiac probe. Using a rectangular transducer, the transmitted energy of a focused ultrasound beam will be concentrated in a cross-like pattern along the planes parallel with the azimuth and elevation axes and crossing along the focus direction. Conventional use of parallel transmissions, both in the scientific literature and in commercial patents, always chose to align the simultaneous transmit directions along a grid. But both the transmit and receive cross-talk artifacts inherent in the MLT techniques, result from the interactions between the main-lobe and side-lobes of simultaneous beams. If we now take into consideration the previously described cross-shape of the ultrasound beam, we may expect that the main-lobe to side-lobe interactions will be avoided if the parallel transmits are not aligned along either the azimuth or the elevation axis. This paper suggest to place the simultaneous transmit directions along the transverse diagonal of the transducer, which was shown to minimize cross-talks. This specific alignment was compared to conventional MLT dispositions through simulations and water tank measurements. The paper concluded on the possibility to align up to 5 MLT along the transverse diagonal while maintaining cross-talk artifacts below -50 dB. Although limited to simulations, this study proposed a promising approach on how to increase the frame rate in 3-D echocardiography while keeping the possibility to transmit focused beams and use second harmonic imaging, and thus maintaining a high spatial resolution and sensitivity. A dedicated scan sequence was proposed, and the gain in frame rate may contribute in removing the need for ECG-based stitching in volume acquisitions.

*This paper was published in IEEE Transactions on Ultrasonics, Ferroelectrics, and Frequency Control, vol. 60, August 2013.*

**Paper no. 3:**
**Motion Compensation Schemes Applied to Synthetic Transmit Beamformation**

While paper 1 and 2 investigated the use of parallel transmission of focused beams to achieve higher frame rate in 3-D echocardiography, this paper addressed how parallel receive beamforming may be used to maximize the frame rate while maintaining an optimal image quality. Using focused transmit beams, the Rayleigh criterion governs the number of beams required to laterally sample a field of view at a resolution optimal for the imaging system. If we reconstruct the transmit focus by combining received image lines from different transmissions, this sampling criterion may be optimized such as it is only governed by the transmit pressure field profile. Synthetic Transmit Beamformation (STB) is probably the most simple application of the synthetic transmit aperture applications, and is proven to be an efficient technique to image

over the full lateral transmit beam width in echocardiography without generating block artifacts. But because it is based on coherent lateral interpolation between image lines acquired from subsequent transmissions, the STB technique is prone to severe degradations in presence of radial motion. This is particularly true in 3-D imaging, where it is impossible to avoid large time delays between transmits in one of the dimensions. In presence of tissue motion with a radial component, the imaging lines will be summed with a non aligned phase, and artifacts appearing as dark stripes are observed in the images. This paper illustrated these effects using both a simple mathematical approach, linear simulations, and *in vivo* measurements. A cross-correlation based algorithm was proposed to estimate and correct for the radial velocities during the imaging process. The method is proven successful both in 2-D and 3-D imaging. In addition, the use of such an algorithm provides an additional unbiased TVI estimation without adding extra transmissions to the scan sequencing.

*This paper has been submitted for publication in IEEE Transactions on Ultrasonics, Ferroelectrics, and Frequency Control.*

**Paper no. 4:**
**Coherent Plane Wave Compounding for Very High Frame Rate Ultrasonography of Rapidly Moving Targets**

Paper 3 addressed the issues appearing with STB in presence of rapidly moving tissues such as the myocardium. The recent availability of channel data processing on receive enables more advanced applications of synthetic transmit aperture. The scientific community is now especially interested in applications where the transmitted beams are no longer focused. Coherent plane wave compounding is probably the more mature of the synthetic transmit aperture technique, and enables very high frame rates as well as a new approach on combining multiple modalities into a single transmit sequence. But as of today there was no work available on its performances when used for B-mode imaging of rapidly moving targets. This paper investigated how motion of the cardiac tissues can influence coherent plane wave compounding techniques. Radial velocities were shown to induce noticeable image degradations: the synthetic focusing mechanism of compounding is degraded, introducing intensity losses, grating-lobes, lateral shifting and radial spreading. The influence of motion can be reduced either by decimating the transmit sequence, but at the cost of an overall degradation in SNR and contrast, or by a correction mechanism in the compounding operation. A motion compensation scheme based on cross-correlation was introduced and tested both with simulations and *in vivo* when imaging a beating rat myocardium. The paper demonstrated the necessity of such a motion correction algorithm for plane wave compounding applications when both a high spatial resolution and sensitivity, and thus a large number of transmit angles per frame, is needed.

*This paper was published in IEEE Transactions on Medical Imaging, vol. 32, July 2013.*

## 1.5 Discussion and conclusion

The work presented in this thesis has explored two different approaches to improve the frame rate for 3-D echocardiography: transmitting simultaneously a plurality of beams (MLT) and taking advantage of the entire span of each transmit beam through parallel beamforming combined with synthetic transmit aperture techniques. However, both of these approaches face major artifacts which prevent a successful implementation for 3-D cardiac imaging: cross-talks between the simultaneously propagating ultrasound fields and phase misalignments in the coherent processing caused by motion of the tissue.

**Cross-talk reduction for Multi-Line Transmission (MLT)**

Transmitting pulses focused along different image lines in parallel is an obvious way to increase the frame rate. We have seen that several challenges appear with a MLT implementation: complex transmit electronics must be designed to excite the transducer elements with independently focused pulses, the pressure levels in the areas where several ultrasound pulses overlap must be controlled such that they do not lead to tissue damages, and the interactions between the parallel propagating wave fields, i.e. the cross-talks, must be reduced to a level where they are no longer distinguishable by the sonographer.

The goal of this thesis was not to evaluate the practical aspects of MLT implementations, but rather to address the more fundamental mechanism that create the cross-talks artifacts. We have distinguished 3 different types of cross-talks, of which the main-lobe to side-lobe interactions were the most severe. These two interactions, the so-called transmit and receive cross-talks, appear as pairs of shadow artifacts in the directions of the simultaneous transmit beams. We know that the intensity of both the transmit and receive cross-talks may be reduced by lowering the side-lobe levels of respectively the transmit and receive beams in the direction of the other beams. Such reductions may be done in various ways, the most simple of them being apodization windows applied to the transducer elements and increased angular separation. More complex approaches are based on isolating the pulses either in the frequency domain using different frequency bands or orthogonal frequency division, or in the time domain using pulse-inversion based sequences... But all of these suggestions are hard to apply to cardiac imaging where the pulse is subject to a restricted temporal bandwidth, a requirement for a high radial resolution, and the necessity to have a high frame rate. An alternative approach which is fully compatible with cardiac B-mode imaging is the use of harmonic imaging. The lower side-lobe levels of the second harmonic component in the propagating wave field lead to reduced transmit cross-talk as shown in Paper 1. As harmonic imaging is as of today a standard modality, knowing it further reduces the influence of parallel beams interactions is central for the potential applications of the MLT techniques.

The contribution on a new approach for 3-D multi-line transmission in Paper 2, while complex to implement, can be the key to higher frame rates for high definition B-mode 3-D cardiac imaging. The use of the transducer geometry as a way to concentrate

the side lobes in planes that will not interact with the other parallel transmits is a new concept, and may according to the presented simulations provide a 5 times higher frame rate while maintaining the cross-talk artifacts at a level that can not be observed with today's scanner sensitivity. Furthermore, we may expect that the results from this 3-D study may be improved using simple isolation principles such as transmit and receive apodization, or even second harmonic imaging as shown with Paper 1.

If MLT has some challenges in the near-field where the pulses overlap, we may expect that reconstructing the transmit focus using a Synthetic Transmit Aperture technique may help obtaining a level of cross-talk similar to what may be obtained in the vicinity of the focal depth. However, no illustration of this principle has been demonstrated in this thesis. Some other key aspects of MLT have not been covered in this thesis as we considered they should be kept for technological implementations. The transmit and receive electronics must evolve to be able to cope with parallel beams. Especially the sub-aperture processors within the modern 2-D matrix phased-array transducers (used to control the probe with a limited number of cables). Beyond this practical challenges, the work presented in this thesis show that MLT has a real potential of application in cardiac ultrasound.

**Motion compensation for Synthetic Transmit Aperture (SAT) techniques**

With the extended possibility to beamform a multitude of image lines in parallel, synthetic transmit aperture techniques have become feasible in many applications. By merging the data acquired over several transmissions, the transmit focus is recreated, i.e. synthesized, in each image location. But since summing of data acquired at different times is the central pillar of all the STA applications, the presence of motion and its impact will play a central role in its success. In this thesis, we have investigated how motion will influence two synthetic transmit aperture techniques. First, Synthetic Transmit Beam (STB) discussed in Paper 3, which has been especially developed for cardiac imaging applications, and is one of the most simple implementations of STA where only the transmit focus direction is reproduced through a lateral interpolation of the beams. Then, Coherent Plane Wave Compounding discussed in Paper 4, which is a more advanced STA application where the transmit focus is recreated on every single image location by the summation of a higher number of lines.

Both the simulations and the experiments presented in this thesis showed that ultrasound imaging systems can be modeled as a low-pass process in the lateral direction, and are thus not utterly impacted by lateral motion. On the contrary, severe degradations may be observed in presence of radial motion. The radial displacement of the observed tissues will result in a simple misalignment during the coherent summation. Furthermore, if this misalignment is large, it can no longer be approximated by a simple phase shift, but must be compensated for using both a delay and a phase shift. This phenomenon is especially true in 3-D applications where there will be large delays between the acquisition times of the image lines in one of the two lateral directions, but may also be present in 2-D imaging when a large number of images lines have to be merged together.

Radial velocity components were shown to cause different artifacts on the STA

imaging applications presented in this work. For STB imaging, the artifacts were limited to signal losses at lateral positions specific to the observed velocities. With coherent plane wave compounding, motion artifacts took the form of general signal losses, lateral shifts of the moving objects, blurring, and formation of grating lobes. We may expect that the other synthetic transmit aperture techniques (based on circular sources, focused or limited diffraction beams, diverging waves...) will produce similar results.

For both STB and plane wave compounding, we proposed simple algorithms based on estimating the phase misalignment through cross-correlation of temporally close imaging lines. These algorithms succeeded in recovering most of the image destructions observed in presence of motion. If these algorithms may be considered as efficient in themselves, more advanced versions could be imagined using for example 2-D/3-D motion estimators and may produced better results. The work presented in this thesis, however, was designed such as efficient real-time implementations could be considered with very little optimization work. In addition, we have seen for both STB and coherent plane wave compounding that such correction algorithms will also provide a tissue velocity estimate (TVI) of the full field of view without increasing the required number of emissions. If the scan sequencing is reordered, one may even expect as presented in Paper 3 that this TVI estimate will have a limited variance and be free of the bias which can be induced by the difference in transmit wavefronts.

While Paper 4 did not discuss any 3-D application, and therefore may be considered as out the scope of this thesis, it was a perfect example of motion compensation applied to a more advanced STA algorithm. This choice resulted from a pragmatic limitation: plane wave imaging was indeed the most advanced STA technique that could be experimented in combination with real-time acquisition at the time this work has been produced. Future work should be to generalize the motion compensation algorithms presented in this thesis to other STA modalities more adapted to cardiac imaging. The first of them is synthetic transmit aperture applied to focused beams beams where the overlap of a plurality of beams both in the near- and far-field may be exploited to synthesize the transmit focus at every location. STA applications based on diverging wavefronts and limited diffraction beams are also to be considered as they are more adapted to the phased-array transducers.

**Towards a gold standard for 3-D echocardiography**

The major research question beyond the scope of this thesis is whether real-time full-volume 3-D echocardiography of the heart can be obtained without sacrificing the image quality compared to what is achieved in 2-D. Todays state-of-the-art 2-D cardiac imaging uses strongly focused beams with harmonic imaging. In this thesis, we have investigated the use of Multi-Line Transmission in 3-D where an increase in frame rate by a factor 5 may be expected without any apparent cross-talk artifact (Paper 2). This parallel transmission acquisition technique is fully compatible with the use of second harmonic imaging (Paper 1), but also with the application of Synthetic Transmit Beam (Paper 3) where a motion compensation algorithm will ensure the image integrity in the third dimension. Finally, the promising results of Paper 4 on

more advanced applications of STA may be extended to the synthetic reconstruction of the transmit focus through STA on the overlap between the focused beams both in the near-field and the far-field. While a lot of the work presented here is based on computer simulations due to the complexity of implementing them on a real scanner, the basic principles were methodically demonstrated with experiments both *in vitro* and *in vivo*. Thus, a combination of all the work presented in this thesis may eventually lead to 3-D imaging capabilities of a large volume ($90 \times 90$ deg, 15 cm depth) at a frame rate close to 20 fps. Of course, a lot of technological challenges both on the simultaneous transmission of several beams and the processing of a large amount of beamformed lines have to be met before the work in this thesis may be evaluated further.

## 1.6 Publication list

**Published in peer-reviewed journals**

1. B. Dénarié, T.A. Tangen, I. Ekroll, N. Rolim, H. Torp, T. Bjåstad and L. Løvstakken ; "Coherent plane wave compounding for very high frame rate ultrasonography of rapidly moving targets" ; *IEEE Transactions on Medical Imaging, vol. 32, July 2013, pp. 1265–1276.*

2. B. Dénarié, T. Bjåstad and H. Torp ; "Multi-line transmission in 3-D with reduced crosstalk artifacts: a proof of concept study" ; *IEEE Transactions on Ultrasonics, Ferroelectrics and Frequency Control, vol. 60, August 2013, pp. 1708–1718.*

3. F. Prieur, B. Dénarié, A. Austeng and H. Torp ; "Multi-line transmission in medical imaging using the second harmonic signal" ; *IEEE Transactions on Ultrasonics, Ferroelectrics and Frequency Control, vol. 60, December 2013.*

**Submitted for publication**

1. B. Dénarié, T. Bjåstad and H. Torp ; "Motion compensation schemes applied to Synthetic Transmit Beamformation" ; *IEEE Transactions on Ultrasonics, Ferroelectrics and Frequency Control.*

2. L. Tong, B. Dénarié, H. Torp, L. Løvstakken and J. D'hooge ; "Comparison of conventional parallel beam forming with plane wave and diverging wave imaging for cardiac applications: experimental validation" ; *IEEE Transactions on Ultrasonics, Ferroelectrics and Frequency Control.*

**Conference presentations and proceedings**

1. B. Dénarié, H. Torp, G. Haugen, A. Sørnes, and T. Bjåstad, "Motion compensated Synthetic Transmit Beam Technique for real-time echocardiography" ; in *IEEE Ultrason. Symp.*, pp. 136–139, 18-21 Oct. 2010.

2. B. Dénarié, O. Bakstad, L. Løvstakken, T. Bjåstad and H. Torp ; "FieldSim3: a unified ultrasound simulation platform" ; *3rd National PhD Conference in Medical Imaging*, Bergen, 21-22 Nov. 2011.

3. B. Dénarié, T. Bjåstad and H. Torp ; "A novel approach for reducing Multi Line Transmission cross talks using 2D transducer arrays" ; *IEEE Ultrason. Symp.*, pp.2242-2245, 7-10 Oct. 2012.

4. B. Dénarié, T. Bjåstad and H. Torp ; "Real-time 3-D echocardiography: can we increase the frame rate by a factor five?" ; *4th National PhD Conference in Medical Imaging*, Trondheim, 28-29 Nov. 2012 ; awarded *best oral presentation.*

5. B. Dénarié, T. Tangen, I. Ekroll, N. Rolim, H. Torp, T. Bjåstad and L. Løvstakken ; "Coherent plane wave compounding for very high frame rate ultrasonography of rapidly moving targets" ; *5th National PhD Conference in Medical Imaging*, Tromsø, 3-4 Oct. 2013

# References


[1] I. Edler and K. Lindström, "The history of echocardiography.," *Ultrasound in Medicine & Biology*, vol. 30, pp. 1565–644, Dec. 2004.

[2] J. M. Griffith and W. L. Henry, "A sector scanner for real time two-dimensional echocardiography," *Circulation*, vol. 49, pp. 1147–52, June 1974.

[3] N. Bom, C. T. Lancee, J. Honkoop, and P. G. Hugenholtz, "Ultrasonic viewer for cross-sectional analyses of moving cardiac structures," *Biomed. Eng.*, June 1971.

[4] J. C. Somer, "Electronic sector scanning for ultrasonic diagnosis," *Ultrasonic*, no. 6, pp. 153–159, 1968.

[5] F. L. Thurstone and O. T. von Ramm, "Electronic beam scanning for ultrasonic imaging," *Proceedings of the Second World Congress on Ultrasonics in Medicine, Rotterdam*, pp. 43–48, June 1973.

[6] M. Kowalski, T. Kukulski, F. Jamal, J. D'hooge, F. Weidemann, F. Rademakers, B. Bijnens, L. Hatle, and G. R. Sutherland, "Can natural strain and strain rate quantify regional myocardial deformation? A study in healthy subjects.," *Ultrasound in Medicine & Biology*, vol. 27, pp. 1087–97, Aug. 2001.

[7] H. Yoshiara, H. Hasegawa, H. Kanai, and M. Tanaka, "Ultrasonic imaging of propagation of contraction and relaxation in the heart walls at high temporal resolution," *Japanese Journal of Applied Physics*, vol. 46, pp. 4889–4896, July 2007.

[8] B. Delannoy, R. Torguet, C. Bruneel, E. Bridoux, J. M. Rouvaen, and H. LaSota, "Acoustical image reconstruction in parallel-processing analog electronic systems," *Journal of Applied Physics*, vol. 50, pp. 3153–3159, 1979.

[9] O. T. Von Ramm, S. W. Smith, and H. G. P. Jr, "High-speed ultrasound volumetric imaging system. ii. parallelprocessing and image display," *IEEE Transactions on Ultrasonics, Ferroelectrics, and Frequency Control*, vol. 38, no. 2, pp. 109–115, 1991.

[10] G. F. Pinton, G. E. Trahey, and J. J. Dahl, "Sources of image degradation in fundamental and harmonic ultrasound imaging: a nonlinear, full-wave,

simulation study.," *IEEE Transactions on Ultrasonics, Ferroelectrics, and Frequency Control*, vol. 58, pp. 1272–83, June 2011.

[11] J. A. Jensen, S. I. Nikolov, K. L. Gammelmark, and M. H. Pedersen, "Synthetic aperture ultrasound imaging.," *Ultrasonics*, vol. 44 Suppl 1, pp. e5–15, Dec. 2006.

[12] T. Shirasaka and K. Toshiba, "Ultrasonic imaging apparatus," *US Patent 4,815,043*, 1989.

[13] R. Mallart and M. Fink, "Improved imaging rate through simultaneous transmission of several ultrasound beams," *Proceedings of SPIE*, vol. 1733, pp. 120–130, 1992.

[14] FDA, "510 (k) information for manufacturers seeking marketing clearance of diagnostic ultrasound systems and transducers," tech. rep., Food and Drug Administration, 1997.

[15] B. Madore, P. J. White, K. Thomenius, and G. T. Clement, "Accelerated focused ultrasound imaging.," *IEEE Transactions on Ultrasonics, Ferroelectrics, and Frequency Control*, vol. 56, pp. 2612–23, Dec. 2009.

[16] L. Tong, *Novel Beam Forming Methods for Fast Cardiac Imaging Using Ultrasound*. PhD thesis, KU Leuven, 2013.

[17] S. Denk, "Ultrasound imaging system and method," *US Patent 20100191115*, 2010.

[18] A. Drukarev and K. Konstantinides, "Beam transformation techinques for ultrasonic medical imaging," *IEEE Transactions on Ultrasonics, Ferroelectrics, and Frequency Control*, vol. 40, pp. 717–26, Jan. 1993.

[19] D. Dubberstein and O. V. Ramm, "Methods and systems for ultrasound scanning using spatially and spectrally separated transmit ultrasound beams," *US Patent 6,159,153*, 2000.

[20] J. Hossack and T. Sumanaweera, "Method and apparatus for medical diagnostic ultrasound real-time 3-D transmitting and imaging," *US Patent 6,179,780*, 2001.

[21] L. Demi, "Parallel transmit beamforming using orthogonal frequency division multiplexing applied to harmonic Imaging-A feasibility study," *IEEE Transactions on Ultrasonics, Ferroelectrics, and Frequency Control*, vol. 59, no. 11, pp. 2439–2447, 2012.

[22] L. Demi, J. Viti, L. Kusters, F. Guidi, P. Tortoli, and M. Mischi, "Implementation of Parallel Transmit Beamforming Using Orthogonal Frequency Division Multiplexing — Achievable Resolution and Interbeam Interference," *IEEE Transactions on Ultrasonics, Ferroelectrics, and Frequency Control*, vol. 60, no. 11, pp. 2310–2320, 2013.

[23] T. Misaridis and J. A. Jensen, "Use of modulated excitation signals in medical ultrasound. Part III: High frame rate imaging.," *IEEE Transactions on Ultrasonics, Ferroelectrics, and Frequency Control*, vol. 52, pp. 208–19, Feb. 2005.

[24] L. Tong and H. Gao, "Multi-transmit beam forming for fast cardiac imaging-a simulation study," *IEEE Transactions on Ultrasonics, Ferroelectrics, and Frequency Control*, vol. 60, no. 8, pp. 1719–1731, 2013.

[25] K. Thiele, "Multi-Beam Transmit Isolation," *US Patent 20100016725*, 2010.

[26] D. P. Shattuck, M. D. Weinshenker, S. W. Smith, and O. T. von Ramm, "Explososcan: A parallel processing technique for high speed ultrasound imaging with linear phased arrays," *The Journal of the Acoustical Society of America*, vol. 75, pp. 1273–1282, 1984.

[27] J. Wright, "Image formation in diagnostic ultrasound," *IEEE International Ultrasonic Symposium Short Course*, 1997.

[28] T. Hergum, T. Bjastad, K. Kristoffersen, and H. Torp, "Parallel beamforming using synthetic transmit beams," *IEEE Transactions on Ultrasonics, Ferroelectrics, and Frequency Control*, vol. 54, no. 2, pp. 271–280, 2007.

[29] J. Wright, S. Maslak, D. Finger, and A. Gee, "Method and apparatus for coherent image formation," *US Patent 5,667,373*, 1997.

[30] T. Bjåstad, S. A. Aase, and H. Torp, "Synthetic transmit beam technique in an aberrating environment.," *IEEE Transactions on Ultrasonics, Ferroelectrics, and Frequency Control*, vol. 56, pp. 1340–51, July 2009.

[31] T. Bjåstad, *High frame rate ultrasound imaging using parallel beamforming*. PhD thesis, NTNU, 2009.

[32] S. Nikolov, J. Kortbek, and J. Jensen, "Practical applications of synthetic aperture imaging," *IEEE Ultrasonics Symposium, Proceedings*, 2010.

[33] W. F. Walker and G. E. Trahey, "The application of k-space in pulse echo ultrasound.," *IEEE Transactions on Ultrasonics, Ferroelectrics, and Frequency Control*, vol. 45, pp. 541–58, Jan. 1998.

[34] K. Thomenius, "Evolution of ultrasound beamformers," in *IEEE Ultrasonics Symposium, Proceedings*, vol. 2, pp. 1615–1622, IEEE, 1996.

[35] M. Tanter, J. Bercoff, L. Sandrin, and M. Fink, "Ultrafast compound imaging for 2-D motion vector estimation: application to transient elastography.," *IEEE Transactions on Ultrasonics, Ferroelectrics, and Frequency Control*, vol. 49, pp. 1363–74, Oct. 2002.

[36] G. Montaldo, M. Tanter, J. Bercoff, N. Benech, and M. Fink, "Coherent plane-wave compounding for very high frame rate ultrasonography and transient elastography.," *IEEE Transactions on Ultrasonics, Ferroelectrics, and Frequency Control*, vol. 56, pp. 489–506, Mar. 2009.

[37] H. Hasegawa and H. Kanai, "High-frame-rate echocardiography using diverging transmit beams and parallel receive beamforming," *Journal of Medical Ultrasonics*, vol. 38, pp. 129–140, May 2011.

[38] L. Tong, H. Gao, H. Choi, and J. D'hooge, "Comparison of conventional parallel beamforming with plane wave and diverging wave imaging for cardiac applications: a simulation study.," *IEEE Transactions on Ultrasonics, Ferroelectrics, and Frequency Control*, vol. 59, no. 8, pp. 1654–1663, 2012.

[39] H. Hasegawa and H. Kanai, "High-frame-rate echocardiography with reduced sidelobe level.," *IEEE Transactions on Ultrasonics, Ferroelectrics, and Frequency Control*, vol. 59, pp. 2569–75, Nov. 2012.

[40] J.-y. Lu, "2D and 3D high frame rate imaging with limited diffraction beams," *IEEE Transactions on Ultrasonics, Ferroelectrics, and Frequency Control*, vol. 44, pp. 839–856, July 1997.

[41] J.-y. Lu, "Experimental study of high frame rate imaging with limited diffraction beams.," *IEEE Transactions on Ultrasonics, Ferroelectrics, and Frequency Control*, vol. 45, pp. 84–97, Jan. 1998.

[42] J. Cheng and J.-y. Lu, "Extended high-frame rate imaging method with limited-diffraction beams.," *IEEE Transactions on Ultrasonics, Ferroelectrics, and Frequency Control*, vol. 53, pp. 880–99, May 2006.

[43] S. Freeman, P. Li, and M. Odonnell, "Retrospective dynamic transmit focusing," *Ultrasonic imaging*, vol. 17, no. 3, pp. 173–196, 1995.

[44] R. Zemp and M. F. Insana, "Imaging with unfocused regions of focused ultrasound beams," *The Journal of the Acoustical Society of America*, vol. 121, no. 3, p. 1491, 2007.

[45] R. Loftman, K. Ustuner, and C. Bradley, "Coherent Image Formation for Dynamic Transmit Beamformation," June 2009.

[46] D. Napolitano, B. Debusschere, G. Mclaughlin, L. Mo, C. Chou, T. Ji, and R. Steins, "Continuous transmit focusing method and apparatus for ultrasound imaging system," Aug. 2011.

[47] J. Udesen, F. Gran, K. L. Hansen, J. A. Jensen, C. Thomsen, and M. B. Nielsen, "High frame-rate blood vector velocity imaging using plane waves: simulations and preliminary experiments.," *IEEE Transactions on Ultrasonics, Ferroelectrics, and Frequency Control*, vol. 55, pp. 1729–43, Aug. 2008.

[48] J. Bercoff and G. Montaldo, "Ultrafast compound doppler imaging: providing full blood flow characterization," *IEEE Transactions on Ultrasonics, Ferroelectrics, and Frequency Control*, 2011.

[49] S. Park, S. R. Aglyamov, and S. Y. Emelianov, "Elasticity imaging using conventional and high-frame rate ultrasound imaging: experimental study.," *IEEE Transactions on Ultrasonics, Ferroelectrics, and Frequency Control*, vol. 54, pp. 2246–56, Nov. 2007.

[50] K. Thiele, P. Scientist, J. Jago, P. Scientist, R. Entrekin, T. Fellow, R. Peterson, and S. Engineering, "Exploring n SIGHT Imaging – a totally new architecture for premium ultrasound," *Whitepaper Philips EPIQ ultrasound system*, pp. 1–12, 2013.

[51] C. Bradley, "Retrospective transmit beamformation," *Whitepaper ACUSON SC2000TM Volume Imaging*, vol. Im, 2008.

[52] G. Mclaughlin, "ZONE Sonography $^{TM}$ : What It Is and How It ' s Different," *Whitepaper ZONARE Medical Systems, Inc*, 2013.

[53] M. Karaman and M. O'Donnell, "Synthetic aperture imaging for small scale systems," *IEEE Transactions on Ultrasonics, Ferroelectrics, and Frequency Control*, vol. 42, pp. 429–442, May 1995.

[54] N. Oddershede and J. A. Jensen, "Effects influencing focusing in synthetic aperture vector flow imaging.," *IEEE Transactions on Ultrasonics, Ferroelectrics, and Frequency Control*, vol. 54, pp. 1811–25, Sept. 2007.

[55] K. S. Kim, J. S. Hwang, J. S. Jeong, and T. K. Song, "An efficient motion estimation and compensation method for ultrasound synthetic aperture imaging.," *Ultrasonic imaging*, vol. 24, pp. 81–99, Apr. 2002.

[56] B. Yiu, I. Tsang, and A. Yu, "A modified synthetic aperture imaging approach with axial motion compensation," *IEEE Ultrasonics Symposium, Proceedings*, pp. 1254–1257, 2008.

# Chapter 2

# Multi-Line Transmission in Medical Imaging Using the Second Harmonic Signal

Fabrice Prieur[1], Bastien Dénarié[2], Andreas Austeng[1] and Hans Torp[2]
[1]Department of Informatics, University of Oslo, Norway
[2]MI-Lab, Department of Circulation and Medical Imaging, Faculty of Medicine, Norwegian University of Science and Technology (NTNU)

The emergence of three-dimensional imaging in the field of medical ultrasound imaging has greatly increased the number of transmissions needed to ensonify a whole volume. With a large number of transmissions follows a low image frame rate. When using classical transmission techniques, as in two-dimensional imaging, the frame rate becomes unacceptably low, prompting for alternative transmission patterns that require less time. One alternative is to use a multi-line transmission (MLT) technique which consists of transmitting several pulses simultaneously in different directions. Perturbations appear when acquiring and beamforming the signal in the direction of one pulse due to the pulses sent in other directions. The edge waves from the pulses transmitted in a different direction add to the signal transmitted in the direction of interest resulting in artifacts in the final image. Taking advantage of the nonlinear propagation of sound in tissue, the second harmonic signal can be used with the MLT technique. The image obtained using the second harmonic signal compared to when using the fundamental signal, should have reduced artifacts coming from other pulses transmitted simultaneously. Simulations backed up by experiments imaging a wire target and an *in vivo* left ventricle confirm that the hypothesis is valid. In the studied case, the perturbations appear as an increase in the signal level around the main echo of a point scatterer. When using the fundamental signal, the measured amplitude level of the perturbations was approximately -40 dB compared to the maximum signal amplitude (-27 dB *in vivo*), while it was around -60 dB (-45 dB *in vivo*) for the second harmonic signal. The MLT technique encounters limitations in the very near field where the pulses overlap and the perturbation level increases as well as for images with strong speckle and low contrast.

## 2.1 Introduction

In medical ultrasound imaging the quality of the image and the usefulness of the diagnostic can be improved through higher data acquisition rates. For volumetric imaging the number of sound emissions needed to produce an image is often squared compared to two-dimensional imaging. Due to the limited speed of sound propagating through the body, acquiring a three-dimensional image made of 2500 transmissions (50 transmissions in elevation and azimuth) travelling 15 cm into the body would take around 0.5 s which translates to a frame rate of 2 frames per second. This is not acceptable for dynamic structures like a beating heart. Several techniques allowing an increase of the frame rate have been studied. One of them called the multi-line acquisition or parallel beamforming consists of transmitting a beam of wide opening angle and beamform the data at reception in several neighbouring directions at the same time [1]. Because the receiving beam is steered off-axis relative to the transmit beam, this method suffers from artifacts that have to be corrected for [2].

Synthetic aperture imaging was originally conceived for radar systems but has been applied to medical ultrasound imaging and yields high frame rates [3]. This techniques uses a subset of elements of the aperture to sequentially transmit a spherical wave and record the echoes using all the elements of the aperture. Fully dynamic focusing for all points can be done at reception producing a low resolution image per transmission. These low resolution images are combined to generate a high resolution image. This system is versatile but encounters limitations due to a low penetration depth when standard pressure pulses are transmitted, a need to compensate for target motion, and a heavy computational burden [3].

The use of limited diffraction beams to increase the frame rate has also been suggested. A weighting of the transducer at reception that produces a diffraction limited response provides signals that are processed to obtain the Fourier transform of the object functions. Using one plane wave at transmission and weighting for low diffraction response at reception allows for high frame rates limited only by the duration of one transmission [4] while using several limited diffraction beams both at transmission and reception allows for a compromise between frame rate and image quality [5].

More recently, a technique using coherent compounding of plane waves has produced high frame rates [6]. It consists of sending sequentially several plane waves at different angles. For each plane wave an image is built by coherently summing the echoes from each element of the receiving array. These images are then coherently summed generating a synthetic focusing. This technique encounters some limitations in the depth of view and opening angle for which the process is applicable.

In 1996, Shen and Ebbini described a technique that uses coded excitation [7]. It consists of using all the elements of the array to simultaneously transmit a number of independent codes each in a separate direction. At reception, the data go through a bank of filters each associated with echoes from a specific direction. The number of image lines that can be acquired simultaneously is equal to the number of filters. The processing of the data consists of estimating a pseudo-inverse operator (PIO) determined by the complex impulse response of the echo generated by each point of

a grid covering the region of interest. Applying this operator to the received data gives an estimate of the complex scatterer strength at each point of the grid. The limitations of this technique are due to the necessary trade-off between robustness of the PIO against noise and effects from scatterers not situated on a point of the grid [8].

Very recently, Demi *et al.* studied the feasibility of multiplexing orthogonal frequencies when imaging with the second harmonic signal [9]. Signals at different frequencies are transmitted at the same time in different directions. At reception, the recorded echo from the second harmonics are separated using band-pass filters. This technique allows to approximately increase the frame rate by the number of signals transmitted at different frequencies. However, in order to be able to discriminate at reception the signals transmitted around different center frequencies, a minimum separation is required between each signal frequency band. If all the frequency bands are to fit within the transducer's bandwidth, each bandwidth has to be small enough to ensure minimum separation. This leads to longer signals and a reduced axial resolution. There is therefore a trade-off between the number of different frequencies simultaneously transmitted, and the length of the transmitted signals that dictates the axial resolution.

The technique studied in this article consists of transmitting pulses simultaneously in several directions and beamform the signal at reception in these directions [10–12]. In this article, it is called multi-line transmission (MLT). The frame rate is improved by a factor corresponding to the number of directions covered for each transmission compared to the frame rate obtained with a standard method where a pulse is sent and received in one direction for each transmission. When acquiring a signal echo in one direction using this technique, perturbations from the beams transmitted in other directions appear [13]. Our hypothesis is that if the second harmonic signal created through nonlinear propagation is used instead of the fundamental signal, those perturbations should be reduced. The second harmonic signal is already used with great success in the field of medical ultrasound imaging through tissue harmonic imaging (THI). THI consists of acquiring the scattered signal by filtering around the second harmonic frequency band instead of the transmitted frequency band. This technique has proven beneficial for image enhancement due to, among others, a narrower main lobe and a higher main-lobe-to-sidelobe ratio of the second harmonic signal compared to the fundamental signal used in conventional imaging [14]. These properties make the second harmonic signal a good candidate to improve the image obtained using the MLT technique.

In the first part or this article, we present the theory behind our hypothesis. The second part describes the methods used for simulations and measurements. In the third part, we present the results of simulations of a point target imaged using the MLT technique and we compare the results obtained with the fundamental and second harmonic signals. The fourth part describes the experiments done to back up the simulations using a medical scanner to image a wire target and the left ventricle of a healthy volunteer. In the last part the results of the experiments are discussed allowing to reach some conclusions on the advantage and limitations of using the second harmonic signal with the MLT technique.

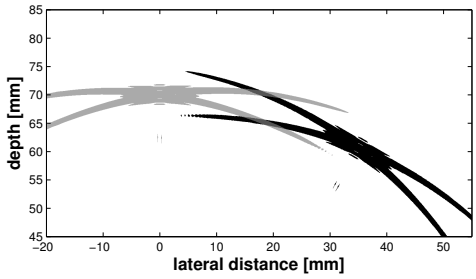


Figure 2.1: Contours of the envelope of two pulses focused at 70 mm depth transmitted at 1.5 MHz with 30° angular separation. The contours defined the spaces where the normalized amplitude is above -40 dB (1%). The edge waves of each beam extend into the direction of the other beam perturbing the beamformed signal at reception.

## 2.2 Theory

When using the MLT technique, two or more pulses are transmitted simultaneously in different steering directions. At reception the received echoes are beamformed in these directions. Compared to an imaging method where the transmitted pulse covers only one direction, the frame rate is multiplied by the number of directions covered per transmission. However, when acquiring a signal echo in one direction perturbations from the beams transmitted in other directions appear (Fig. 2.1). The first type of perturbations is the receive crosstalk due to the effect of echoes coming from scatterers not situated in the direction of interest. They can easily be limited by applying an apodization to the aperture at reception [15]. The other type of perturbations is the transmit crosstalk due to the energy transmitted outside the steering direction. They can also be limited by a similar apodization applied to the aperture at transmission. However it is more problematic in this case as it requires an individual amplification of the signal transmitted to each element of the transducer and it limits the maximum energy that can be transmitted. Since the receive crosstalk can be reduced by a simple weighting of the data, this article will focus on the transmit crosstalk that cannot be reduced when using common systems without individual amplifiers. To limit both types of perturbations it is beneficial to use a large angular separation between the beams transmitted simultaneously. A more directive beam with low sidelobe levels is also beneficial for reducing those perturbations. The second harmonic signal generated by nonlinear propagation of sound presents such characteristics.

When the sound propagates in biological tissue, the variations of density with sound pressure distort the transmitted pulse. These distortions translate into energy transfer from the emitted frequency band to frequency bands centered around multiples of the transmit center frequency. When filtering the received echo around the second harmonic frequency, the second harmonic signal obtained presents a narrower main lobe and a higher main-lobe-to-sidelobe ratio compared to the fundamental signal. In this study, the center frequency of the transmitted pulse when imaging with the second harmonic signal is $f_0$ while it is $2f_0$ when imaging with the fundamental signal. This

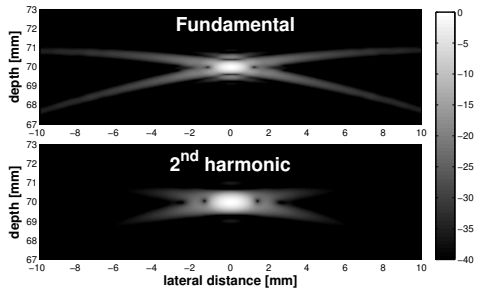


Figure 2.2: Edges waves generated when filtering the signal around the fundamental frequency (top) for a pulse transmitted at 3.0 MHz and around the second harmonic frequency (bottom) for a pulse transmitted at 1.5 MHz. Here the amplitude of the pulse envelopes is displayed in decibel after normalization.

means that the received signals are filtered around the same frequency in both cases: $2f_0$. The main lobe of the second harmonic signal at $2f_0$ is slightly larger than the mainlobe of the fundamental at $2f_0$, but the main-lobe-to-sidelobe ratio is lower for the second harmonic signal [16].

This feature is beneficial for improving the image obtained when using the MLT technique. Indeed, the level of the perturbing edge waves in the steering direction should be relatively lower for second harmonic signal than for the fundamental signal at the same frequency as shown in Fig. 2.2.

In the next sections, this hypothesis is tested using simulations and experimental data.

## 2.3 Method

In order to verify the potential improvements of MLT with the second harmonic signal, we used both simulations and measurements to compare the perturbation levels when using the second harmonic signal or the fundamental signal. In all the simulations, the transducer is a rectangular array of dimensions 19.2 mm in azimuth ($x$ direction) and 14 mm in elevation ($y$ direction) made of 64 elements with a center frequency of 2.5 MHz and a focus depth of 61 mm in both directions. The center frequency of the transmitted pulse is 1.5 MHz when studying the second harmonic signal and 3.0 MHz when studying the fundamental signal.

Due to restrictions in the shape of the electrical input signal that can be sent to the probe's elements, it was not possible to send two pulses in different directions simultaneously during the experiments. We therefore chose to send two pulses in different directions sequentially and add the channel data acquired after each transmission during the data processing. This approach was used both in the measurements and in the simulations.

The sound field resulting in adding the fields generated by two pulses transmitted in

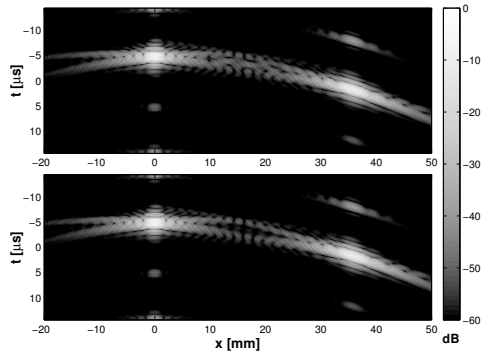


Figure 2.3: Second harmonic pressure sound fields at focus point in the zero elevation plane when two pulses separated by 30° are transmitted simultaneously (top), or sequentially before addition (bottom).

different directions is not exactly the same as the field generated when both pulses are transmitted simultaneously if nonlinear effects are taken into account. To estimate their difference we used a simulation package for nonlinear wave propagation of wideband pulses called Abersim [17–19] to simulate both scenarios. In the simulations, the pulse transmitted has a 6-dB (full width half maximum) relative bandwidth of 80% and the peak pressure at focus is 600 kPa. Two pulses are sent in the zero elevation plane, one in the direction perpendicular to the transducer plane, 0°, and the other with a 30° angular separation. The second harmonic sound fields obtained at focus depth in the zero elevation plane in the case of simultaneous and sequential transmissions are shown in Fig. 2.3. When filtered around the fundamental frequency, the fields are almost identical and their difference does not exceed 3 dB. The same simulation was repeated where the angular separation between the two pulses was changed from 30° to 15°. The comparison of the fields in this case is very similar to the case using 30° angular separation.

Fig. 2.4 compares lateral profiles for the second harmonic field in the case of simultaneous and sequential transmissions. It shows the root mean square (RMS) value over the pulse duration as shown in Fig. 2.3 for every value of the azimuth coordinate $x$ for 15° and 30° angular separations. The largest difference is located in the area between the focus points and is around 10 dB when considering the pulse RMS value. The corresponding profiles for the fundamental signal could not be distinguished from each other.

These simulations allow us to conclude that the sound field obtained by summing the field generated by one pulse transmitted in two directions is a good approximation of the sound field generated by two pulses transmitted simultaneously in each direction for an angular separation above 15°. This is therefore the mode of operation that is used in the subsequent simulations and experiments.

Strictly speaking, our mode of operation does not improve the frame rate compared to traditional B-mode imaging but the results are a good approximation of the imaged

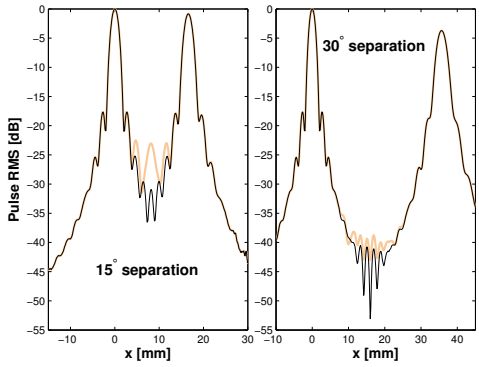


Figure 2.4: (Color online). Lateral profiles showing the normalized RMS value of the obtained pulse filtered around the second harmonic frequency when two pulses are transmitted simultaneously (thick lines) or sequentially then summed (thin lines). Profiles are shown for an angular separation between the pulses of 15° (left) and 30° (right).

produced by the MLT technique when transmitting several pulses simultaneously.

## 2.4 Simulations

### 2.4.1 The simulator

Numerical experiments were run using a simulator based on the quasi-linear approximation. In the quasi-linear approximation, the fundamental signal is assumed to propagate linearly. The fundamental field can be seen as localized sources for the second harmonic signal. The amplitude of these sources is proportional to the square of the the fundamental signal's amplitude. More details on the theoretical background and implementation of the simulator can be found in [20] and [21]. To simulate the beams transmitted during acquisition of a B-scan sector image in medical ultrasound, N beams need to be simulated with a steering direction in azimuth varying from $-\theta_m$ to $\theta_m$ relative to the normal to the transducer ($z$ direction). This covers an angular sector in the zero elevation plane as shown in Fig. 2.5. In the simulations, the sound field when steering in the direction $\theta$ is approximated by the field generated by a probe transmitting the beam at 0° steering angle and whose dimension has been multiplied by $\cos\theta$.

To check that this last approximation is valid, the lateral profiles at the focus point obtained when using the quasi-linear simulator were compared to the results given by Abersim. In the simulations, the pulse described in Sec. II was assumed to propagate in a lossless and homogeneous media. The comparisons were done for the steering directions 15°, 30°, and 45° from the $z$ direction. The match between the results is satisfactory with a root mean square (RMS) value for the difference between the lateral

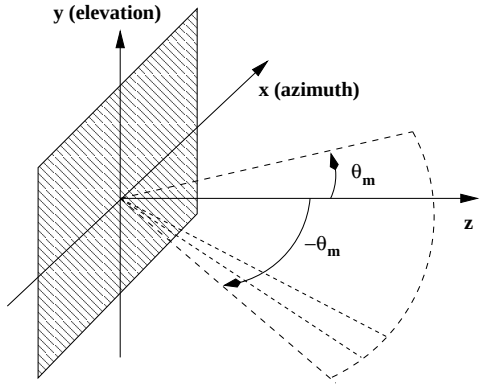


Figure 2.5: Steering directions that cover an angular sector extending from $-\theta_m$ to $\theta_m$ in the zero elevation plane.

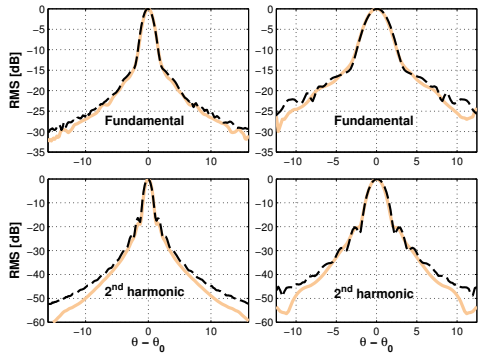


Figure 2.6: (Color online). Lateral profiles along the azimuth (left) and elevation (right) directions obtained by the quasi-linear method (solid line) and Abersim (dashed line) for the fundamental (top) and the second harmonic (bottom) signals at focus depth (61 mm) when steering to 15° from the $z$ direction. The horizontal axis shows the difference between the direction of look $\theta$ and the steering direction $\theta_0$. Note the different vertical scales used for the fundamental and second harmonic signals.

profiles below 0.4 dB. The lateral profiles along the azimuth and elevation directions obtained by both methods for the 15° steering direction are shown in Fig. 2.6. The vertical scales were adapted between the fundamental and the second harmonic signals in order to better show where the lateral profiles differ. The reason why we favoured the quasi-linear simulator instead of Abersim in the rest of the presented work is due to its greater speed that is decisive when simulating many transmit directions.

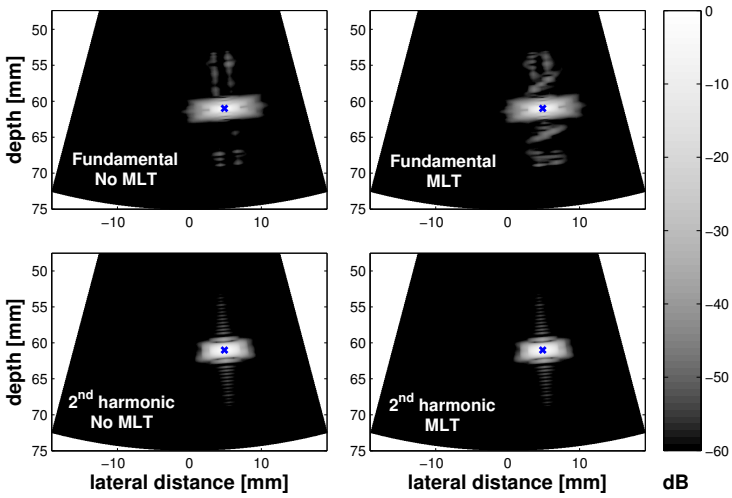


Figure 2.7: Images obtained when simulating the echo of a point scatterer when using the fundamental signal (top) from a pulse transmitted at 3.0 MHz and the second harmonic signal (bottom) from a pulse transmitted at 1.5 MHz in the case of the standard method (left) and the MLT method (right). The envelope of the received echo is displayed in decibel after normalization. The placement of the scatterer is indicated by a cross in each image and the display is limited to the angular sector contained within $\pm 15°$.

### 2.4.2 Results

Keeping the same simulation parameters as in the previous section a point scatterer with a unitary reflectivity coefficient was simulated at 61 mm along the steering direction that creates a 5° angle with the $z$ direction. The scattered signal is assumed to propagate spherically back to the transducer. The signals at reception are dynamically focused using a delay-and-sum method and the receiving aperture is weighted using a Hanning window of the same length as the aperture to minimize the sidelobe levels. The angular sector simulated extends from $-30°$ to $30°$ and is divided into 60 directions. For the MLT method, 30 pairs of beams separated by 30° are transmitted sequentially then added. In the case of simultaneous transmissions, the final image is obtained after 30 transmissions multiplying the frame rate of the standard method (one beam transmitted in one direction for each transmission) by a factor two.

Fig. 2.7 shows the images obtained when using the standard method and the MLT method for both the fundamental and the second harmonic signals. The center frequency of the transmitted pulse is 3.0 MHz when filtering the echo in the fundamental frequency band, and 1.5 MHz when filtering in the second harmonic frequency band.

In the case of the fundamental signal, the image obtained with the MLT method

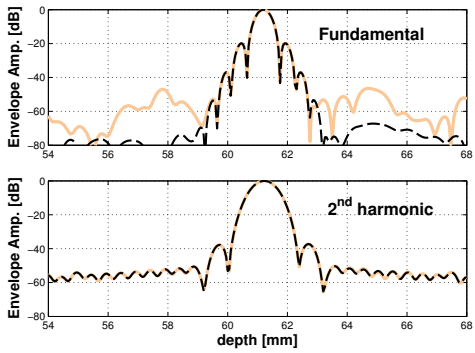


Figure 2.8: (Color online). Axial profile of the signal amplitude in the direction of the point scatterer (5°) after beamforming. The echo amplitude for the fundamental (top) and second harmonic (bottom) signals, both at 3.0 MHz, are shown in the case of the MLT method (solid lines) and standard method (dashed lines).

presents artifacts in form of additional stains above and below the main echo compared to the image obtained when using the standard method. Those are the echoes of the edge waves generated by the beam transmitted 30° from the receiving direction. The image created with the second harmonic signals look similar in the case of the standard method or the MLT method. The small ripples that appear above and below the main echo in the case of the second harmonic signal are artifacts from the quasi-linear simulator and are not due to perturbations. The simulator solves the propagation in the frequency domain and ripples appear during the inverse Fourier transform process due to the finite extent of the frequency domain used in the computation.

Fig. 2.8 shows a cut of the planes shown in Fig. 2.7 along the direction where the scatterer is situated (5° from the main propagation axis). It shows the envelope of the signals after beamforming both for the fundamental and the second harmonic signals in the case of the standard method and the MLT method. The echo from the fundamental signal with the MLT method presents perturbations before and after the main echo. Theses perturbations increase the signal level around its maximum by approximately 20 dB bringing it to 50 dB below the maximum amplitude. This explains the stains above and below the main echo on Fig. 2.7. Such perturbations cannot be distinguished for the second harmonic signal.

## 2.5 Experiments

### 2.5.1 Setup

A M5S cardiac probe was connected to a Vivid E9 scanner (GE Vingmed Ultrasound AS, Horten, Norway). The system was modified in our laboratory so that it is possible to record the data received by each element of the probe before beamforming. The beamforming was done separately on a personal computer using MATLAB® (version

2013a, The MathWorks, Natick, MA).

In a first experiment, the target was a nylon wire immersed in GlycoShell Kons.(Norske Shell, Stavanger, Norway) which is a concentrated anti-freezing additive containing more than 90% of monoethylene glycol. The wire is parallel to the elevation direction and placed around 59 mm, while the focus depth was 60 mm. The pulse used consists of 1.5 periods of a square wave convolved with the impulse response of the transducer's elements. The transmitted frequency was 1.67 MHz when imaging with the second harmonic signal, and 3.34 MHz when imaging with the fundamental signal. Despite the theoretical bandwidth of the probe, these frequencies were found to be optimal to maximize the signal to noise ratio and minimize the pulse distortion when imaging with the second harmonic signal. The transmitted amplitude corresponds to a mechanical index in water of approximately 1.5 at 1.67 MHz and 1 at 3.34 MHz.

In a second experiment, the left ventricle of a healthy volunteer was imaged using a similar setup at the fundamental and at the second harmonic frequency and a frame was recorded corresponding to the same time in the cardiac cycle.

### 2.5.2 Results

#### Wire target

The angular sectors imaged with the fundamental signal are shown in Fig. 2.9(a) in the case of a conventional transmit pattern (one pulse in one direction for each transmission) and of the MLT technique. The same images in the case of the second harmonic signal are shown in Fig. 2.10(a). Figs. 2.9(b) and 2.10(b) show a zoom of both figures around the location of the wire target. The beamforming stage uses the delay-and-sum method and a Hanning window is used at reception to limit the effect of the receive crosstalk. In order to visualize the differences more clearly, the difference between the images obtained with and without the MLT technique was computed before envelope compression and displayed in the lower panels with a higher gain. In Figs. 2.9(a) and 2.10(a), we distinguish between the transmit crosstalks (on the right side of the image) appearing around the wire target, and receive crosstalks (on the left side of the image) appearing in the direction of the second transmit beam when the wire target is ensonified. The perturbations amplitude displayed in those figures is normalized to the maximum amplitude of the image obtained without the MLT technique. For the fundamental signal, the perturbations coming from the pulse sent in another direction appear around the main echo from the target when using the MLT technique. They spread around the azimuth 7 mm and cover the depths 56 mm to 63 mm. These perturbations have a lower level for the second harmonic signal and the images obtained with or without using the MLT technique are more similar in this case (Figs. 2.9(b) and 2.10(b)). One can see that the echo from the target has a smaller tail with the second harmonic signal than with the fundamental signal. This is expected as only the parts of the transmitted pulse presenting sufficiently high pressure variations will generate some second harmonic signal.

Fig. 2.11 shows the echo amplitude along the line of the angular sector corresponding to the direction of the wire target with and without using the MLT

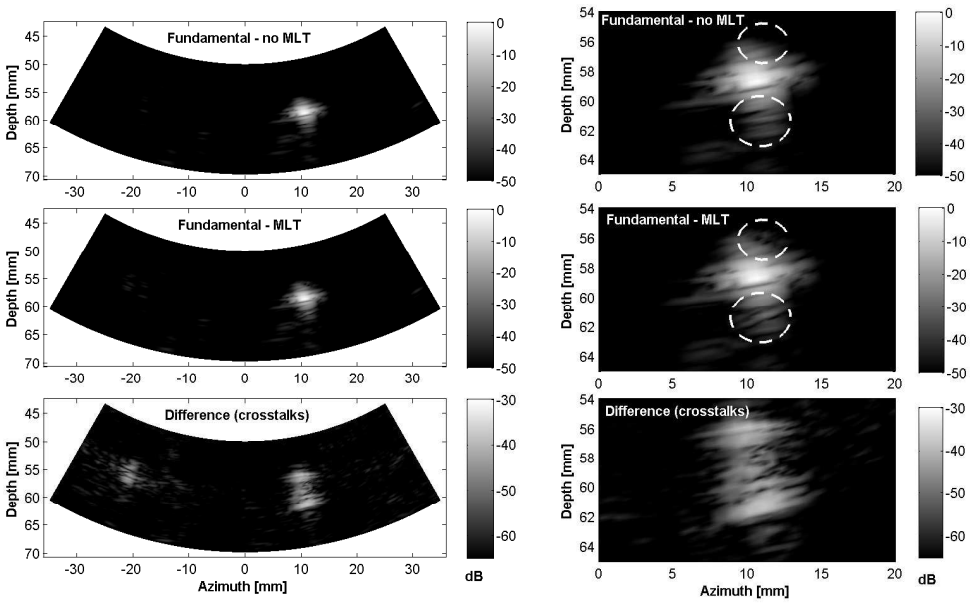


Figure 2.9: Images of a wire target immersed in anti-freezing additive when using the fundamental signal at 3.34 MHz in the case of a conventional transmit pattern (top) and the MLT technique (middle). The difference before envelope detection, i.e. the MLT crosstalks, is displayed in the lower panel. The image on the right is a zoom of the image on the left in the area where the wire target is located. The circles indicate the areas where large difference can be seen.

technique for the fundamental signal (top) and the second harmonic signal (bottom). They also show the amplitude of the perturbing crosstalks normalized to the maximum amplitude of the line obtained without MLT. These perturbations due to the edge waves when using the MLT technique add on to the echo of the pulse transmitted in the direction of the wire target. For the fundamental signal, the amplitude of those perturbations reaches the level of the signal scattered by the wire target at depths below 57 mm and above 62.5 mmm, approximately. At those depths the amplitude of the scattered signal and of the MLT transmit crosstalks is about -40 dB. This means that perturbations due to crosstalk are significant when the scattered signal falls beyond -40 dB around the focus point. In the case of the second harmonic signal, the amplitude of the perturbations reaches the level of the scattered signal around the same depths, but at those depths the amplitude of the scattered signal and of the transmit crosstalks is around -60 dB. This means that when using the second harmonic, the perturbations due to crosstalk are significant only when the signal around focus point has fallen beyond -60 dB.

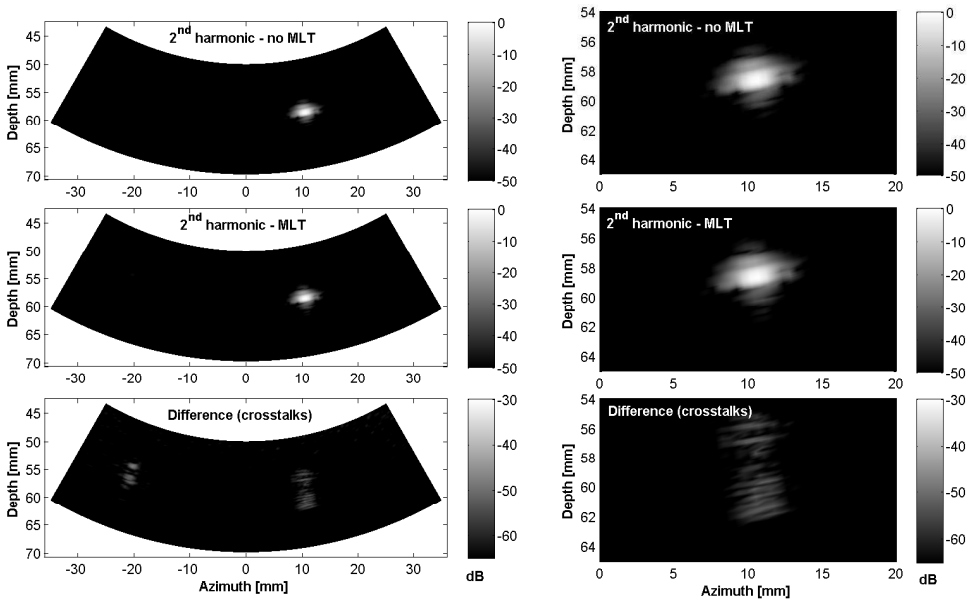


(a) (b)

Figure 2.10: Images of a wire target immersed in anti-freezing additive when using the second harmonic signal at 1.67 MHz in the case of a conventional transmit pattern (top) and the MLT technique (bottom). The difference before envelope detection, i.e. the MLT crosstalks, is displayed in the lower panel. The image on the right is a zoom of the image on the left in the area where the wire target is located.

### Left ventricle

The high contrast between the heart walls and the blood pool of the ventricle provides a situation of choice for observing the perturbations caused by the MLT crosstalks. In the case of the fundamental signal at 3.34 MHz (Fig. 2.12(a)), the interferences between the simultaneous beams result in perturbing crosstalks whose amplitude is over -30 dB when normalized to the maximum amplitude of the image obtained without MLT. When using the MLT technique those perturbations appear as an additional overall noise pattern. Using the second harmonic signal at 1.67 MHz (Fig. 2.13(a)), these artifacts are less pronounced, and the main degradation is caused by the receive crosstalk which could be reduced further using a stronger apodization window during beamforming. In both figures, artifacts resulting from the receive crosstalks are observable on the lower left corner of the images, where the myocardium is reproduced, while transmit crosstalk artifacts can be observed on the lower right part of the image around the myocardium. We distinguish a clear separation between the right and left part of the image (especially visible in the fundamental signal crosstalk image), which is caused by the time gap between the acquisition of last beam of the left side and of

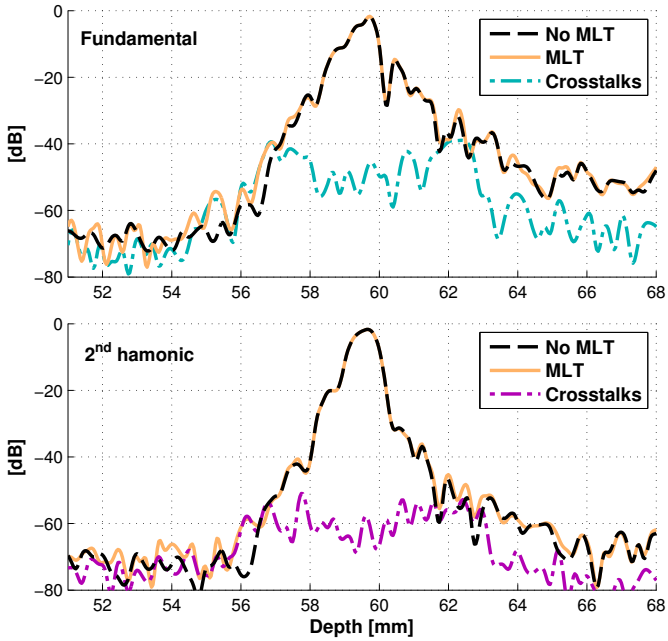


Figure 2.11: (Color online). Axial profile of the signal amplitude in the direction of the wire target after beamforming. The echo amplitude along this line in the case of the MLT technique (solid brown lines), the conventional transmission technique (dashed black lines) and the crosstalks (dash-dotted cyan/magenta lines) are shown for the fundamental (top) and second harmonic (bottom) signals. The amplitude of the crosstalk signals is normalized to the maximum of the amplitude of the line obtained without the MLT technique

the first beam of the right side.

### 2.5.3 Discussions

The simulations and experiments confirmed that the level of perturbations due to transmit crosstalk when using the MLT technique is lower with the second harmonic signal than with the fundamental signal. The amplitude of these perturbing signals is around -40 dB below the maximum amplitude for the fundamental signal and around -60 dB for the second harmonic signal.

In the simulations, around 3 mm away from the focus point, most of the fundamental signal comes from the crosstalk perturbations when using the MLT technique (Fig. 2.8). Its level is around -40 dB compared to the maximum amplitude. This is comparable to the level of the crosstalk signal measured in the experiment with the wire target (Fig. 2.11). At these depths, however, the amplitude of the scattered signal originating from the pulse transmitted in the receiving direction is

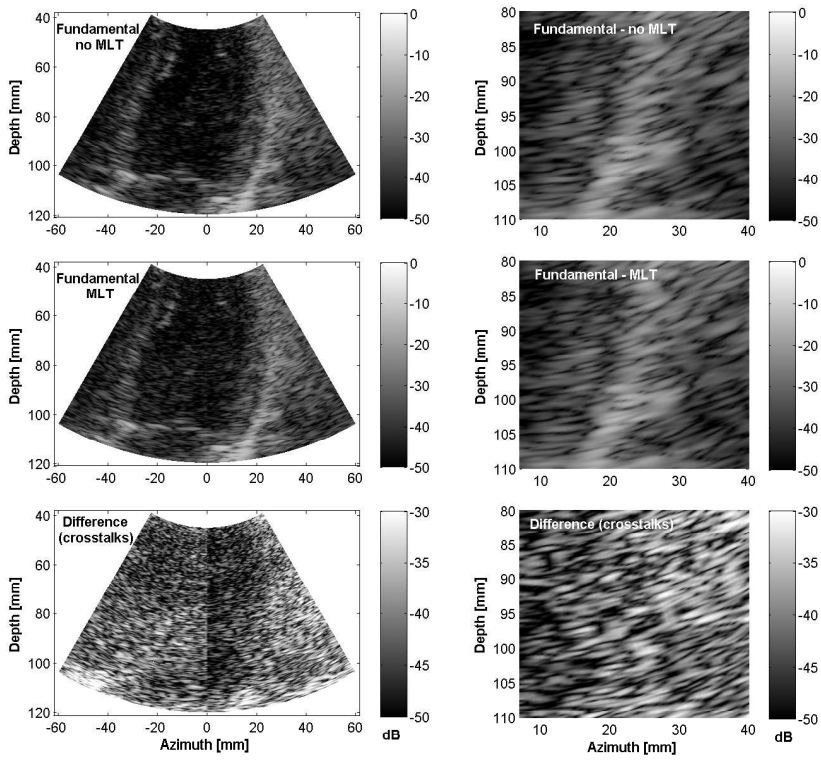


Figure 2.12: Images of the left ventricle of a healthy volunteer when using the fundamental signal at 3.34 MHz in the case of a conventional transmit pattern (top) and the MLT technique (bottom). The difference before envelope detection, i.e. the MLT crosstalks, is displayed in the lower panel. The image on the right is a zoom of the image on the left from the right part of the myocardium.

only around -40 dB below the maximum in the experiment while it is below -80 dB in the simulations. This difference can be explained by a larger spatial extent of the transmitted pulse. Indeed, in the simulations, the impulse response of the transducer is approximated to a Dirac function that does not alter the shape of the received pulse. In the experiments, the impulse response of the transducer of finite bandwidth affects the transmitted pulses and received echoes by spreading them in time. This is visible when comparing the horizontal scales of Figs. 2.8 and 2.11.

Other explanations for the higher amplitude of the received echoes away from focus without using the MLT technique is the fact that the wire is not exactly a point source and that it is not placed exactly at the focus point. Indeed the fluid used being opaque, it was not possible to visually check if the wire was positioned at focus. Additionally there was an uncertainty on the estimated speed of sound in the fluid that could

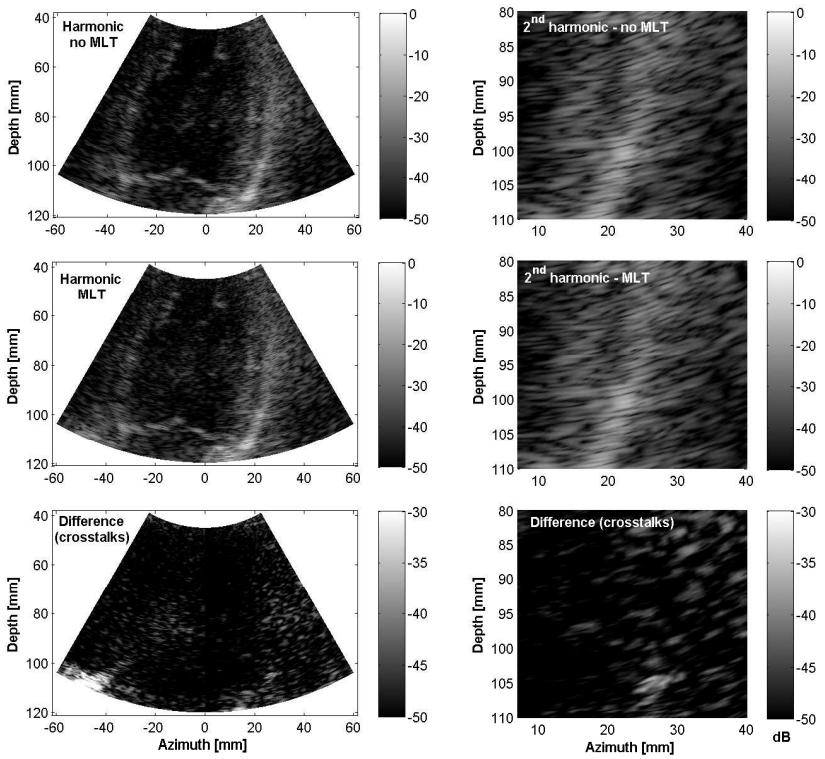


Figure 2.13: Images of the left ventricle of a healthy volunteer when using the second harmonic signal at 1.67 MHz in the case of a conventional transmit pattern (top) and the MLT technique (bottom). The difference before envelope detection, i.e. the MLT crosstalks, is displayed in the lower panel. The image on the right is a zoom of the image on the left from the right part of the myocardium.

impact the focusing of the transmitted pulse. This could explain why the crosstalk perturbations due to the MLT technique are harder to see for the fundamental in the wire target experiment than predicted by the simulations.

Despite this, the variations of the measured perturbations with depth for the fundamental signal are comparable to the results given by the simulations around focus. This appears clearly when comparing Figs. 2.8 and 2.11.

For the second harmonic signal, the measured amplitude of the crosstalk signal is around -60 dB. This is slightly higher than what is observed in the simulations where the echoes with or without using the MLT technique cannot be separated. This could be explained by the leakage of energy coming from the transmitted pulse into the frequency bandwidth surrounding the second harmonic frequency. Indeed, the theoretical level of perturbations for the second harmonic signal at 3.34 MHz is lower

than for the fundamental signal at the same frequency due to the combined effects of lower sidelobe levels and the nonlinear pressure build-up during propagation. If some energy is transmitted in the second harmonic frequency band, it will impact the level of the transmit crosstalk when filtering in this frequency band. In the simulations, the problem of energy leakage into the second harmonic frequency band does not exist because the quasi-linear simulator propagates the fundamental and second harmonic signals as two independent signals.

These results are confirmed by *in vivo* images of the left ventricle on a healthy volunteer. The perturbations caused by the crosstalks when using the MLT technique appear as noise around the cardiac walls and in the ventricle pool for the fundamental signal at 3.34 MHz. Their amplitude goes up to -30 dB below the maximum amplitude recorded in the image formed without using the MLT technique. For the second harmonic signal the level of the perturbations caused by the transmit crosstalk is lowered by 10 to 15 dB reaching -40 to -45 dB below the maximum amplitude recorded. This reduction in the amplitude of the transmit crosstalk is in line with what was observed when imaging the wire target. In this case too, the impact of the perturbing crosstalks is less visible than in the simulations. This could be explained by the presence of speckle. In this configuration, other challenges were highlighted, such as the need for a strong apodization window at reception, as well as an adequate scanning sequence to avoid a large time gap at the center of the image.

## 2.6 Conclusions

Using computer simulations and measurements, we have shown that the perturbations coming from pulses transmitted in different directions when using the MLT technique are lower when the second harmonic signal is used instead of the fundamental signal. These perturbations appear as stains around the main echo of a point target. Their measured level around focus is approximately -40 dB below the maximum amplitude for the fundamental signal, and below -60 dB for the second harmonic signal when imaging a wire target. Both simulations and measurements show a signal level increase around the maximum echo level when using the fundamental signal. This increase is much less noticeable in the case of the second harmonic signal, where the perturbations remain below -60 dB. The second harmonic signal can therefore be used with the MLT technique. In addition to reducing reverberation and clutter level, it reduces the effect of transmit crosstalk compared to the fundamental signal.

The limitations of the method appear when trying to image the very near field. In the vicinity of the transducer, the pulses sent in different directions overlap. In a given transmit direction, the perturbations from pulses transmitted in different directions have a much higher amplitude than farther from the source. In the experiments, the first 2 cm of the image were affected by this effect. The extent of this perturbed near field can be somewhat reduced by increasing the angular separations between beams transmitted simultaneously.

Likewise, the benefit of using the second harmonic signal with the MLT technique is reduced in presence of strong speckle or images with low contrast. Indeed, if the

amplitude dynamic of the image is below 30 dB, crosstalk perturbations with an amplitude 40 dB below the maximum amplitude level, as in the case of the fundamental signal, would have very little impact on the quality of the image. Reducing their level to 60 dB below the maximum level by using the second harmonic would therefore not improve the image quality much.

A future work could consist of combining the multi-line transmission technique with the multi-line acquisition technique. Several broader beams would be transmitted at the same time and several directions within each beam would be acquired improving further the increase in frame rate.

## Acknowledgment

The authors wish to thank GE Vingmed Ultrasound for providing access to a Vivid E9 ultrasound scanner.

# References


[1] D. P. Shattuck, M. D. Weinshenker, S. W. Smith, and O. T. von Ramm, "Explososcan: A parallel processing technique for high speed ultrasound imaging with linear phased arrays," *J. Acoust. Soc. Am.*, vol. 75, pp. 1273–1282, Apr. 1984.

[2] T. Hergum, "Parallel Beamforming in 3D Ultrasound using Synthetic Transmit Beams: a k-space Simulation Approach," Master's thesis, Norwegian University of Science and Technology, Faculty of Natural sciences and Technology, 2004.

[3] J. A. Jensen, S. I. Nikolov, K. L. Gammelmark, and M. H. Pedersen, "Synthetic aperture ultrasound imaging," *Ultrasonics*, vol. 44, pp. e5–e15, Aug. 2006.

[4] J. Lu, "2D and 3D high frame rate imaging with limited diffraction beams," *IEEE Trans. Ultrason. Ferroelectr. Freq. Control*, vol. 44, pp. 839–856, July 1997.

[5] J. Cheng and J. Lu, "Extended high-frame rate imaging method with limited-diffraction beams," *IEEE Trans. Ultrason. Ferroelectr. Freq. Control*, vol. 53, pp. 880–899, May 2006.

[6] G. Montaldo, M. Tanter, J. Bercoff, N. Benech, and M. Fink, "Coherent plane-wave compounding for very high frame rate ultrasonography and transient elastography," *IEEE Trans. Ultrason. Ferroelectr. Freq. Control*, vol. 56, pp. 489–506, Mar. 2009.

[7] J. Shen and E. S. Ebbini, "A new coded-excitation ultrasound imaging system−Part I: basic principles," *IEEE Trans. Ultrason. Ferroelectr. Freq. Control*, vol. 43, pp. 131–140, Jan. 1996.

[8] J. Shen and E. S. Ebbini, "A new coded-excitation ultrasound imaging system−Part II: operator design," *IEEE Trans. Ultrason. Ferroelectr. Freq. Control*, vol. 43, pp. 141–148, Jan. 1996.

[9] L. Demi, M. D. Verweij, and K. W. A. Van Dongen, "Parallel transmit beamforming using orthogonal frequency division multiplexing applied to harmonic imaging - A feasibility study," *IEEE Trans. Ultrason. Ferroelectr. Freq. Control*, vol. 59, pp. 2439–2447, Nov. 2012.

[10] K. E. Thomenius and S. D. Silverstein, "Method and apparatus for high-frame-rate high-resolution ultrasonic image data acquisition," May 23 2000. US patent 6,066,099.

[11] D. T. Dubberstein and O. T. Von Ramm, "Methods and systems for ultrasound scanning using spatially and spectrally separated transmit ultrasound beams," Dec. 12 2000. US Patent 6,159,153.

[12] T. A. Whittingham, "New and future developments in ultrasonic imaging," *Br. J. Radiol.*, vol. 70, pp. 119–132, Nov. 1997.

[13] A. Drukarev, K. Konstantinides, and G. Seroussi, "Beam transformation techinques for ultrasonic medical imaging," *IEEE Trans. Ultrason. Ferroelectr. Freq. Control*, vol. 40, pp. 717–726, Nov. 1993.

[14] F. A. Duck, "Nonlinear acoustics in diagnostic ultrasound," *Ultrasound Med. Biol.*, vol. 28, no. 1, pp. 1–18, 2002.

[15] L. Tong, H. Gao, H. F. Choi, and J. D'hooge, "Multi-transmit beam forming for fast cardiac imaging," in *Proc. IEEE Ultrason. Symp. 2011*, (Orlando, FA), pp. 140–143, 2011.

[16] R. J. Fedewa, K. D. Wallace, M. R. Holland, J. R. Jago, G. C. Ng, M. R. Rielly, B. S. Robinson, and J. G. Miller, "Effect of changing the transmit aperture on the spatial coherence of backscatter for the nonlinearly generated second harmonic," in *Proc. IEEE Ultrason. Symp. 2002*, vol. 2, (Munich, Germany), pp. 1665–1668, 2002.

[17] T. Varslot and G. Taraldsen, "Computer simulation of forward wave propagation in soft tissue," *IEEE Trans. Ultrason. Ferroelectr. Freq. Control*, vol. 52, pp. 1473–1482, Sept. 2005.

[18] T. Varslot and S. E. Måsøy, "Forward propagation of acoustic pressure pulses in 3D soft biological tissue," *Model. Identif. Contr.*, vol. 27, pp. 181–200, July 2006.

[19] M. E. Frijlink, H. Kaupang, T. Varslot, and S. E. Måsøy, "Abersim: A simulation program for 3D nonlinear acoustic wave propagation for arbitrary pulses and arbitrary transducer geometries," in *Proc. IEEE Ultrason. Symp. 2008*, (Beijing, China), pp. 1282–1285, Nov. 2008.

[20] H. Torp, T. F. Johansen, and J. S. Haugen, "Nonlinear wave propagation - a fast 3D simulation method based on quasi-linear approximation of the second harmonic field," in *Proc. IEEE Ultrason. Symp. 2002*, vol. 1, (Munich, Germany), pp. 567–570, Oct. 2002.

[21] F. Prieur, T. F. Johansen, S. Holm, and H. Torp, "Fast simulation of second harmonic ultrasound field using a quasi-linear method," *J. Acoust. Soc. Am.*, vol. 131, pp. 4365–4375, June 2012.

# Chapter 3

# Multi-Line Transmission in 3-D with Reduced Cross-Talk Artifacts: a Proof of Concept Study

Bastien Dénarié[1], Tore Bjåstad[2] and Hans Torp[1]
[1]MI-Lab, Department of Circulation and Medical Imaging, Faculty of Medicine, Norwegian University of Science and Technology (NTNU)
[2]GE Vingmed Ultrasound AS, Horten, Norway

Multi-Line Transmission (MLT) is a technique where ultrasound pulses for several directions are transmitted simultaneously. The purpose is increased framerate, which is especially important in 3-D echocardiography. Compared to techniques purely based on parallel beamformation, MLT avoids the need for reducing the transmit aperture and thus maintains a high harmonic signal level. The main disadvantage is artifacts caused by cross-talk between the simultaneous beams.

In a conventional MLT implementation, simultaneous transmits would be spaced regularly in the azimuth and elevation planes. However, using rectangular geometry arrays, most of the acoustic side-lobe energy is concentrated along these planes. The results in this work show that the cross-talks can be pushed below the typical display range of 50 dB used in cardiac applications if the parallel transmit directions are aligned along the transverse diagonal of the array. Dispositions with 2 to 5 MLT for a typical cardiac 2-D phased-array were investigated using Field II. Using the proposed alignment, the maximal cross-talk artifact amplitudes decreased 20 dB to 30 dB compared to conventional MLT dispositions. In water-tank measurements, side-lobes levels of a commercially available rectangular probe were 15 dB to 25 dB lower along the transverse diagonal, confirming that similar suppressions can be expected using actual transducers.

## 3.1 Introduction

Over the last decade, advances in technology have made 3-D ultrasound imaging an accessible modality for establishing medical diagnostics. But despite its potential, three dimensional imaging of the heart has not been adopted fully by the clinicians due to the inherent trade-off between image quality and framerate [1].

Imaging a 3-D sector requires squaring the number of pulses transmitted into the body to keep the image quality of conventional 2-D ultrasound. While the heart kinematics contains components higher than 100 Hz, most of the pathologies can today be diagnosed with a framerate of 50 Hz [2, 3]. Hence, a clinician might prefer a $75 \times 75$ degrees sector at 50 Hz, however, current systems cannot capture more than approximately $60 \times 15$ degrees at a real-time minimum of 20 frames per second in good quality.

Several techniques have been proposed to keep a high framerate while maintaining the resolution and contrast of 2-D echography. Sub-volumes of data can be acquired over several heart cycles and stitched together using the ECG information to recreate a full volumetric image of the heart [4]. Although this technique is available on today's scanners, it is often affected by various distortions in the image due to the fusion of different datasets.

Parallel acquisition systems where several narrow receive beams are formed in parallel have been proposed [5]. To achieve increased frame rates using such systems, the transmit beam width must be increased. The broadness of the transmitted beam can be easily controlled by varying the size of the transmit aperture, but according to the Fresnel zone for a phased array this has an impact on how deep we can focus, as well as a direct limitation on the level of energy transferred into the body. Second harmonic imaging brought a non-negligible improvement in echocardiography [6], and the pressure level required for the nonlinear effects to appear in tissue cannot be associated with a too broad beam. Therefore, the transmitted beam must be narrow enough and the number of parallel beams is in practice often limited.

Coherent plane wave compounding has been demonstrated as an efficient way to increase the framerate without significant losses in image quality for applications where linear array transducers can be used [7]. In a similar way, it has been proposed to use diverging waves emanating from a virtual point source behind the surface of the transducer to cover an imaging sector appropriate for phased-array imaging at a very high framerate [8]. Despite its ingenuity, the use of defocused waves results in a poor image quality because of the wide lateral spreading of the transmitted energy. Such techniques will generally present high side-lobes and will not be able to generate second harmonics [9]. In addition, motion within the field of view such as observed in echocardiography will result in destructive interferences during the compounding operation, also known as motion artifacts [10, 11].

In order to increase the framerate while keeping the advantages of harmonic imaging, it has been proposed to transmit simultaneously two ultrasound pulses focused along different steering directions [12–14]. A straightforward extension, known as Multi-Line Transmission (MLT), is to transmit a higher number of beams, with a gain in framerate equal to the number of parallel beams. But even with an electric

circuitry supporting the transmission of several simultaneous pulses, the interactions between the ultrasound fields on transmit as well as on receive generated non negligible cross-talk artifacts [15].

In order to reduce MLT cross-talk artifacts, several options were proposed. One could use different frequency bands for each transmitted beams [16, 17], use techniques such as pulse inversion to cancel the effects of the other transmit directions [18], or modulate the apodization of the transmitted and received beams so that the direction of the main-lobes of the beams of interest corresponded to direction of the zeros in the side-lobe patterns of the other beams [19]. Unfortunately, none of these methods were proven successful in removing the cross-talk artifacts from the field of view without negatively impacting on the time or spatial resolution of the system.

In this work, we propose a new approach for multi-line transmission, getting rid of the cross-talk artifacts in the visible range, and allowing MLT to be effectively used in 3-D echocardiographic applications. By aligning the simultaneously transmitted beams along what we introduce as the transverse diagonal of the transducer, one can reduce the cross-talks without impact on the system resolution. After a theoretical description of the cross-talk artifacts appearing using MLT, we discuss how we can take advantage of the transducer geometry to choose a disposition of the MLT resulting in highly reduced cross-talk levels. Then we investigate the pressure field of a transducer in order to verify the practical validity of our approach. Finally, we conduct simulations to determine how the number of parallel transmit-lines will influence the amplitude of the cross-talk artifacts, when using both conventional MLT dispositions and our proposed alignment along the transverse diagonal of the transducer.

## 3.2 Multi-Lines Transmission

### 3.2.1 Implementation

Transmitting simultaneously several pulses requires a complex implementation. Several approaches have been experimented: one may use several transducers, or split the aperture of a single transducer into several subsets of elements, each transmitting one of the beams [20]. All of these approaches have a simple implementation from an electronic point of view, but will lead to beams which have different origins or different pitch, causing severe artifacts in the propagating pressure fields.

In this article, we will consider that we use a single transducer with a multitude of signal generators. The signals from each generator will be delayed independently to steer the beam in the desired direction, before all the signals are summed together. The final signal is then transferred to the transducer array elements, as depicted on Fig. 3.1 for a situation with 2 parallel transmits. Such an implementation avoids the generation of undesired artifacts in the transmitted pressure field.

In this work, MLT is used to refer to either one of the parallel transmit beams, or an imaging system using multiple parallel transmissions (as opposed to Single Line Transmission, SLT).

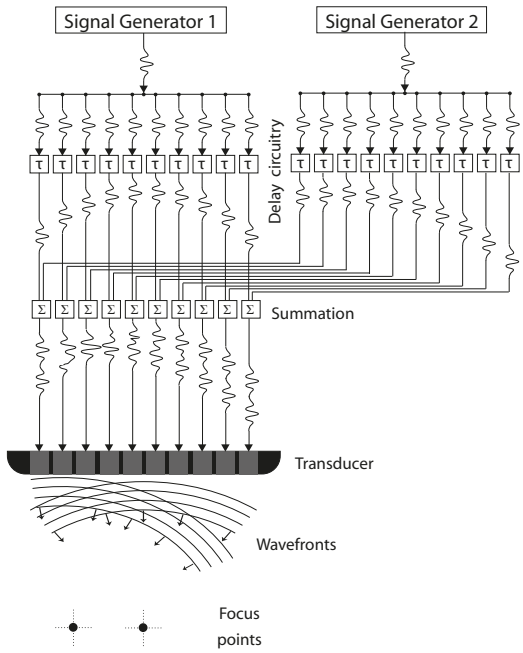


Figure 3.1: Implementation of a 2 MLT ultrasound system. Two signals are generated and pre-focused using an independent circuitry before being summed and sent to a 1-D phased-array probe, generating the simultaneous transmission of two focused ultrasound beams.

### 3.2.2 Scan Sequencing

On receive, parallel acquisition is done to generate the desired number of receive beams around the transmit directions. The scan sector is then typically divided in sub-zones, and each of the transmit lines will cover one of the zones independently, as illustrated in Fig. 3.2 (a).

In the presence of motion in the imaged medium, an artifact may appear in between each of these zones, due to the long time interval between the transmission of the first beam (on the left hand side of each zone) and the transmission of the last beam (on the right hand side of each zone). In order to avoid this artifact, it has been proposed [21] to transmit alternatively the pulses at the left and the right part of each zone, scanning towards the inside of each zone as illustrated in Fig. 3.2 (b). Using such an alternated scan sequencing, the maximum delay between two adjacent receive directions will be reduced to two times the pulse repetition time (PRT).

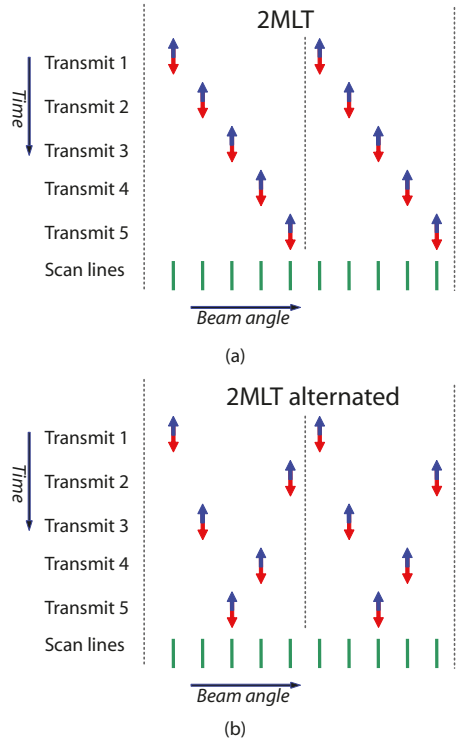


Figure 3.2: Illustration of simple scan sequencing scenarios using multiple line transmission, MLT. In these situations, only one receive beam is generated for each transmit. The scan direction of each transmit line goes from left to right of each sub-zone in (a), while it goes alternatively towards the center of each sub-zone in (b) to limit artifacts at the edge of each zone in case of motion of the imaged object.

### 3.2.3 Cross-talk Artifacts

The major disadvantage of using the MLT technique is the artifacts resulting from the interaction between the different simultaneous beams; the so called cross-talk artifacts. We can separate these cross-talks in three categories, also illustrated in Fig. 3.3:

- *Transmit cross-talk*: energy from the side-lobes of a definite transmit beam that is picked up in the main-lobe of a receive beam focused in a different direction.
- *Receive cross-talk*: energy from the main-lobe of a definite transmit beam that is picked up in the side-lobes of a receive beam focused in a different direction.
- *Two-ways cross-talk*: energy from the side-lobes of a definite transmit beam that is picked up in the side-lobes of a receive beam focused in a different direction.

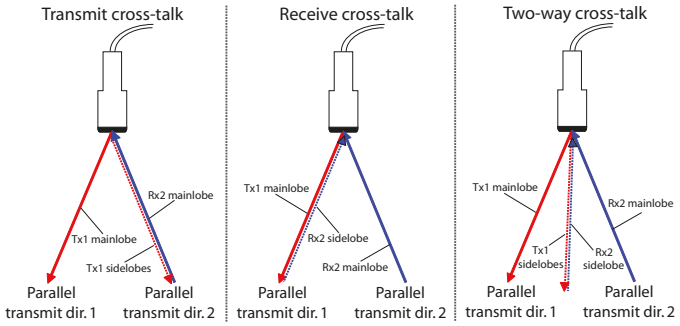


Figure 3.3: Illustration of MLT cross-talks. Parallel transmit beams are named Tx1 and Tx2, while the corresponding receive beams are named Rx1 and Rx2.

The effects of the transmit and receive cross-talks can be easily visualized from imaging a single point scatterer, as shown in Fig. 3.4 for a 2 MLT system. Transmit cross-talks will appear as two point reflections above and below the object of interest, while receive cross-talks will appear as two points in the directions where the other transmit beams were located when the scatterer was hit.

These two additional points can be explained by the fact that the side-lobes of a typical beam are usually mainly constituted by two successive edge waves. Cross-talk artifacts are then mainly echoes caused by the interaction between the edge waves and main lobes of simultaneous transmit and receive beams. Edge waves are caused by the limited physical size of the aperture: since the transducer size is not infinite, there is nothing to cancel the outermost components of the propagating pressure field, resulting in waves which seem to originate from the outermost parts of the aperture. Consequently, edge waves propagate in parallel with the borders of the transducer, i.e. around the azimuth and elevation planes. As we shall see later, this observation is of major importance for the rest of this study.

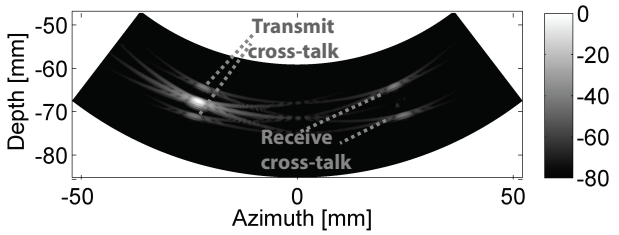


Figure 3.4: Cross-talks appearing when imaging a single point scatterer using a 2 MLT system. Both transmit and receive cross-talks are clearly visible using a high dynamic display range (80 dB).

While a typical order of magnitude for transmit and receive cross-talks is around $-35/40$ dB, the amplitude of the so-called two-way cross-talk is usually much lower,

below $-60\,\mathrm{dB}$, making them invisible in a B-mode image.

It is obvious that the amount of cross-talks will depend on different factors. The location and amount of side-lobes of transmit and receive beams can be adjusted by e.g. apodization or use of second harmonic imaging [15, 22]. A typical ultrasound system implements dynamic receive apodization and will therefore be able to limit the receive cross-talks. The distance between the parallel transmit directions will also influence the amount of cross-talks, and a rule of thumb would be to separate the parallel transmit directions as much as possible. Other techniques can be used to limit the interaction between the different beams, such as differentiating the different beams with different frequency bands or coded excitation [17, 23], or combining several transmits in a pulse inversion scheme [18].

In this study, we will consider that the cross-talks are invisible if they can be reduced at a level below $-50\,\mathrm{dB}$. Typical cardiac imaging scanners operate with a dynamic display range of $40-45\,\mathrm{dB}$, and therefore we can ensure that the artifacts will be invisible if they are below or close to $-50\,\mathrm{dB}$. The measure we will use to evaluate this level is the maximum of the envelope of the received pulse, which is suited for cardiac applications where strong scatterers in the pericardium contrast with a low amplitude blood pool in the ventricles. In order to maximize the framerate, we will typically want to use a high number of parallel transmit lines, and therefore reduce the distance between the simultaneous transmits to the minimum acceptable. In addition, we will not use any apodization. We can hence consider that our study consists in a worst case scenario, and levels of cross-talks which are considered as invisible here can be even more attenuated using apodization on both transmit and/or receive.

## 3.3 A New Approach For Multi-Lines Transmission in 3-D

### 3.3.1 Taking Advantage of the Transducer Rectangular Geometry

Applying the Fraunhofer approximation, it can be shown that a transducer array transmitting a focused beam will radiate in the focal plane a pressure field proportional to the Fourier transform of the aperture [24]. A short and widely used derivate of this observation is that the pressure field radiated by a rectangular transducer will have the shape of a *sinc* function in the focal plane. If we now consider the focal plane as a full 2-D plane parallel to the transducer surface, one can expect to observe such *sinc* profiles along both the azimuth and elevation axes. Within the hypothesis of a linear propagation, the total pressure field will indeed result from the two-dimensional spatial convolution between the *sinc* profiles located along the azimuth and elevation axes; thereby forming a cross-shaped pressure field, as schemed in Fig. 3.5.

As explained above, the main source of artifacts using MLT were the transmit- and receive-cross-talks; a direct result from the interaction of one main-lobe with the side-lobes of other beams. By considering the field in the focal plane, we can see that the main-lobe/side-lobe interactions can be avoided if we place the other

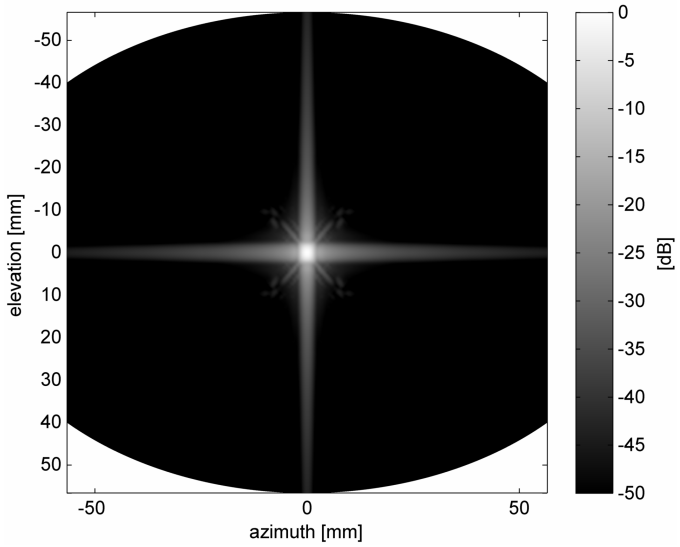


Figure 3.5: Illustration of the pressure field transmitted by a rectangular phased-array probe in the focal plane generated using Field II. The energy is concentrated along the azimuth ($y = 0$) and elevation ($x = 0$) planes. The profile was obtained by taking the maximum of the envelope of the pressure pulse at each location.

transmit directions in the areas which are not covered by the pressure field, i.e. away from the "cross". A common measure of the width of the pressure field in azimuth and/or elevation is given by $\lambda \cdot F_{\#}$, where the F-number $F_{\#} = F/A$ is defined by the focal depth $F$ and the aperture size $A$. It means that, as a rule of thumb, the thickness of the "cross" edges along the azimuth and elevation planes are inversely proportional to the aperture size of the transducer respectively in the azimuth and elevation directions. A good choice would hence be to place the different transmits along the line perpendicular with one of the diagonals of the transducer, the so called transverse diagonal depicted in Fig. 3.6. This would result in a situation where the overlap between the transmitted beams is limited to side-lobes/side-lobes interactions, and where we could expect the cross-talk artifacts to be below a visible threshold.

One of the advantages of this principle is that it will be valid for both transmit and receive beams, reducing both types of cross-talks.

### 3.3.2 Proposed 3-D Scan Sequence

Taking advantage of the previous observations, we have developed a special scan sequence adapted to a full volume acquisition with a large number of simultaneous transmit beams, as depicted in Fig. 3.7.

The 3-D imaging sector is tilted around the z-axis compared to conventional acquisition sequences, and is divided in sub-zones. Each sub-zone is covered by one of

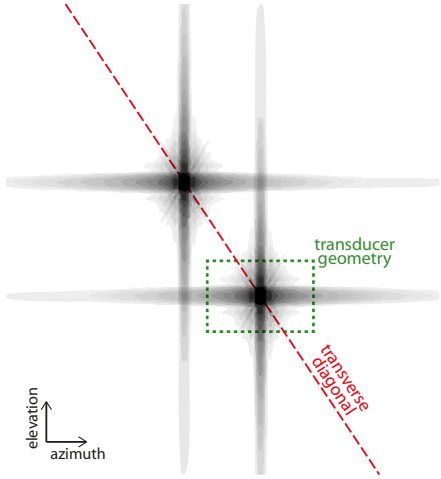


Figure 3.6: Aligning the transmit directions along the transverse diagonal of the transducer, as depicted in (a), will reduce the interaction between the simultaneous transmit pulses to a minimum as shown in (b).

the parallel transmit lines. The parallel transmit lines are aligned along the transverse diagonal of the transducer geometry so that there is no direct interaction between the main-lobes and the side-lobes of the different simultaneous transmit beams.

Instead of scanning along the azimuth plane, the successive transmits will be fired in the planes perpendicular to the chosen transverse diagonal of the transducer (i.e. along one of the diagonal of the transducer). Each sub-zone is then covered by the acquisition of several planes in an alternated pattern, so that the acquisition tends to the center of the zones, avoiding the artifacts explained in chapter 3.2.2.

The proposed scan sequence allows the acquisition of large 3-D sectors, while using focused and narrow beams in transmission.

## 3.4 Material and Methods

### 3.4.1 Cross-talk Evaluation

The three types of cross-talks presented in chapter 3.2.3 can all be described as the result of the interaction between one receive beam and the transmitted energy which differs from a normal SLT situation. Let us call $\theta_i, i \in [1, N]$, the steering angles of the $N$ parallel transmits. The cross-talks response in the receive direction $\theta_k$ can be expressed as the difference between the two-way response of a MLT transmission and regular SLT transmission:

$$A_{xt}\left(\theta_k, \vec{r}, t\right) = h\left(\theta_{1\ldots N}|\theta_k, \vec{r}, t\right) - h\left(\theta_k|\theta_k, \vec{r}, t\right),$$

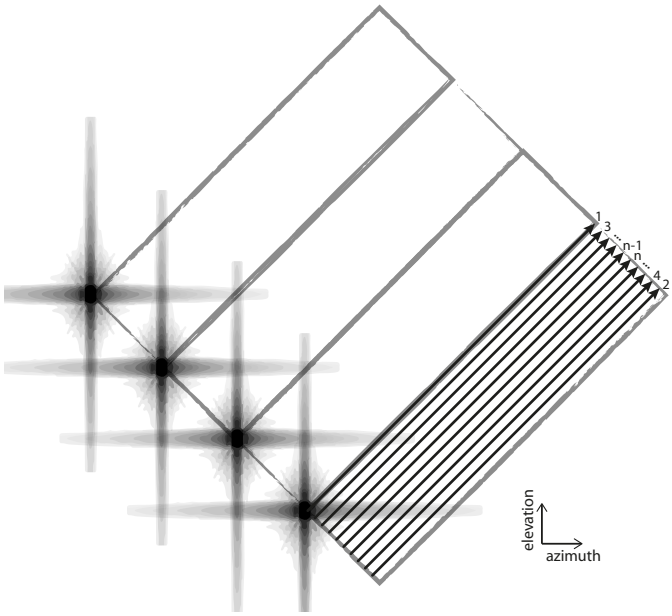


Figure 3.7: Illustration of the proposed scan pattern (here with 4 MLT). The parallel transmits are placed on the transverse diagonal defined by the transducer geometry, and the imaging sector shape will be tilted compared to the classical azimuth/elevation shape. Each transmit beam will cover its sub-zone, scanning plane by plane, while each second plane is alternated to scan towards the center of the zone.

where $h\left(\theta_{i\ldots j}|\theta_k, \vec{r}, t\right)$ is the two-way response where the transmit beams are fired in the directions $\theta_i$ to $\theta_j$ and where the receive beam is steered along the direction $\theta_k$. These functions are evaluated at the position $\vec{r}$ and at time $t$.

In order to evaluate the power of these cross-talks in decibels $A_{xt}^{dB}$ compared to the scattering of tissue in the direction of interest $\theta_k$, we just need to normalize the previous difference as:

$$A_{xt}^{norm}\left(\theta_k, \vec{r}\right) = \frac{\text{maxenv}\left\{A_{xt}\left(\theta_k, \vec{r}, t\right)\right\}}{\text{maxenv}\left\{h\left(\theta_k|\theta_k, \vec{r}, t\right)\right\}},$$

$$A_{xt}^{dB}\left(\theta_k, \vec{r}\right) = 20 \cdot \log_{10}\left[A_{xt}^{norm}\left(\theta_k, \vec{r}\right)\right], \tag{3.1}$$

The function maxenv $\{x\}$ is the maximum of the envelope and was computed taking the maximum of the absolute value of the Hilbert transform of $x$.

This principle is illustrated in Fig. 3.8 for a simple situation with 2 MLT aligned in the azimuth plane steered at angles $\theta_1$ and $\theta_2$. The two-way response of the system when transmitting two beams simultaneously and receiving in the leftmost direction $\theta_1$ is presented in Fig. 3.8 (a). This beam profile contains both the normal response of the system (Fig. 3.8 (b), with transmit and receive beams are both steered at $\theta_1$),

and the cross-talks response (Fig. 3.8 (c)) which is computed from the subtraction of the two-way responses of the two previous profiles.

In this simple situation, one can easily distinguish the transmit cross-talk (located on the left of Fig. 3.8 (c)) from the receive cross-talk (located on the right part). Both these cross-talks vary with depth, with maximum of amplitudes located at the steering directions. In a case where the transmit beams are not aligned within the same plane, the strongest interactions will happen in each of the crossings between the side-lobes of the beams.

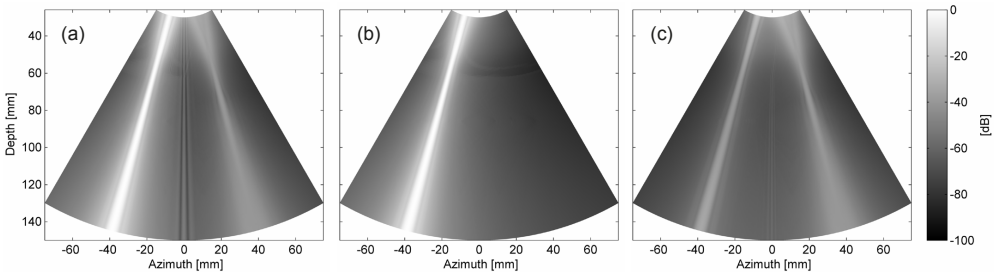


Figure 3.8: Two-way beam profiles for a 2MLT system. (a) Both beams are transmitted simultaneously and reception is only done in the leftmost direction. (b) Only the leftmost beam is transmitted while reception is along the leftmost direction. (c) Only the rightmost beam is transmitted while reception is along the leftmost direction. All the beam profiles are normalized so that the SLT system response in the direction of the receive beam (b) is constant with depth.

In the remainder of this work, we will measure the amplitude of the cross-talks using equation (3.1). This measure will be normalized at each depth, so that we get a cross-talk estimate that corresponds to the amplitude of the artifacts appearing in a time-gain-compensated (TGC) B-mode image.

Using phased arrays, we can expect a wider main-lobe and higher side-lobes for large steering angles due to smaller effective aperture. Therefore, the cross-talks are estimated for all the receive directions corresponding to all the transmit directions, so that we have an estimate of the worst case scenario.

### 3.4.2 Transmit Pressure Evaluation

In order to validate the shape of the transmitted pressure field of a rectangular transducer in the focal plane, water tank experiments were conducted.

The pressure field of a M5S cardiac probe (GE Vingmed Ultrasound AS, Horten, Norway) was recorded in the plane corresponding to the depth $z = 80\,\text{mm}$, which is an approximate to the focal plane (the plane at a distance $r = 80\,\text{mm}$ from the center of the probe). The transmit pressure field was characterized in a water tank using a Onda HGL-0200 hydrophone with a tip diameter of 200 µm connected to a Onda AH-2020 20 dB-preamplifier (Onda, Sunnyvale, CA, USA), and attached to a Physik xyz translation stage robot (Physik Instrumente PI GmbH & Co. KG, Karlsruhe,

Table 3.1: Setup parameters used with the 2-D cardiac probe

| | |
|---|---|
| Active aperture size (az × el) | 22 × 13 mm |
| Pulse center frequency | 2.5 MHz |
| Pulse length | 2 periods |
| Transmit focus | 80 mm |
| Transmit apodization | none |
| Propagation medium | water (T = 22.4°C) |

Germany). The probe was covered with a thin layer of ultrasound gel and wrapped into a plastic foil for waterproofing, before the probe surface was submerged in water. In order to reduce the high noise level in the water-tank, the temporal response of 128 pulse occurrences were registered and averaged at each plane position. The pressure fields are presented using the maximum of the envelope (max. peak) of these datasets. Details about the probe geometry and the scanner configuration can be found in Table 3.1.

The pressure field of the same probe and setup was simulated using Field II [25, 26]. The impulse response of the transducer elements was previously recorded in a water tank and fed through the simulation environment.

### 3.4.3 Cross-talk Simulations for MLT Scan Sequences

The cross-talk amplitudes were evaluated according to equation (3.1) by simulating a combination of two-way responses. These two-way responses were generated for a 2-D phased-array probe using Field II.

The transducer dimensions were chosen to match the overall geometry of a real 3-D cardiac probe. Details about the probe geometry and the setup configuration can be found in Table 3.2.

In order to investigate the advantages of the proposed 3-D MLT scan sequence, we chose to simulate a wide set of dispositions for the simultaneously transmitted beams, as illustrated in Fig. 3.9. Conventional MLT spatial configurations were chosen (first row) as a benchmark to compare with the proposed MLT spatial configurations (second row). More specifically, they were chosen in order to highlight the amplitude of the cross-talks when using:

- **1-A**: 2 MLT aligned in the azimuth direction.
- **1-B**: 2 MLT aligned in the elevation direction. Here the side-lobes should be expected to be higher than in 1-A due to a smaller aperture, leading to more intense artifacts.
- **1-C**: 3 MLT aligned in the azimuth direction.

Table 3.2: Setup parameters used with the 3-D cardiac probe

| | |
|---|---|
| Number of elements (az × el) | 120 × 96 mm |
| Aperture size (az × el) | 20.5 × 16.4 mm |
| Pulse center frequency | 2.5 MHz |
| Pulse length | 2 periods |
| Transmit focus | 80 mm |
| Receive focus | dynamic |
| Transmit apodization | none |
| Receive apodization | none (growing aperture) |
| Transmit $F_{\#}$ (az × el) | 3.9 × 4.6 |
| Receive $F_{\#}$ (az × el) | 2.5 × 2.5<br>until depth 51 mm, then increasing |

- **1-D**: 4 MLT aligned in a grid pattern in both azimuth and elevation directions. This is the direct evolution from disposition 1-A if we want to add more MLT without increasing the artifacts more than in 1-C.

- **2-A to 2-D**: 2 to 5 MLT aligned along the transverse diagonal of the transducer geometry, as proposed in this study. This will allow a choice between the gain in framerate and the influence of cross-talks.

The dispositions were all adapted to cover a $90 \times 90$ degree 3-D sector. The angular separations between the transmit beams for each spatial disposition can be found in Table 3.3.

All the simulations results were estimated on the spherical surfaces with origin at the center of the transducer and with a radius of 40 mm, 80 mm (the transmit focal length), and 120 mm. The beam profiles were obtained by taking the maximum of the temporal envelope of the pressure field at each location.

As mentioned previously, steering at higher angles will give a generally higher level of side-lobes, and therefore we can expect more intense cross-talks between the MLT depending on the directions of the beams. In this study, we found for each of the dispositions 1-A to 2-D the combination of the steering angle of the MLT group and the receive beam direction that generated the most intense cross-talk artifacts, within the boundary of a 3-D sector of $90 \times 90$ deg. In this way, we ended up with a worst-case evaluation of the cross-talks amplitude.

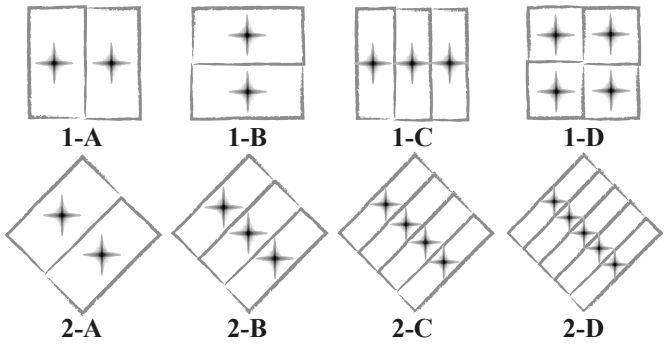


Figure 3.9: Illustration of the different MLT spatial configurations used for cross-talk estimation. Conventional MLT dispositions for up to 4 parallel transmit beams are represented by dispositions 1 (A-D). The proposed scan sequences with the MLT aligned on the transverse diagonal of the transducer are represented in dispositions 2 (A-D).

Table 3.3: Angular separations between the different transmit directions for the simulated spatial dispositions

| | **Azimuth [deg]** | **Elevation [deg]** |
|---|---|---|
| **1-A** | 45 | 0 |
| **1-B** | 0 | 45 |
| **1-C** | 30 | 0 |
| **1-D** | 45 | 45 |
| | **Along the transverse diagonal [deg]** | |
| **2-A** | 45 | |
| **2-B** | 30 | |
| **2-C** | 22.5 | |
| **2-D** | 18 | |

## 3.5 Results

### 3.5.1 Water-tank Measurements

The measured and simulated pressure fields transmitted using the M5S probe in the plane corresponding to depth $z = 80\,\text{mm}$ are both presented in Fig. 3.10 (a) and (b). In addition, cuts along the azimuth axis, elevation axis, and one of the transverse diagonal (represented as a white dashed line in Fig. 3.10 (a)) are displayed in Fig. 3.10 (c) and (d). We observe that the pressure profiles are roughly similar until $-40\,\text{dB}$, and with a higher level of perturbations in the water-tank experiment. The transmitted pressure

is gathered around the azimuth and elevation axes as expected.

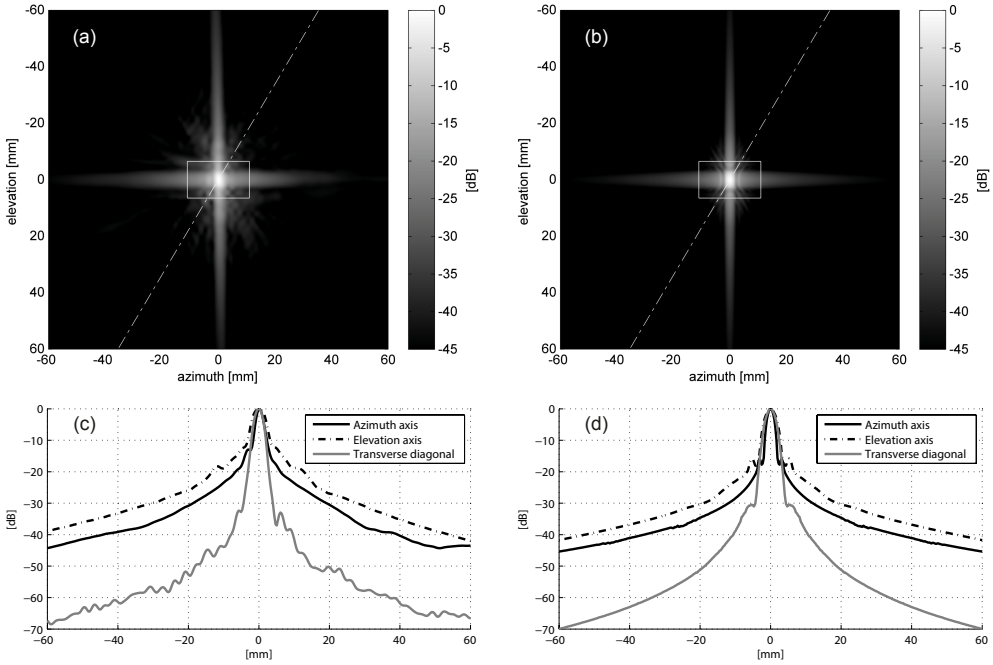


Figure 3.10: Transmit pressure field (max. peak) of a M5S probe measured in a water tank (a) and simulated (b) at a depth z = 80 mm. Cuts are presented for both measurements (c) and simulations (d).

### 3.5.2 Simulations

The amplitude of the MLT cross-talks was evaluated according to equation (3.1) for all the geometrical dispositions 1-A to 2-D at depths 40 mm, 80 mm and 120 mm, and the worst-case amplitude of these artifacts is displayed in Fig. 3.11. An example comparison of these cross-talk profiles can be shown for illustration purpose for the 3 MLT situations 1-C and 2-B in Fig. 3.12, where no additional steering is given in transmit and where the receive beam is chosen to be steered in the centermost transmit direction. Fig.3.11 is built by taking the maximum values of the envelope profiles such as the ones presented in Fig. 3.12.

We can see in Fig. 3.11 that the cross-talks from conventional MLT dispositions 1-A to 1-D are more pronounced than when the MLT are aligned along the transverse diagonal of the transducer geometry. Except for near field, the artifact levels in dispositions 2-A to 2-D are under the visibility threshold of a 50 dB display range.

It is interesting to notice that the level of cross-talks depends on the depth. The maximum amplitude of the cross-talk artifacts are about 10 dB higher in the near-field

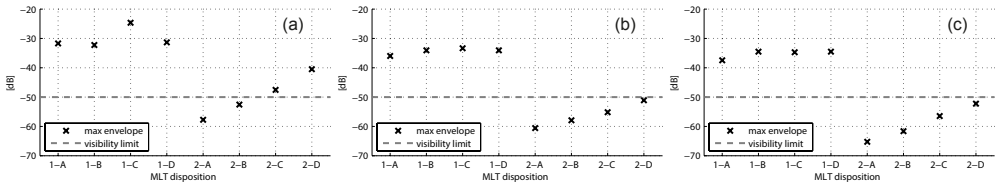


Figure 3.11: Maximum amplitude of the MLT cross-talks for the different MLT dispositions 1-A to 2-D. The artifacts amplitude is calculated in three planes corresponding to a distance 40 mm (a), 80 mm (b) and 120 mm (c) from the center of the transducer. The maximum amplitude is found by choosing the steering angle on transmit and the receive beam that maximize the artifacts. The −50 dB visibility limit corresponds to the dynamic display range typically present in cardiac imaging.

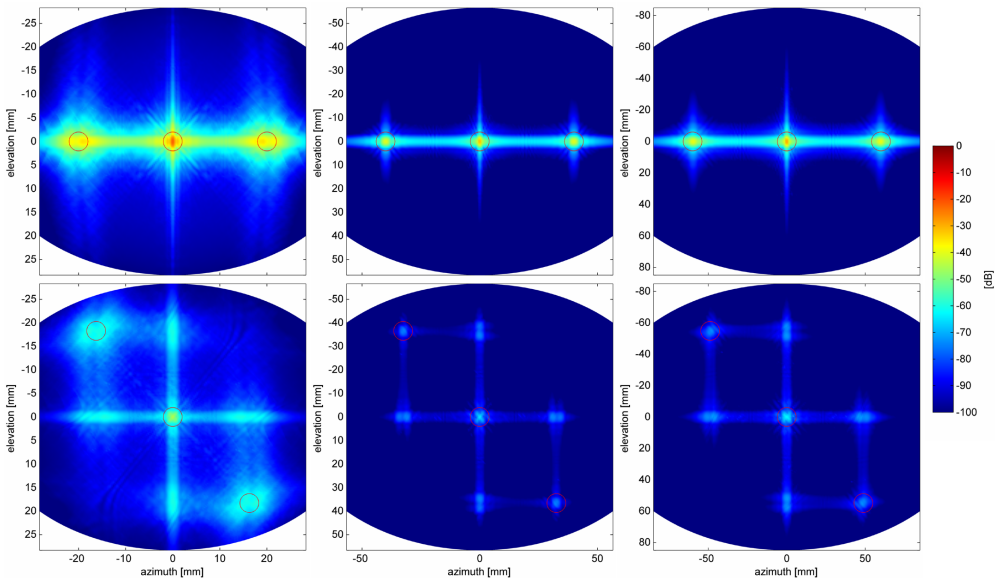


Figure 3.12: Example envelope profiles of the cross-talks, here for the MLT dispositions 1-C (top row) and 2-B (bottom row) with the transmit beams directed on the center of each zone (each indicated by a red circle). The profiles were evaluated at depths 40 mm (left column), 80 mm (center column) and 120 mm (right column), for the receive direction corresponding to no steering, i.e. the centermost transmit beam direction.

(depth 40 mm) than at focal depth, and 3 dB lower at depth 120 mm. This can easily be noticed from Fig. 3.12.

## 3.6 Discussion

The starting point of this study was the observation that the energy radiated by a rectangular transducer should be gathered in the azimuth and elevation planes. The hydrophone measurements presented in Fig. 3.10 (a) tends to confirm this principle. Along the azimuth axis and the transverse diagonal of the transducer geometry (Fig. 3.10 (c) and 3.10 (d)), we could observe a very good match between the simulated and measured profiles. On the elevation axis, one can see that the main-lobe is wider in the water-tank measurements compared to the simulations, which means the focusing in elevation is probably not perfect on the probe. Outside of the cross formed by the principal side-lobes along the azimuth and elevation axes, secondary side-lobes could be measured in an irregular pattern with pressure levels below −35 dB of what can be observed in the main-lobe, and below −40 dB along the studied transverse diagonal. This phenomenon along all the differences with the equivalent Field II simulation presented in Fig. 3.10 (b) could have different causes: the probe is statically focused in elevation with a lens that could have an imperfect shape; some of the transducer elements may be misshaped or inactive, leading to the formation of additional grating lobes; the probe surface was covered by a thin plastic foil for waterproofing purposes, which may act as an additional lens defocussing the transmitted beam; a small amount of the energy could have reflected along the walls of the water tank and be registered with the next pulse firings; the low speed of sound in the water may be the source of errors in the focusing both electronically and by the elevation lens. Having taken into account all those considerations, we can conclude on a fair match between the hydrophone and simulated transmit field profiles. It is important to note that the difference between the amplitude of the side-lobes along the azimuth and elevation axes, and the side-lobes along the transverse diagonal is contained between 15 dB and 25 dB as soon as we are located outside of the main-lobe (i.e. at a distance larger than 18 mm). This side-lobe amplitude difference will result in lower interactions, and therefore lower cross-talk artifacts in the image.

The amplitude of the cross-talks was simulated for different situations corresponding to both conventional MLT dispositions and our proposed alignment along the transverse diagonal of the transducer geometry. If we consider the maximum dynamic display range in cardiac imaging application to be of 50 dB, we can see in Fig. 3.11 that the MLT cross-talk artifacts will be visible for all the conventional dispositions 1-A to 1-D. Using our proposed dispositions 2-A to 2-D, these artifacts could be neglected, except in the near-field where the pressure waves from the simultaneously transmitted beams are overlapping. An explanation for the cause of this cross-talk artifact reduction can be found in Fig. 3.12. When the simultaneous transmits are aligned along the azimuth axis, there will be one or several main-lobe to side-lobe interactions, leading to severe artifact levels; whereas the alignment of the transmit directions along the transverse diagonal reduced the cross-talks to interactions between

pairs of side-lobes.

It is interesting to look at how the cross-talk amplitudes vary with an increasing number of MLT. In conventional dispositions 1-A/B/D, where only two of the simultaneous transmits are aligned along the azimuth or elevation axis, and where the angular separation is as much as 45 deg, the magnitude of the worst artifacts will be contained between $-32$ dB and $-30$ dB. We denote a slightly higher level of artifacts when aligning the beams along the elevation direction. This is due to the fact that the aperture is smaller in the elevation, generating wider side-lobes and therefore more intense cross-talks. When putting four transmit directions in a grid pattern as in 1-D, we observe a level of artifacts similar to the ones observed in 1-B, while we may have expected an increase in the cross-talks. Indeed, when using a grid disposition, the maximum amplitude of the artifacts is approximately equal to the maximal one observed along one single line of the grid. What happens in this case is that the artifacts in the image will be present in more radial positions. As seen in Fig. 3.4, the position of the cross-talk artifacts is dependent on the location of the MLT. An increase in the number of the simultaneous transmits will lead to a corresponding increase in the number of visible cross-talk artifacts at different locations in the image; but not necessary a direct gain in their intensity. When increasing the number of MLT to three along the same line, as in 1-C, we can see that the artifact level is increased, due to the reduced transmit beam separation. This can be especially well observed in the near-field where stronger interactions between the beams happen. Similarly, the magnitude of the cross-talks is also observed to increase with reduced MLT spacing for the dispositions along the transverse diagonal. It is interesting to note that the level of interactions between the MLT is kept below visible both at focal depth and in the far-field, while the superposition of the pressure fields in near-field results in stronger interactions, and thus visible cross-talk artifacts for dispositions 2-C and 2-D where more than 3 beams were simulated.

In this study, we restricted ourselves to a basic implementation of a 3-D MLT system that we can consider as a worst-case scenario. Different considerations and improvements can indeed be done to lower the amplitude of the cross-talk artifacts even further:

Second harmonic imaging is a widely used modality, which allows for an improved image quality in cardiac imaging applications. The second harmonic pressure field has the property of possessing narrower and lower side-lobes, as well as a smaller and more defined main-lobe. Taking advantage of the second harmonic, we can expect to reduce the interactions between the harmonic pressure fields, and therefore reduce the amplitude of the cross-talk artifacts even further. Accurate simulations of the second harmonic pressure fields require the resolution of the non-linear equations for the sound propagation. Even though some approaches have been proposed to solve these equations with the help of limiting hypothesis [27–29], this was considered as beyond the scope of this work.

Apodization functions applied to the transducer elements on transmit and/or receive allow to modulate the spatial response of our system. Applying an apodization function, one may expect transmit and/or receive beam profiles with a reduced side-lobe level, resulting in lower cross-talk levels [15]. In our study, we did not use any

apodization on transmit, since it is not a widely spread technology, nor receive, since we wanted to focus on the impact of the spatial disposition of the MLT only. Therefore, we can expect further improvements in the reduction of the cross-talk artifacts in all the studied MLT dispositions using apodization functions.

The level of artifacts observed in the near-field in Fig. 3.11 (a) is higher for all the studied MLT dispositions, and is critical for eventual MLT applications. Close to the probe, the pressure field of each simultaneously transmitted beam is so wide that it results in interactions and therefore cross-talk artifacts. In order to reduce the level of artifacts in the near-field, one may try to limit the size of the point-spread function (PSF) in the near-field. This could be achieved using synthetic aperture techniques such as retrospective transmit beam-formation [30, 31]. By combining the information gathered from successive acquisitions, one may synthetically recreate a beam with a transmit focus position located at the position of choice.

Two aspects that may be a limiting factor but that have not been studied in this article are specular reflections and shadowing of the probe surface.

Specular reflections may happen in the presence of a sharp and defined boundary between two mediums. Energy transmitted by a first beam may be reflected in another direction, passing through the main-lobe of a different transmit beam, and resulting in strong artifacts. Even though this was considered unlikely in cardiac applications due to the irregularity characterizing the inner walls of the heart cavities, this may have a negative impact on MLT applications in general.

The proposed dispositions along the transverse diagonal of the probe are based on the observation that the pressure field emitted by a rectangular transducer will be gathered along two planes aligned with the elevation and azimuth axes, forming a cross-shaped pattern. This will no longer be entirely true if the surface of the probe is partially covered by for example the ribs. This shadowing may happen in difficult patients and may in such cases cause limitations to the proposed method. Nonetheless, we can estimate that our proposed MLT dispositions will work perfectly in applications where we can be sure that the effective surface of the transducer will not be shadowed and will hence stay rectangular, such as in trans-esophageal echocardiography (TEE) applications.

## 3.7 Conclusion

This work presents a novel method for multi-line transmission taking advantage of the shape of the pressure field emitted by a rectangular transducer. We propose to align multiple transmit lines along the transverse diagonal of the transducer geometry. Spatial dispositions with up to 5 MLT could be combined without triggering a level of cross-talk artifacts above the visible threshold of a 50 dB dynamic display range. Simulations showed 20 to 30 dB lower cross-talks than compared to conventional dispositions with the same number of MLT. This reduction in cross-talks was also demonstrated by water tank measurements of a commercially available probe.

A 3-D scan sequence was adapted to the proposed method. This enabled acquisition of wide 3-D sectors without artifacts between the internal MLT sectors. The proposed

method combined with parallel receive beamforming can potentially remove the need for stitching of data from several cardiac cycles in real-time 3-D echocardiography (from 3 Hz to 15 Hz for a wide cardiac sector of 90 × 90 degrees). These gain in frame rate can be achieved without transmitting broader beams, and hence without sacrificing the use of harmonic imaging.

## Acknowledgment

The researchers thank GE Vingmed Ultrasound for access to a Vivid E9 ultrasound scanner.

# References


[1] L. P. Badano, R. M. Lang, and J. L. Zamorano, *Textbook of Real-Time Three Dimensional Echocardiography*, vol. 129. Springer, 2011.

[2] H. Yoshiara, H. Hasegawa, H. Kanai, and M. Tanaka, "Ultrasonic Imaging of Propagation of Contraction and Relaxation in the Heart Walls at High Temporal Resolution," *Japanese Journal of Applied Physics*, vol. 46, pp. 4889–4896, July 2007.

[3] L. Hatle and B. Angelsen, *Doppler Ultrasound in Cardiology - Physical Principles and Clinical Applications*. Lea & Febiger, Philadelphia, 2nd ed. ed., 1986.

[4] S. Brekke, S. I. Rabben, A. Støylen, A. Haugen, G. Haugen, E. N. Steen, and H. Torp, "Volume stitching in three-dimensional echocardiography: distortion analysis and extension to real time.," *Ultrasound in medicine & biology*, vol. 33, pp. 782–96, May 2007.

[5] D. P. Shattuck, M. D. Weinshenker, S. W. Smith, and O. T. von Ramm, "Explososcan: a parallel processing technique for high speed ultrasound imaging with linear phased arrays.," *The Journal of the Acoustical Society of America*, vol. 75, pp. 1273–82, Apr. 1984.

[6] F. Duck, "Nonlinear acoustics in diagnostic ultrasound," *Ultrasound in medicine & biology*, vol. 28, no. 1, pp. 1–18, 2002.

[7] G. Montaldo, M. Tanter, J. Bercoff, N. Benech, and M. Fink, "Coherent plane-wave compounding for very high frame rate ultrasonography and transient elastography.," *IEEE transactions on ultrasonics, ferroelectrics, and frequency control*, vol. 56, pp. 489–506, Mar. 2009.

[8] M. Couade, M. Pernot, M. Tanter, E. Messas, A. Bel, M. Ba, A. Hagege, and M. Fink, "Ultrafast imaging of the heart using circular wave synthetic imaging with phased arrays," in *IEEE International Ultrasonics Symposium (IUS)*, pp. 515–518, IEEE, 2009.

[9] H. Hasegawa and H. Kanai, "High-frame-rate echocardiography using diverging transmit beams and parallel receive beamforming," *Journal of Medical Ultrasonics*, vol. 38, pp. 129–140, May 2011.

[10] B. Dénarié, H. Torp, G. Haugen, A. Sørnes, and T. Bjåstad, "Motion Compensated Synthetic Transmit Beam Technique for Real-time Echocardiography," in *IEEE Ultrasonics Symposium, 2011*, 2011.

[11] B. Dénarié, T. Tangen, I. Kinn Ekroll, N. Rolim, H. Torp, T. Bjåstad, and L. Løvstakken, "Coherent plane wave compounding for very high frame rate ultrasonography of rapidly moving targets," *Medical Imaging, IEEE Transactions on*, vol. PP, no. 99, pp. 1–1, 2013.

[12] K. Thomenius and S. Silverstein, "Method and apparatus for high-frame-rate high-resolution ultrasonic image data acquisition," *US Patent 6,066,099*, vol. 99, no. 19, pp. 1–18, 2000.

[13] R. Mallart and M. Fink, "Improved imaging rate through simultaneous transmission of several ultrasound beams," *Proceedings of SPIE*, vol. 1733, pp. 120–130, 1992.

[14] A. Drukarev and K. Konstantinides, "Beam transformation techinques for ultrasonic medical imaging," *Ultrasonics, Ferroelectrics and Frequency Control, IEEE Transactions on*, vol. 40, pp. 717–26, Jan. 1993.

[15] L. Tong, H. Gao, H. Choi, and J. D'hooge, "Multi-transmit Beam Forming for Fast Cardiac Imaging," *IEEE Ultrasonics Symposium*, 2011.

[16] D. Dubberstein and O. V. Ramm, "Methods and systems for ultrasound scanning using spatially and spectrally separated transmit ultrasound beams," *US Patent 6,159,153*, 2000.

[17] L. Demi, M. D. Verweij, and K. W. A. van Dongen, "Parallel Transmit Beamforming Using Orthogonal Frequency Division Multiplexing Applied to Harmonic Imaging — A Feasibility Study," *Ultrasonics, Ferroelectrics and Frequency Control, IEEE Transactions on*, vol. 59, no. 11, pp. 2439–2447, 2012.

[18] K. Thiele, "Multi-Beam Transmit Isolation," *US Patent 20100016725*, 2010.

[19] J. Hossack and T. Sumanaweera, "Method and apparatus for medical diagnostic ultrasound real-time 3-D transmitting and imaging," *US Patent 6,179,780*, 2001.

[20] T. Shirasaka, "Ultrasonic imaging apparatus," *US Patent 4,815,043*, 1987.

[21] S. Denk, "Ultrasound imaging system and method," *US Patent 20100191115*, 2010.

[22] B. Angelsen, *Ultrasound imaging*. Emantec Norway, 2000.

[23] B. Madore, P. J. White, K. Thomenius, and G. T. Clement, "Accelerated focused ultrasound imaging.," *IEEE transactions on ultrasonics, ferroelectrics, and frequency control*, vol. 56, pp. 2612–23, Dec. 2009.

[24] R. Cobbold, *Foundations of biomedical ultrasound*. Oxford University Press, 2006.

[25] J. Jensen, "Field: A program for simulating ultrasound systems," *Medical and Biological Engineering and Computing*, vol. 34, pp. 351–353, 1996.

[26] J. Jensen and N. Svendsen, "Calculation of pressure fields from arbitrarily shaped, apodized, and excited ultrasound transducers," *Ultrasonics, Ferroelectrics and Frequency Control, IEEE Transactions on*, vol. 39, no. 2, pp. 262–267, 1992.

[27] M. E. Frijlink, H. Kaupang, T. Varslot, and S. E. Måsøy, "Abersim : a Simulation Program for 3D Nonlinear Acoustic Wave Propagation for Arbitrary Pulses and Arbitrary Transducer Geometries," in *IEEE Ultrasonics Symposium (IUS)*, pp. 1282–1285, 2008.

[28] F. Prieur, T. F. Johansen, S. Holm, and H. Torp, "Fast simulation of second harmonic ultrasound field using a quasi-linear method.," *The Journal of the Acoustical Society of America*, vol. 131, pp. 4365–75, June 2012.

[29] F. Varray, M. Toulemonde, O. Basset, and C. Cachard, "Fast and accurate nonlinear pressure field simulation : a finite-difference scheme into the Fourier domain," *IEEE International Ultrasonics Symposium*, 2012.

[30] S. Freeman, P. Li, and M. Odonnell, "Retrospective dynamic transmit focusing," *Ultrasonic imaging*, vol. 17, no. 3, pp. 173–196, 1995.

[31] C. Bradley, "Retrospective transmit beamformation," *Whitepaper ACUSON SC2000TM Volume Imaging*, vol. Im, 2008.

# Chapter 4

# Motion Compensation Schemes Applied to Synthetic Transmit Beamformation

Bastien Dénarié[1], Tore Bjåstad[2] and Hans Torp[1]
[1]MI-Lab, Department of Circulation and Medical Imaging, Faculty of Medicine, Norwegian University of Science and Technology (NTNU)
[2]GE Vingmed Ultrasound AS, Horten, Norway

Synthetic Transmit Beamformation (STB) is a previously published technique for removing image artifacts caused by parallel beamforming. Since it is based on lateral coherent interpolation between overlapping beams acquired from subsequent transmit events, it is vulnerable to motion. This is especially the case in 3-D cardiac imaging where the acquisition time between two successive planes is long. As a result, stripe-shaped artifacts with up to 15 dB gain losses are observed in the images.

The objective of this work was to develop a motion compensated STB algorithm capable of compensating for motion in cardiac imaging. The algorithm presented is based on the cross-correlation product between the IQ data of overlapping scan lines from neighboring transmit events, and has a sufficiently small computational demand to be implemented in real-time. The technique was tested using simulations and by post processing of recorded *in vivo* data, both in 2-D and 3-D acquisitions.

Applying the proposed motion compensation algorithm, stripe artifacts appearing in the STB images were successfully corrected. The estimates obtained from the motion correction algorithm also provide an additional tissue velocity imaging (TVI) modality at the frame rate of the B-mode acquisition.

## 4.1 Introduction

As of today, 2-D trans-thoracic echocardiography remains a modality of choice for establishing clinical diagnostics. A high image quality and the real-time capability are among the main benefits over the more recent 3-D ultrasound imaging modalities [1]. However, in order to make clinical decisions from 2-D images, the cardiologist must be able to mentally reconstruct the full 3-D morphology of the heart. As such, 3-D echocardiography combining a good spatial resolution with frame rates compatible with real-time acquisition would ensure better and automatized diagnostics, thus becoming a gold standard for the evaluation of the cardiac function. However, the high image quality obtained in 2-D cardiac echography is based on second harmonic imaging using tightly focused transmit beam. Translating this acquisition directly into 3-D will result in an unacceptable frame rate since the number of transmissions is squared.

To obtain higher frame rates, it has been proposed to beamform a plurality of image lines for each transmission. With this technique, called parallel receive beamformation or Multiple Line Acquisition (MLA), a given volume is covered with fewer transmissions. As of today, the use of parallel receive beamformation makes it possible to acquire small sub-volumes of data for each transmit beam in most commercial scanners [2–4]. On some research platforms, parallel receive beamforming has also been used to generate a full image per transmission [5, 6]. Theoretically, the Nyquist theorem states that the image sector will be fully sampled laterally if two neighboring transmit beams overlap over at least half of their lateral span [7]. However, the misalignment of the transmit and receive directions may lead to block-like image artifacts caused by the warping and skewing of the two-way beam profile [8]. A coherent combination of the data received from overlapping transmit beams can be used to achieve a high lateral resolution and prevent block artifacts. Synthetic transmit beamformation (STB) is a previously published technique for removing image artifacts caused by parallel beamforming [7]. Due to its simplicity, STB has shown to be especially well suited for real-time cardiac imaging applications, where a high frame rate combined with a good spatial resolution and a robustness against aberrations is required to acquire the heart kinematics [9–11].

However, as the STB technique is based on lateral coherent interpolation between overlapping beams acquired from subsequent transmit events, it is vulnerable to motion in the imaged medium. Velocities from both the myocardium and the blood in the cavities are sufficiently high to cause visible artifacts. These artifacts are generated by the coherent summation of out-of-phase signals acquired at two different times in the cardiac cycle. Similar phenomenons have been observed in a wide range of applications using coherent summation across several transmissions, such as synthetic transmit aperture [12–16] and plane wave compounding [17, 18]. They have proposed to estimate the in-plane motion over the entire field of view using diverse 2-D correlations between low- and high-resolution images in order to correct for these artifacts. However, due to the large number of transmissions combined in each receive direction, these methods rely on heavy computations which do not meet the real-time requirements of ultrasound imaging. In 3-D imaging the difficulty of correcting

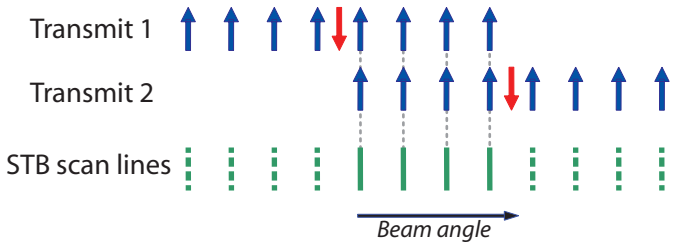


Figure 4.1: Acquisition pattern for 4 STB. The figure shows transmit and receive steering angles (on the x-axis) for two neighboring transmit events. Receive directions are indicated with arrows pointing upwards and transmit direction with arrows pointing downwards. Resulting STB scan line positions are indicated with solid lines.

for motion is increased as the time gap between two sub-volumes overlapping in the elevation direction is typically 10 to 50 times longer than the time gap between two successive in-plane emissions. To the author's knowledge, no algorithm has yet been proposed for motion correction in 3-D imaging.

In this article, we propose an algorithm for motion compensation in Synthetic Transmit Beam imaging, both in 2-D and 3-D. First the theoretical effects of motion on the STB technique are presented in Section 4.2. In Section 4.3, a simple compensation scheme for 2-D imaging using STB is proposed and validated against both simulations and *in vivo* acquisitions. Finally, the motion compensation strategy is extended to real-time 3-D STB imaging in Section 4.4, and the algorithm is used to provide an additional tissue velocity imaging (TVI) modality covering the entire field of view.

## 4.2 Synthetic Transmit Beams in Presence of Motion

### 4.2.1 Motion Artifacts

The Synthetic Transmit Beamforming technique is based on coherent lateral interpolation between the channel data of neighboring transmit beams. In practice, this is achieved by combining data from identically steered parallel receive lines from two successive overlapping ultrasound pulses, as illustrated in Fig. 4.1. Each synthetic line $\vec{y}_\theta$ will then be computed using linear interpolation

$$\vec{y}_\theta = \xi \cdot \vec{x}_{n,\theta} + (1 - \xi) \cdot \vec{x}_{n+1,\theta} \tag{4.1}$$

where $\vec{x}_{n,\theta}$ and $\vec{x}_{n+1,\theta}$ denotes the IQ beamformed signals from two successive transmits $n$ and $n+1$ focused on receive in the same angular direction $\theta$, and $\xi = (\theta_{n+1} - \theta)/(\theta_{n+1} - \theta_n)$ is the relative distance between the receive direction $\theta$ and the transmit directions $\theta_n$ and $\theta_{n+1}$.

We will now consider a group of scatterers moving at a given velocity with component $v_{\text{ax}}$ towards the transducer. The difference in the scatterers position at

the time they are insonified by two successive pulses is reflected as a time shift in the received RF-signals. After IQ demodulation, and as long as the time shift is less than the pulse length, we may estimate the displacement locally as a phase shift by computing the cross-correlation $\hat{R}_{n,\theta}$ between two successive beams:

$$\hat{\Phi}(n,\theta) = \angle\left\langle \hat{R}_{n,\theta} \right\rangle = \angle\left\langle \vec{x}^{*}_{n+1,\theta} \cdot \vec{x}_{n,\theta} \right\rangle \tag{4.2}$$

This phase shift estimate $\hat{\Phi}(n,\theta)$ may be improved using spatial averaging over a region where the motion is considered as uniform.

The axial velocity $v_{\text{ax}}$ can then be evaluated from the phase shift estimate $\hat{\Phi}(n,\theta)$:

$$\begin{aligned} v_{\text{Nyquist}} &= \frac{c \cdot PRF}{4 f_0}, \\ v_{\text{ax}} &= \frac{\hat{\Phi}(n,\theta)}{\pi} \cdot v_{\text{Nyquist}} \end{aligned} \tag{4.3}$$

where $f_0$ is the pulse center frequency, $c$ is the speed of sound, and PRF is the Pulse Repetition Frequency of the system.

Motion of the imaged medium will therefore be directly reflected in the cross-correlation estimate. In (4.3), we see that for the critical axial velocity $v_{\text{ax}} = v_{\text{Nyquist}}$, this phase shift will reach a value of $\pi$. This will cause maximal destructive interferences in the synthetic line generated in (4.1). This destructive interference will be seen in the final image as a dark stripe in the axial direction around the location of the moving target, and is further referred as "motion artifact".

### 4.2.2 Quantification of Motion Artifacts

The power of each STB scan line can be expressed from (4.1) as

$$\begin{aligned} \hat{P}_{y,\theta} = \xi^2 \cdot \hat{P}_{n,\theta} + (1-\xi)^2 \cdot \hat{P}_{n+1,\theta} \\ + 2 \cdot \xi \cdot (1-\xi) \cdot \left| \hat{R}_{n,\theta} \right| \cdot \cos \hat{\Phi}(n,\theta) \end{aligned} \tag{4.4}$$

where $\hat{P}_{n,\theta} = \left\langle \vec{x}^{*}_{n,\theta} \cdot \vec{x}_{n,\theta} \right\rangle$ is the power of the received line corresponding to the $n$-th transmitted pulse focused in the angular direction $\theta$.

Assuming a uniform speckle ($\hat{P}_{n,\theta} \approx \hat{P}_{n+1,\theta}$), one can approximate the extent of the stripes, i.e. the loss of intensity in the resulting B-mode image caused by the motion of the scatterers, by combining (4.2), (4.3) and (4.4):

$$E = \frac{\xi^2 + (1-\xi)^2 + 2 \cdot \xi \cdot (1-\xi) \cdot \cos\left( \frac{4\pi \cdot f_0}{\text{PRF}} \cdot \frac{v_{\text{ax}}}{c} \right)}{\xi^2 + (1-\xi)^2 + 2 \cdot \xi \cdot (1-\xi)} \tag{4.5}$$

The extent of the motion artifacts is presented for an example cardiac application (PRF = 5.133 kHz, $f_0$ =3.34 MHz) in Fig. 4.2, and for various values of the PRF in Fig. 4.3. This expression constitutes a narrow band approximation only, but gives a

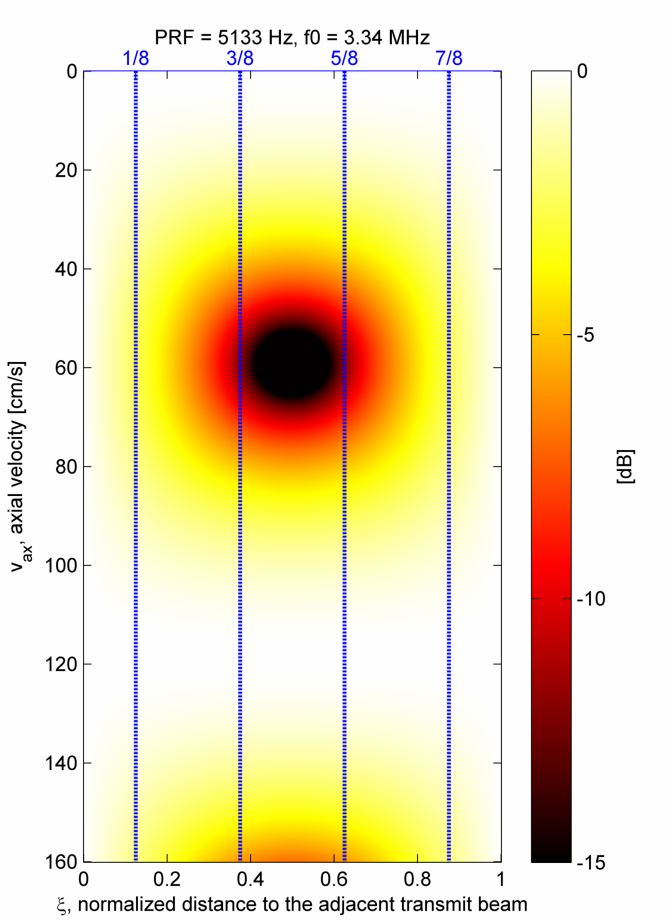


Figure 4.2: Amplitude of the negative interferences due to motion on the final STB image, as expressed in (4.5), as a function of the observed velocities and of the receive directions (e.g. in a 4 STB pattern, $\xi = [1/8; 3/8; 5/8; 7/8]$). The PRF is 5.133 kHz and the IQ demodulation frequency is $f_0$ =3.34 MHz.

good illustration of the mechanisms behind motion artifacts using STB. For a receive beam steered in an angle close to the middle of two overlapping transmit beams ($\xi \to 0.5$), we observe that some velocities generate a gain loss exceeding 10 dB. Put in other words, dark stripes may be observed on the image in the areas in between the transmit steering angles in presence of some definite tissue or blood velocities.

Note also that the appearance of the artifact is periodic with motion. This is due to the fact that we are sampling the observed velocities at a frequency defined by the PRF of the system, and that the repetitive pattern corresponds to aliasing when the

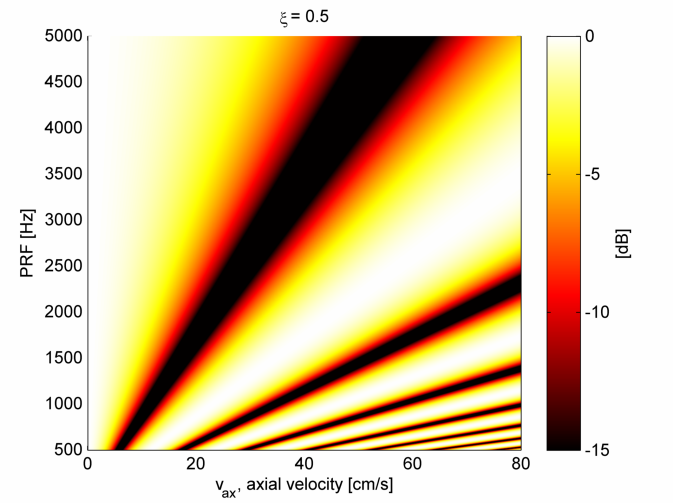


Figure 4.3: Amplitude of the negative interferences due to motion on the final STB image, as expressed in (4.5) for $\xi = 0.5$, as a function of the PRF and of the observed velocities.

imaged velocities are over the Nyquist limit.

## 4.3 Suppressing Motion Artifacts with the 2-D STB Imaging Technique

### 4.3.1 Cross-correlation Based Motion Compensation

The phase of the cross-correlation process (4.2) can be used to estimate the axial velocities using (4.3). These cross-correlation estimates can also be used to prevent artifacts generated by motion in the STB interpolation (4.1).

The estimated velocity in term of phase angle will take the form of a phase shift within the interval $[-\pi; \pi]$. Assume now that the velocities are lower than the Nyquist limit (e.g. for cardiac tissue moving with velocities under 20 cm/s, as seen in Fig. 4.3 with a PRF around 5 kHz). We can compensate for this motion using the narrow band approximation of the effect of motion on the received IQ signal expressed in (4.3): a simple phase shift. This shift is applied via a phase rotation of the IQ vectors. This gives the motion compensated STB process:

$$\begin{aligned} \vec{y}_\theta = & \xi \cdot e^{i\cdot(1-\xi)\cdot\hat{\Phi}(n,\theta)} \cdot \vec{x}_{n,\theta} \\ & + (1-\xi) \cdot e^{-i\cdot\xi\cdot\hat{\Phi}(n,\theta)} \cdot \vec{x}_{n+1,\theta} \end{aligned} \tag{4.6}$$

The complex exponential rotation vectors introduced in (4.6) are factorized by the normalized distance to the transmit beam so that the phase correction is smooth along

the lateral direction. This prevents the generation of stronger stripes when following the STB merging with lateral interpolation.

For larger velocities above the Nyquist limit ($v > 55\,\text{cm/s}$ for the example setup with PRF $= 5.133\,\text{kHz}$ and $f_0 = 3.34\,\text{MHz}$), aliasing will occur for the pulse center frequency and the estimated phase shift $\hat{\Phi}(n,\theta)$ will no longer correspond to the exact displacement of the scatterer. However, the STB motion compensation process (4.6) will ensure that no pure negative interference between the signals are generated at the pulse center frequency $f_0$, resulting only in a small loss in axial resolution. Hence, the quality of the proposed motion compensation scheme is gradually reduced with increasing velocities. In an extreme scenario, one may consider a axial displacement such as the envelope of the signals $\vec{x}_{n,\theta}$ and $\vec{x}_{n+1,\theta}$ do not overlap. In this case, the signals become uncorrelated and the correction process will fail.

The cross-correlation (4.2) used to correct for motion is a local estimate, while tissue motion is a rather spatially continuous phenomenon. To improve the estimate, averaging of the cross-correlation estimate can be considered. Axially, one must choose an averaging region over which the tissue is susceptible to remain approximately constant. Laterally, one may average between all the beams corresponding to the same pair of transmit beams, as the displacement observed between the two emissions should be comparable over those receive directions. If no averaging is applied to the cross-correlation estimates, the signals $\vec{x}_{n,\theta}$ and $\vec{x}_{n+1,\theta}$ in the motion compensated STB process (4.6) will always be summed in-phase. The STB operation becomes equivalent to a scenario where the weighted STB summation is done after detection of the IQ data, also called incoherent STB (iSTB) [19].

### 4.3.2 Field II Simulations: Setup

In order to validate the motion compensation algorithm, a B-mode image of a moving phantom was generated using Field II [20, 21]. The phantom consists of a rectangle filled with randomly distributed scatterers in the azimuth plane (4 scatterers per resolution cell) and contains in addition three spherical cysts of diameter 16.7, 12.5 and 10 mm, as well as 12 point scatterers with a 20 dB brighter amplitude. In addition, random white Gaussian noise was generated with an amplitude 20 dB below the phantom speckle signal to account for thermal noise. The field of view is a 75° sector acquired with a 96 elements cardiac probe using 62 transmit beams as described in Table 4.1. On transmit, the lateral spacing was determined such that the Rayleigh sampling criterion is fully met [22], and the apodization function was set to a triangular window such as to mimic the pressure field generated by the second harmonic component of the signal [23]. On receive, 8 parallel beams (MLA) are generated and combined into a 4 STB pattern as detailed in Fig. 4.1, with or without motion correction. The beams are then further interpolated laterally before envelope detection. In order to reduce estimation variance, the cross-correlation is computed using a sliding hamming window in the axial direction (2.5 mm long), and then averaged laterally between all the beams corresponding to the same pair of transmit beams.

Table 4.1: Experimental 2-D Setup Parameters

| | |
|---|---|
| Transducer geometry | 96 elements, 230 µm pitch |
| Transmit center frequency | 1.67 MHz, 60% bandwidth |
| Demodulation frequency $f_0$ | 3.34 MHz |
| Transmit focal distance | 85 mm |
| $f$-number transmit | 4.33 |
| $f$-number receive | 2 until 44 mm, then increasing |
| Sector size | 75° |
| Number of transmit beams | 62 |
| Parallel receive lines | 8 |
| PRF | 5.133 kHz (2 kHz *in vivo*) |

### 4.3.3 Field II Simulations: Results

The results of the simulations are presented in Fig. 4.4. As expected, motion artifacts appear as lateral gain variations in the STB image (top row). Each of these artifacts stretch across a plurality of receive lines. This is due to the fact that all the receive lines close to $\xi = 0.5$ are impacted by the motion artifacts as illustrated in Fig. 4.2. In addition, we observe the strongest motion artifacts when the phantom moves with a velocity $v = 60\,\text{cm/s}$, as expected from the theory.

The motion compensation algorithm presented in 4.3.1 is successful in recovering those gain losses (middle row). However, we observe that the axial resolution is maintained only for velocities below $v < 60\,\text{cm/s}$ (especially seen with the center-most bright point scatterer at 13 cm depth). This phenomenon can be explained by looking at the averaged phase estimate $\hat{\Phi}(n, \theta)$ used by the motion compensation algorithm (bottom row). We observe aliasing of the phase estimate appearing from $v = 60\,\text{cm/s}$. As mentioned when introducing (4.3), the axial velocities will directly reflect in the phase shift between the received IQ lines as long as the motion is inferior the pulse length. When aliasing is added, the correctness of the motion compensation based on a phase-shift (4.6) will be gradually degraded.

When looking closer to the phase estimate (especially for small velocities $v < 60\,\text{cm/s}$), we observe a bias in the phase estimate: the phase is both under- and over-estimated respectively on the left-side and the right-side of each bright scatterer at small depths (5 and 8 cm), while the opposite phenomenon is observed at larger depths beyond transmit focus (13 cm). The same phenomenon may be observed when looking at the edges of the rectangular speckle phantom and along the border of the cysts.

### 4.3.4 In vivo Experiment: Setup

A Vivid E9 ultrasound scanner along with a M5S cardiac probe (GE Vingmed Ultrasound AS, Horten, Norway) were used to acquire the beamformed IQ data

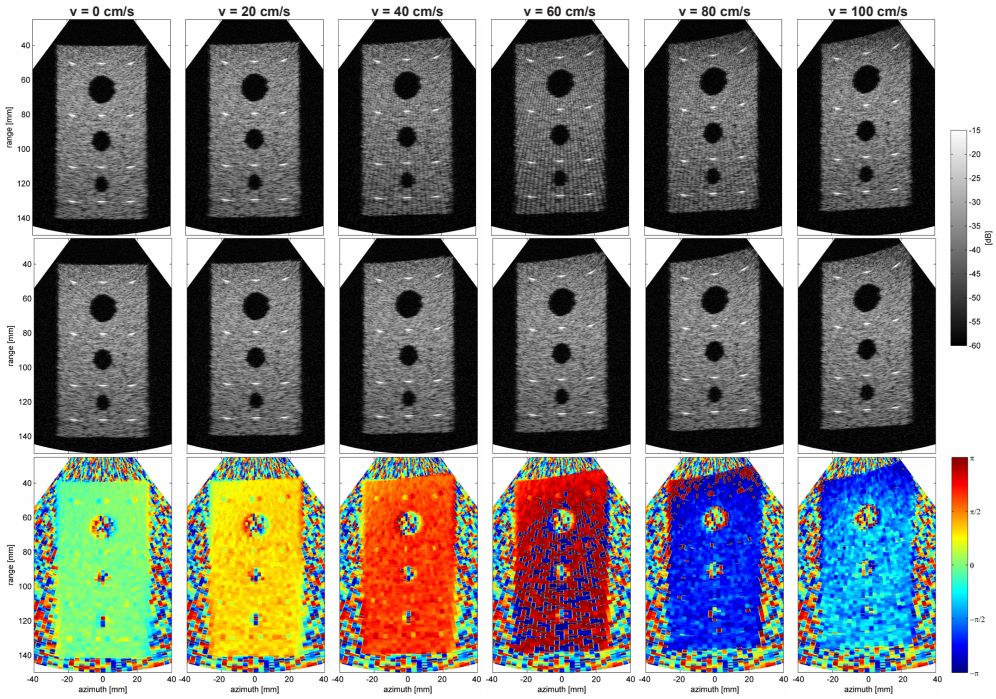


Figure 4.4: B-mode images of a simulated phantom moving upwards. Top row: 4 STB. Middle row: 4 STB with motion compensation. Bottom row: Phase estimates used by the motion correction algorithm.

corresponding to a 75° sector scan on an entire heart cycle. The acquisition setup was similar to what is presented in Table 4.1, except for the PRF which was reduced to 2000 Hz in order to provoke motion artifacts. As for the simulations, 8 parallel receive lines were combined using the STB technique, and lateral interpolation was applied before detection.

In order to evaluate the influence of the motion artifacts on the STB technique, it was chosen to compute the mean intensity per STB line. In a 4 STB pattern, the intensity from all the lines have been averaged, normalized and grouped along the 4 different STB lines to which it corresponds. This averaging has been limited to the depths ranging from 40 mm to 120 mm where high velocities are observed in the myocardium.

### 4.3.5 In vivo Experiment: Results

An example frame exhibiting motion artifacts is presented in Fig. 4.5. The image is processed with and without the motion compensation algorithm and an associated bar chart indicates the mean intensity per STB line. We observe that the STB lines 1 and 4 exhibit a high intensity with or without motion compensation: they correspond to

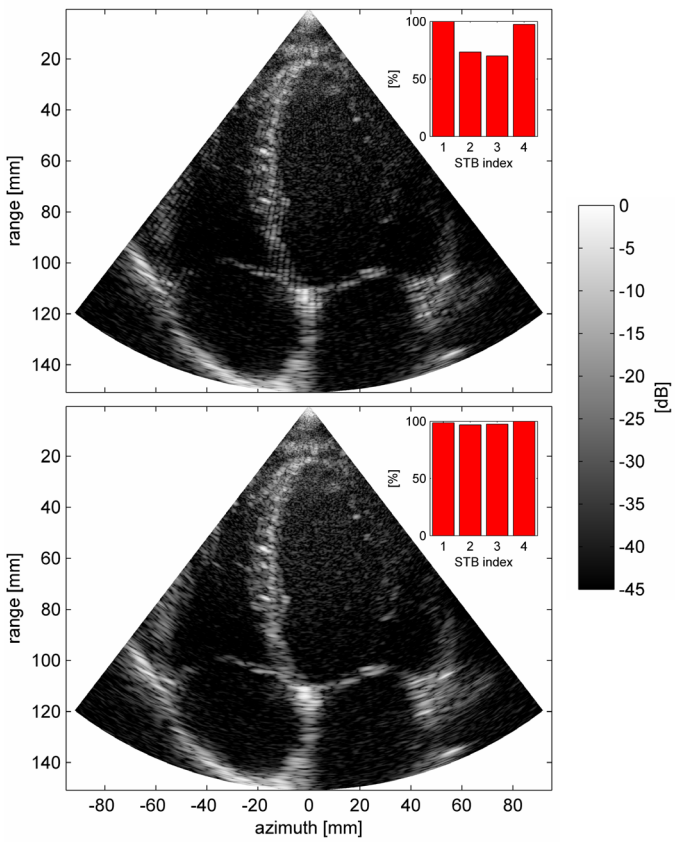


Figure 4.5: Four chambers view of a healthy volunteer acquired with the STB technique at a rather low PRF (2 kHz). Motion artifacts are clearly visible in the myocardium when using the STB technique (top), while they disappear once corrected with the proposed algorithm (bottom). The bar chart indicates the mean intensity per STB scan line. Two corresponding movies, covering several heart cycles, are located at http://folk.ntnu.no/denarie/thesis.

values of $\xi = 1/8$ and $\xi = 7/8$ in Fig. 4.2. The mean intensity of the STB lines 2 and 3 (corresponding to $\xi = 3/8$ and $\xi = 5/8$), however, is reduced when no motion compensation is applied. This reduction is about 26-30%, which is consistent with the loss observed in Fig. 4.2.

On the bottom row, we observe that the motion compensation algorithm successfully recovers the gain losses in the STB image. After compensation, the gain variations along the STB lines is inferior to 3%.

### 4.3.6 Discussion on motion compensation in 2-D STB imaging

The STB technique relies on coherent summation of signals acquired at different times; it will therefore be susceptible to degradations in presence of motion. Using both simulations and *in vivo* 2-D acquisitions, we observed that lateral gain losses appear in the STB images when certain axial velocities are attained by the imaged target. These gain losses are located at fix lateral directions in between the transmit beam directions. As expected from theory, the phenomenon is not only dependent on the observed velocities, but also on the chosen PRF and the center frequency of the received signal.

Using phantom simulations, we were able to confirm the theory that the motion artifacts have a negative impact on the image in a repetitive pattern with increasing velocities. In our simulation setup, with a PRF 5.1333 kHz corresponding to the optimal PRF for an image with 15 cm depth, the darker stripes were appearing for velocities around $v = 60\,\text{cm/s}$, and the phenomenon may be expected to reproduce for velocities as high as 180 cm/s. However, such velocities are not observed in the tissues *in vivo*, since the myocardium has a velocity below 20 cm/s [24]. Higher velocity components are only observed in the blood and around the valves. Hence, in order to illustrate the apparition of this phenomenon *in vivo*, we had to reduce our PRF to 2 kHz according to Fig. 4.3, which may correspond to a real situation setup were both a B-mode and a color-flow sequence are interleaved.

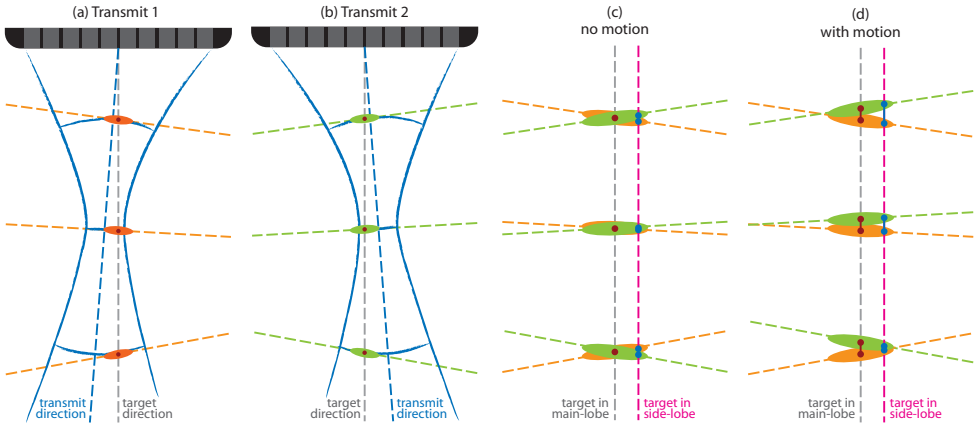


Figure 4.6: The velocity bias in the estimation process is caused by the difference of the transmit wavefronts. Close to the location of a scatterer, the PSF is aligned with the transmit wavefront as depicted in (a) and (b). When the receive direction is located in the main-lobe of the transmit beam, the velocity estimated along the targets direction is equal to the motion of the scatterers, as depicted in (c) and (d). When the receive direction is aligned with the side-lobe of the transmit beam, the velocity estimated is different from the real motion.

When looking at the phase estimates $\hat{\Phi}(n, \theta)$ computed on the simulated phantom,

we observed a bias around the bright scatterers or at the edges of the rectangular phantom. This bias is caused by the difference in the transmit wave fronts of the two receive lines $\vec{x}_{n,\theta}$ and $\vec{x}_{n+1,\theta}$, as illustrated in Fig. 4.6. When an ultrasound beam illuminates a given scatterer, the resulting PSF will be locally aligned with the wave front of the propagating pulse. If the scatterer is aligned with the transmit line direction, this effect will not be noticed: the scatterer will appear at its exact location and any axial motion of the target will result in a similar dephasing in the cross-correlation (4.2). However, if the point target is aligned with the direction of the side-lobes the transmit beam, its point spread function will be aligned with the transmit wavefront and the scatterer will present a small axial shift in the receive direction, even in the absence of motion. The cross-correlation may then under-estimate or over-estimate the target axial velocities based on the the spatial location of the target and the difference in the wave-front orientations at this location, as depicted in Fig. 4.6 (c) and (d). A similar phenomenon has already been observed when trying to image tissue velocities using the STB technique [19].

This phenomenon will appear as soon as the contrast between a target (or a medium) and its surrounding is high enough. The motion compensation algorithm is based on computing the cross-correlation between the two receive line and re-phasing the signals together. If the phase estimate presents a bias, we may expect the correction to produce erroneous results. Especially when a target with high reflection coefficient is located in the side-lobes of the transmit beams, the motion compensation scheme may have the effect of coherently summing the side-lobes of the two receive lines instead of summing them with a phase shift that would have decreased the side-lobe amplitudes. This means that the proposed STB motion compensation algorithm potentially has the drawback of reducing the spatial resolution at the boundaries between targets with a high contrast difference. However, both our phantom simulations and our *in vivo* acquisitions show no sign of this potential drawback. The bias phenomenon seems to be a major drawback only if displaying the velocities estimated in the STB phase compensation algorithm, such as in [19].

In conclusion, we have seen that the 2-D STB technique presents artifacts when velocities exceed about a quarter of wavelength per PRT. These artifacts can be compensated by a simple phase correction, but we cannot use the phase estimates as a safe basis for tissue velocity imaging (TVI) as it presents a systematic bias.

## 4.4 Extension to 3-D Imaging Applications

### 4.4.1 Synthetic Transmit Beams in 3-D

The Synthetic Transmit Beam technique can easily be extended to 3-D imaging by overlapping the receive beams both in the azimuth and elevation directions, as illustrated in Fig. 4.7(a). Using such a disposition, 4 receive lines corresponding to different transmit directions are coherently summed together for each receive direction. It is interesting to note that the STB interpolation is separable in azimuth and elevation, and can henceforth be divided in two stages as illustrated in Fig. 4.7(b):

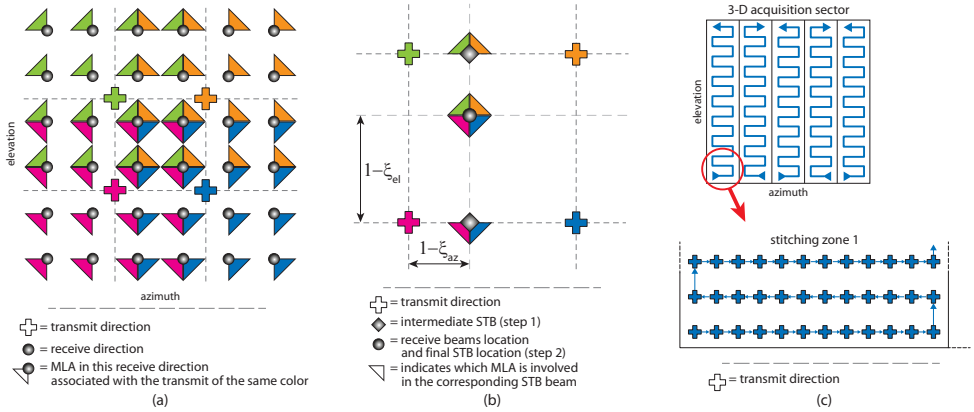


Figure 4.7: (a) Illustration of the transmit and parallel receive beams positions when used in combination with the 3-D STB technique. (b) The 3-D STB summation can be decomposed in two successive summations. (c) Proposed scan sequencing using both stitched acquisition zones synchronized with the ECG and an alternated scan direction (scanning back and forth) for each elevation plane.

- *step 1*: the beams transmitted in the same elevation planes but in different azimuth directions are merged together, forming two intermediate synthetic beams:

$$\vec{y}_{\theta}^{\,m} = \xi_{\text{az}} \cdot \vec{x}_{n,\theta}^{\,m} + (1-\xi_{\text{az}}) \cdot \vec{x}_{n+1,\theta}^{\,m} \tag{4.7}$$

$$\vec{y}_{\theta}^{\,m+1} = \xi_{\text{az}} \cdot \vec{x}_{n,\theta}^{\,m+1} + (1-\xi_{\text{az}}) \cdot \vec{x}_{n+1,\theta}^{\,m+1} \tag{4.8}$$

  where $\vec{x}_{n,\theta}^{\,m}$ denotes the IQ beamformed signals from transmit direction $n$ in azimuth and $m$ in elevation, focused on receive in the angular direction $\theta = \langle \theta_{\text{az}}, \theta_{\text{el}} \rangle$.

- *step 2*: these two intermediate synthetic beams resulting from two different elevation directions are summed together to form the final synthetic beam:

$$\vec{y}_{\theta} = \xi_{\text{el}} \cdot \vec{y}_{\theta}^{\,m} + (1-\xi_{\text{el}}) \cdot \vec{y}_{\theta}^{\,m+1} \tag{4.9}$$

The difference in the acquisition times of the beams merged in step 1 is always equal to the PRT. Therefore, we may expect motion artifacts similar to what was observed in 2-D STB. But, as seen previously, cardiac tissue does not move at axial velocities capable of triggering any STB motion artifact if an optimal PRF is chosen.

However, the difference in the acquisition times of the the intermediate synthetic beams merged in step 2 is much higher as it is typically equal to the time necessary to acquire one full 2-D plane. Therefore, we may expect motion artifacts even for smaller axial velocities such as observed in the myocardium. An obvious technique to minimize the effect of motion on our image is to reduce the time necessary to

acquire each elevation plane of our 3-D volume. In Section 4.3.2, we have seen that we needed about 60 transmissions to generate a fully sampled plane of 75°. Dividing the acquisition of our full 3-D volume over 5 heart cycles using an ECG-based stitching technique [25], we may limit the number of transmission for each elevation plane to $60/5 = 12$.

### 4.4.2 Obtaining Unbiased Velocity Estimates

Looking at Fig. 4.3, we observe that a division by 12 of the PRF will result in a very small upper limit for which tissue velocities can be corrected for using the cross-correlation method of Section 4.3.1 (i.e. the velocities leading to a signal phase shift under half a period). Practically, this means that tissue velocities must be corrected for using both a phase shift and a delay correction.

In order to obtain this delay correction, one must determine the displacement of the observed tissues between the time they were hit by the ultrasound pulse emissions and the time corresponding to our final STB beam. In a 3-D imaging situation, this time interval can be as large as the time required to acquire one full plane of data. The velocity estimations, however, must be computed between two in-plane transmissions to ensure a high correlation between the signals. The delay correction will thus be computed from the product between the estimated in-plane velocities and the number of transmissions between two planes (here, 12). Hence, any error in the in-plane velocity estimate will be multiplied: we need to ensure a robust velocity estimate.

In Section 4.3, we have observed that the estimation of the target velocity from cross-correlation presents a bias which is dependent on the difference in the transmit wave fronts combined into one STB line. If this biased velocity estimate is used in the 3-D motion compensation scheme where both a phase shift and a delay are applied, the bias will be multiplied by the number of transmit beams in a plane and will lead to incorrect delay compensations.

But in the vicinity of the transmit direction, one may consider the pulse wavefront to be locally planar with an angle perpendicular to the transmit beam steering direction. Doing so, the bias caused by the difference in the transmit wavefronts will be linearly dependent on the difference in steering direction between the beams (Fig. 4.6). When scanning in 3-D, the STB process can be seen as a summation of the STB beams synthesized from two elevation planes. If we estimate the tissue velocities from the first summation (step 1 in Fig. 4.7(b)) in both elevation planes, we should obtain two velocity estimations per spatial location. Merging these estimations will contribute to a lower variance in the estimator, but should not change the bias. If we now consider a scan sequencing as illustrated in Fig. 4.7(c), where the elevation planes are successively scanned in an alternated direction (back and forth), we will obtain two velocity estimations per spatial location with opposite bias (since the bias is proportional to the transmit angle difference). Averaging those two estimations should contribute to an estimate with both a lower variance and a canceled bias.

Therefore, a simple change in the 3-D STB scan sequencing (scanning back and forth in the successive elevation planes) allows for an unbiased estimation of the axial velocity, that can be used both as a TVI measurement and for a correction of eventual

motion artifacts in the STB technique.

### 4.4.3 Motion compensation algorithm for 3-D STB

Using the proposed alternated scan sequencing (Fig. 4.7(c)), the axial component of the velocities observed in a given receive direction can be estimated using the average of the cross-correlation estimates computed individually in the two elevation planes $m$ and $m+1$:

$$\begin{aligned}\hat{\Psi}_{\text{az}}(m,n,\theta) &= \angle\sqrt{\left\langle \hat{R}^{m}_{n,\theta}\right\rangle \cdot \left\langle \hat{R}^{m+1}_{n,\theta}\right\rangle},\\ \hat{R}^{m}_{n,\theta} &= \left(\vec{x}^{m}_{n+1,\theta}\right)^{*}\cdot \vec{x}^{m}_{n,\theta},\\ \hat{R}^{m+1}_{n,\theta} &= \left(\vec{x}^{m+1}_{n,\theta}\right)^{*}\cdot \vec{x}^{m+1}_{n+1,\theta}\end{aligned} \tag{4.10}$$

The cross-correlation can be averaged axially and in the azimuth direction between the beams corresponding to the same pair of transmit beams. As mentioned previously, $\hat{\Psi}_{\text{az}}(m,n,\theta)$ is an unbiased estimate that can be related to the tissue velocity using (4.3).

In order to minimize the influence of the so-called motion artifacts in the 3-D STB B-mode images, both a phase-shift and a delay correction are applied while generating our synthetic beams in the previously described step 1:

$$\begin{aligned}\vec{y}^{m}_{\theta}(t) = \xi_{\text{az}}\cdot e^{i\cdot\varphi_1(m,n,\theta)}\cdot \vec{x}^{m}_{n,\theta}(t+\tau_1(m,n,\theta))\\ +(1-\xi_{\text{az}})\cdot e^{i\cdot\varphi_2(m,n,\theta)}\cdot \vec{x}^{m}_{n+1,\theta}(t+\tau_2(m,n,\theta))\end{aligned} \tag{4.11}$$

$$\begin{aligned}\vec{y}^{m+1}_{\theta}(t) = \xi_{\text{az}}\cdot e^{i\cdot\varphi_3(m,n,\theta)}\cdot \vec{x}^{m+1}_{n,\theta}(t+\tau_3(m,n,\theta))\\ +(1-\xi_{\text{az}})\cdot e^{i\cdot\varphi_4(m,n,\theta)}\cdot \vec{x}^{m+1}_{n+1,\theta}(t+\tau_4(m,n,\theta))\end{aligned} \tag{4.12}$$

where the applied correction phase shifts and delays are respectively given by:

$$\begin{aligned}\varphi_i(m,n,\theta) &= \chi^{m,n}_{i}\cdot\hat{\Psi}_{\text{az}}(m,n,\theta),\\ \tau_i(m,n,\theta) &= \frac{\varphi_i(m,n,\theta)}{2\pi\cdot f_0},\\ i &\in \{1,2,3,4\}\end{aligned} \tag{4.13}$$

and the $\chi^{m,n}_{i}$ are defined as the normalized temporal distance between each individual transmit timing $t^{m}_{n}$ and the desired synthesized transmit direction timing $t_\theta$:

$$\begin{aligned}\chi^{m,n}_{1} &= PRF\cdot(t_\theta - t^{m}_{n})\\ \chi^{m,n}_{2} &= PRF\cdot(t_\theta - t^{m}_{n+1})\\ \chi^{m,n}_{3} &= PRF\cdot(t_\theta - t^{m+1}_{n})\\ \chi^{m,n}_{4} &= PRF\cdot(t_\theta - t^{m+1}_{n+1})\end{aligned} \tag{4.14}$$

This first correction scheme is not sufficient, as small errors in the phase-shift estimator will have a different impact on the resulting image depending on the location of the receive beam in the azimuth plane. Using the alternated scan sequencing presented in Fig. 4.7(c), one can see that the time difference between two elevation planes is different in the right-hand side and the left-hand side of the images. As a result, a small error in the estimation of $\hat{\Psi}_{\text{az}}(m,n,\theta)$ will be increased many folds on one side of the plane, by a factor $\chi_i^{m,n}$. Using 12 transmission directions in azimuth, the estimation error will be multiplied by a factor up to 12. If this multiplication leads to delay correction errors comparable with the pulse length, the motion correction process is susceptible to fail. In order to cope with this phenomenon, a second cross-correlation is computed between the intermediate synthetic beams:

$$\begin{aligned}\hat{\Psi}_{\text{el}}(m,\theta) &= \angle\left\langle \hat{R}_\theta^m \right\rangle \\ &= \angle\left\langle \left(\vec{y}_\theta^{m+1}\right)^* \cdot \vec{y}_\theta^m \right\rangle\end{aligned} \tag{4.15}$$

This cross-correlation estimate is then used to correct for misalignments introduced by the multiplication of small errors on the phase estimate $\hat{\Psi}_{\text{az}}$ in (4.13) when merging the two intermediate synthetic beams into the final STB line:

$$\begin{aligned}\vec{y}_\theta =& \xi_{\text{el}} \cdot e^{i\cdot(1-\xi_{\text{el}})\cdot\hat{\Psi}_{\text{el}}(m,\theta)} \cdot \vec{y}_\theta^m \\ &+ (1-\xi_{\text{el}}) \cdot e^{-i\cdot\xi_{\text{el}}\cdot\hat{\Psi}_{\text{el}}(m,\theta)} \cdot \vec{y}_\theta^{m+1}\end{aligned} \tag{4.16}$$

### 4.4.4 Simulation - Method

Simulations were conducted using Field II in order to evaluate the effects of motion on the STB technique in 3-D. The phantom is similar to the one used for the 2-D simulations (4 scatterers per resolution cell), but extended in the elevation direction. The phantom is moving vertically with a velocity varying from 0 cm/s to 20 cm/s. The field of view is set up to a 15° × 75° sector, which is comparable with what can be acquired using ECG-stitching in the azimuth direction. The scan sequencing follows the alternated direction described in Fig. 4.7(c), and is described more in depth in Table 4.2. On transmit, the lateral spacing is equal to the Rayleigh criterion for full sampling, and the apodization function was set to a triangular window such as to mimic the pressure field generated by the second harmonic component of the signal. On receive, 4 × 4 parallel beams (MLA) are generated and combined into a 2 × 2 STB pattern as detailed in Fig. 4.7(a), with or without motion correction. The beams are then further interpolated laterally (both in the azimuth and elevation directions) before envelope detection. In the motion compensation algorithm, the cross-correlation (4.10) was computed using a sliding hamming window in the axial direction (2.5 mm long), and then averaged laterally between all the beams corresponding to the same pair of transmit beams.

Table 4.2: Experimental 3-D Setup Parameters

| | Azimuth | Elevation |
|---|---|---|
| Transducer geometry | 20.5 mm | 16.4 mm |
| Transmit focal distance | 85 mm | 85 mm |
| $f$-number transmit | 4.62 | 5.78 |
| $f$-number receive | 2 until 40.5 mm | 2 until 32.3 mm |
| Sector size | 15° | 75° |
| Number of transmit beams | 12 | 46 |
| Parallel receive lines | 4 | 4 |
| Transmit center frequency | 1.67 MHz, 60% bandwidth | |
| PRF | 5.133 kHz | |

### 4.4.5 Simulation - Results

The centermost planes of the 3-D sector, both in the azimuth and elevation directions, are presented in Fig. 4.8 when using the STB technique. Axial motion is seen to generate motion artifacts which take the form of darker stripes. These stripes are no longer disposed in a regular pattern in the azimuth plane as visualized for the 2-D acquisition pattern, but show up at different lateral positions. At these lateral positions, the difference in transmit time between the four firings involved in the STB summation is prone to generate artifacts corresponding to the observed motions.

A second version of these 3-D STB images when using the proposed motion compensation algorithm is given in Fig. 4.9. We observe that the compensation scheme successfully recovered the losses in intensity caused by motion during the STB summation, without introducing any major damage to the image. We may observe that the speckle after the compensation algorithm has lost a bit of its granularity, but this phenomenon is minor and hard to quantify.

The velocity estimated for every situation from the cross-correlation angle $\hat{\Psi}_{\text{az}}$ is displayed in Fig. 4.10. When comparing with the velocity estimates from the 2-D STB sequence (Fig. 4.5, bottom row), we observe that the bias observed at the edge of the phantom and around the scatterers have disappeared. The noise in the estimated velocity is also more concentrated, between $[-\pi/2; \pi/2]$, due to the averaging of equation (4.10).

## 4.5 Discussion

We have shown that using STB to image rapidly moving targets leads to noticeable artifacts in the image. In practice, this phenomenon may be observed in applications where the acquisition rate is slow, such as interleaved B-mode / Doppler, B-mode when the range span is large or 3-D B-mode volume acquisitions. While this

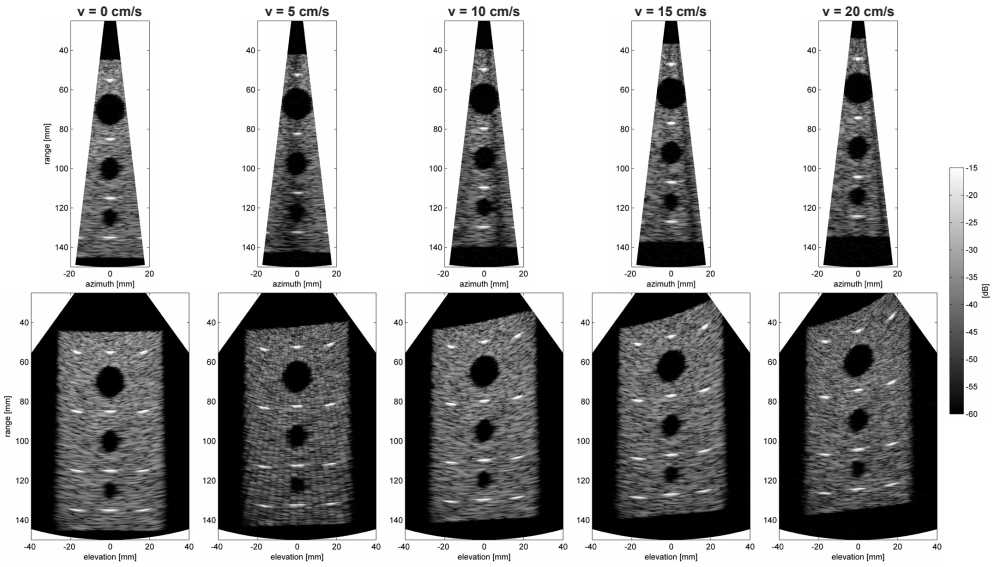


Figure 4.8: B-mode images of a simulated phantom moving upwards using a $2 \times 2$ STB pattern. The central planes of a 3-D stitching volume both in the azimuth and elevation directions are represented.

phenomenon may lead to severe image degradations, it follows a simple model and can be compensated for using a cross-correlation based algorithm. Furthermore, the phase estimates obtained in the compensation algorithm may be used as a supplementary tissue velocity (TVI) estimate without requiring any addition in the acquisition scheme.

Initially we have simulated the effects of axial motion on a simple phantom using a STB based 2-D acquisition. While simulated phantom velocities (up to 1 m/s) seem unrealistic for *in vivo* tissues (the myocardium has components up to 20 cm/s), they provided a perfect example of the phenomenon we wanted to observe.

When going to 3-D imaging, two important considerations must be taken: the time between two successive planes in the elevation direction is much larger than the interval between two successive in-plane beams; and the acquisition process is done by scanning back and forth each plane, leading to unequal time difference at different azimuth positions within two successive planes. As a result, the motion artifacts will happen for lower axial velocities compared to 2-D, as illustrated in Fig. 4.8, but will also appear in more irregular positions in the image.

The main result of this study is the observation that both our correction algorithms succeeded in compensating for the velocity artifacts without reducing the overall image quality. In 3-D, though, we observed a small loss in the granularity of the speckle. This loss is caused by the second correction step in the motion compensation algorithm. This second correction step has been implemented to cope with small errors in the estimation of the tissue velocities which will be multiplied when applying the delay

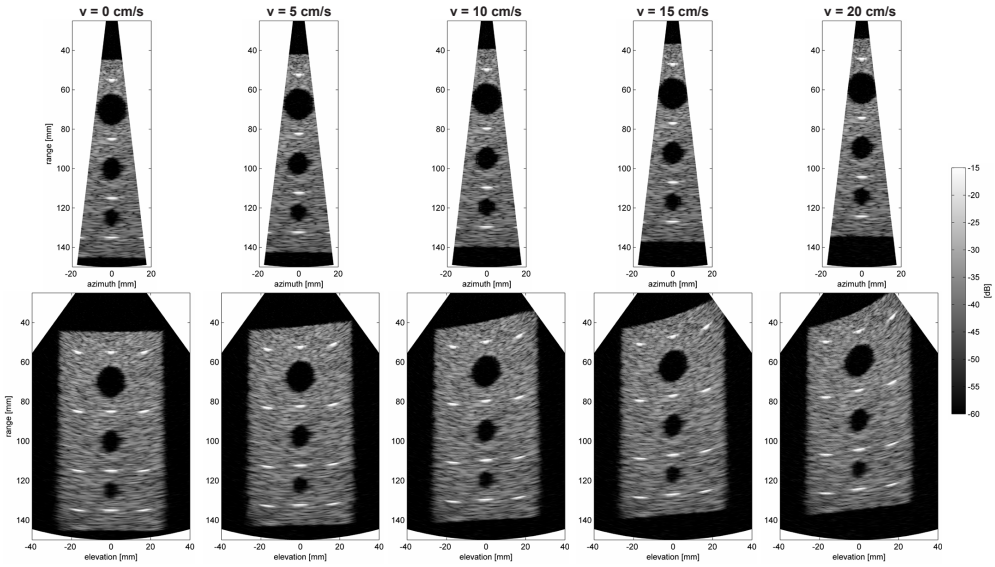


Figure 4.9: B-mode images of a simulated phantom moving upwards using a $2 \times 2$ STB pattern with the proposed motion correction algorithm. The central planes of a 3-D stitching volume both in the azimuth and elevation directions are represented.

and phase correction over two elevation planes in (4.13). While this second step is necessary, it has for effect of detecting the small phase difference naturally present in the speckle and to align them, resulting in a speckle more homogeneous. This phenomenon is more present in the elevation direction where the side-lobes of the system are more intense and hence more prone to be detected and amplified by the second step of the correction scheme.

The cross-correlation between different beamformed lines as presented in this study is an operation with a rater low computational load. While the processing for this study was done in Matlab, we believe that the algorithms presented may be implemented for real-time applications on a modern ultrasound scanner.

The quality of the correction algorithm is based on the correctness of the cross-correlation estimates. Using the 2-D STB acquisition, we have seen that the phase estimates suffer from a bias caused by the difference between the transmit wave fronts of the successive transmit beams. This bias is particularly visible around strong point scatterers or at the edge of the phantom. When going to 3-D, we proposed a new way to estimate the axial velocity by averaging the estimates from two successive elevation planes scanning in opposite directions. This estimation is improved compared to the 2-D situation as the bias is canceled. But in order to provide a correct value, the velocity of the tissues must remain constant during the interval it takes to acquire two planes (with 12 transmit per plane). This assumption may be considered as valid during most of the cardiac cycle [24].

There are several other ways to further improve the cross-correlation estimates.

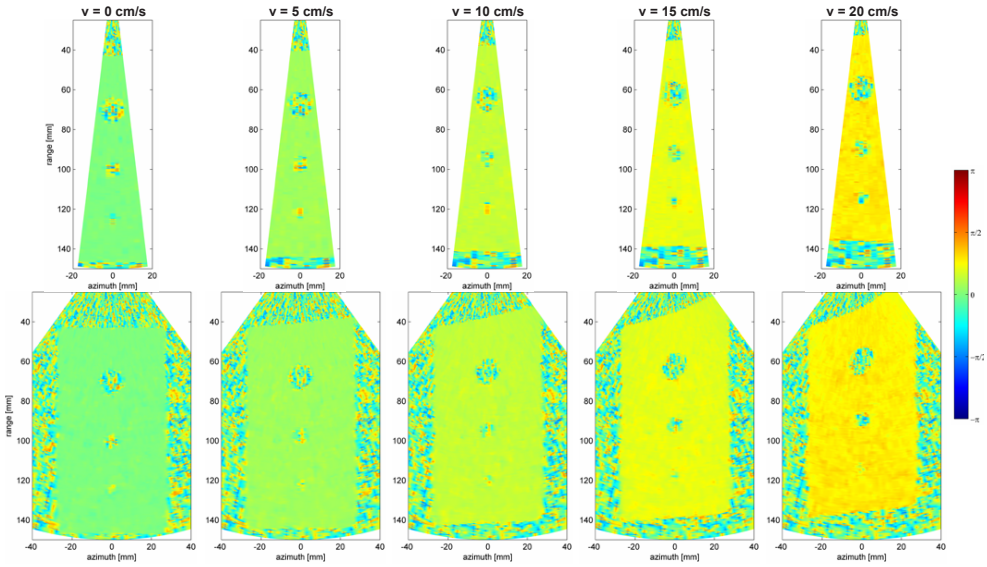


Figure 4.10: Phase estimates used by the motion correction algorithm for the simulated phantom. The central planes of a 3-D stitching volume both in the azimuth and elevation directions are represented.

Spatial averaging is a method which is used in this study, but needs to be dimensioned according to how quickly the velocity changes in the averaging dimension, so that the spatial resolution will not be degraded. In addition, one may consider an alternative scan sequencing where the adjacent transmit beams are not fired right after the other, but with a longer time interval equivalent to 3 times the PRT, by using packet interleaving techniques such as in [19]. By increasing the effective time between two adjacent beams, the phase estimate resulting from cross-correlation will have the same variance but with a higher observed displacement, resulting in a decreased variance for the velocity estimates. Note that using this technique will also reduce the maximal velocity which can be observed without aliasing, but this seems appropriate for tissue imaging in 3-D echocardiography, since the maximal phase estimates in Fig. 4.10 were about $\pi/3$ for a velocity component of 20 cm/s.

In our simulations, even though the velocity estimates are suboptimal (the variance could have been reduced as described previously, and the 2-D simulations present an additional bias), the results of the motion correction process do not seem to be affected. According to the principles presented in Fig. 4.6, the phase bias and the estimation errors may result in undesired coherent summation of side-lobes, which will lead to poorer lateral resolution and reduce the sharpness of boundaries. These phenomenons could however not be observed either in simulations or in our *in vivo* measurements. Thus, the estimation errors were only a concern when using the phase estimates as an additional TVI modality as in Fig. 4.4.

While the motion artifact phenomenon may be observed in a clear and regular

pattern in 2-D (Fig. 4.5), the irregularity of the artifacts position in a 3-D volume made it complicated to provide an *in vivo* example. The artifacts were clearly noticeable in our 3-D simulations (Fig. 4.8), but *in vivo* the motion stripes will appear at rather random locations since there is no spatial uniformity of the velocity field as provided in the simulations.

## 4.6 Conclusion

Targets moving rapidly in the axial direction will cause noticeable image artifacts when using Synthetic Transmit Beamforming. This is particularly true in 3-D imaging, where it is impossible to avoid large time delays between transmits in one of the dimensions. In this study, we have illustrated these effects using both a simple mathematical approach, linear simulations, and *in vivo* measurements. Artifacts appearing as dark stripes with up to 15 dB gain reduction were observed as a result of axial velocities.

A cross-correlation based algorithm was proposed to estimate and correct for the axial motion. The method has proven successful both in 2-D and 3-D imaging and provides an additional TVI modality without impairing the frame rate.

This work might be adapted to similar coherent processing techniques such as Coherent Plane Wave Imaging or other Synthetic Transmit Aperture applications.

## Acknowledgment

The researchers thank GE Vingmed Ultrasound for access to a Vivid E9 ultrasound scanner.

# References


[1] L. P. Badano, R. M. Lang, and J. L. Zamorano, *Textbook of Real-Time Three Dimensional Echocardiography*, vol. 129. Springer, 2011.

[2] O. T. Von Ramm and S. W. Smith, "Real time volumetric ultrasound imaging system.," *Journal of digital imaging the official journal of the Society for Computer Applications in Radiology*, vol. 3, no. 4, pp. 261–266, 1990.

[3] O. T. Von Ramm, S. W. Smith, and H. G. Jr Pavy, "High-speed ultrasound volumetric imaging system. II. Parallelprocessing and image display," *IEEE Transactions on Ultrasonics, Ferroelectrics, and Frequency Control*, vol. 38, no. 2, pp. 109–115, 1991.

[4] K. Thomenius, "Evolution of ultrasound beamformers," in *IEEE Ultrasonics Symposium, Proceedings*, vol. 2, pp. 1615–1622, IEEE, 1996.

[5] G. Montaldo, M. Tanter, J. Bercoff, N. Benech, and M. Fink, "Coherent plane-wave compounding for very high frame rate ultrasonography and transient elastography," *IEEE Transactions on Ultrasonics, Ferroelectrics, and Frequency Control*, vol. 56, no. 3, pp. 489–506, 2009.

[6] J. Jensen, H. Holten-Lund, and R. Nilsson, "SARUS: A synthetic aperture real-time ultrasound system," *IEEE Transactions on Ultrasonics, Ferroelectrics, and Frequency Control*, vol. 60, no. 9, pp. 1838–1852, 2013.

[7] T. Hergum, T. Bjåstad, K. Kristoffersen, and H. Torp, "Parallel beamforming using synthetic transmit beams," *IEEE Transactions on Ultrasonics, Ferroelectrics, and Frequency Control*, vol. 54, no. 2, pp. 271–280, 2007.

[8] T. Bjåstad, *High frame rate ultrasound imaging using parallel beamforming*. PhD thesis, NTNU, 2009.

[9] T. Bjåstad, S. A. Aase, and H. Torp, "The impact of aberration on high frame rate cardiac B-mode imaging.," *IEEE Transactions on Ultrasonics, Ferroelectrics, and Frequency Control*, vol. 54, pp. 32–41, Jan. 2007.

[10] T. Bjåstad, S. A. Aase, and H. Torp, "Synthetic transmit beam technique in an aberrating environment.," *IEEE Transactions on Ultrasonics, Ferroelectrics, and Frequency Control*, vol. 56, pp. 1340–51, July 2009.

[11] T. Hergum, T. Bjåstad, L. Løvstakken, K. Kristoffersen, and H. Torp, "Reducing color flow artifacts caused by parallel beamforming.," *IEEE Transactions on Ultrasonics, Ferroelectrics, and Frequency Control*, vol. 57, pp. 830–8, Apr. 2010.

[12] K. S. Kim, J. S. Hwang, J. S. Jeong, and T. K. Song, "An efficient motion estimation and compensation method for ultrasound synthetic aperture imaging.," *Ultrasonic imaging*, vol. 24, pp. 81–99, Apr. 2002.

[13] J. Jeong and J. Hwang, "Effects and limitations of motion compensation in synthetic aperture techniques," *IEEE Ultrasonics Symposium, Proceedings*, pp. 1759–1762, 2000.

[14] C. Hazard and G. Lockwood, "Effects of motion on a synthetic aperture beamformer for real-time 3D ultrasound," *IEEE Ultrasonics Symposium, Proceedings*, pp. 1221–1224, 1999.

[15] M. Karaman, H. S. Bilge, and M. O'Donnell, "Adaptive multi-element synthetic aperture imaging with motion and phase aberration correction.," *IEEE Transactions on Ultrasonics, Ferroelectrics, and Frequency Control*, vol. 45, pp. 1077–87, Jan. 1998.

[16] M. Bae and J. Ham, "Method of removing an effect of side lobes in forming an ultrasound synthetic image by motion estimation and compensation," *EP Patent 2,053,420*, vol. 1, no. 3, pp. 458–464, 2009.

[17] J. Wang and J.-y. Lu, "Motion artifacts of extended high frame rate imaging.," *IEEE Transactions on Ultrasonics, Ferroelectrics, and Frequency Control*, vol. 54, pp. 1303–15, July 2007.

[18] B. Denarie, T. A. Tangen, I. K. Ekroll, N. Rolim, H. Torp, T. Bjåstad, and L. Løvstakken, "Coherent plane wave compounding for very high frame rate ultrasonography of rapidly moving targets.," *IEEE Transactions on Medical Imaging*, vol. 32, pp. 1265–76, July 2013.

[19] T. Bjåstad and H. Torp, "Single-pulse tissue doppler using synthetic transmit beams.," *IEEE Transactions on Ultrasonics, Ferroelectrics, and Frequency Control*, vol. 56, pp. 2134–44, Oct. 2009.

[20] J. Jensen and N. Svendsen, "Calculation of pressure fields from arbitrarily shaped, apodized, and excited ultrasound transducers," *IEEE Transactions on Ultrasonics, Ferroelectrics, and Frequency Control*, vol. 39, no. 2, pp. 262–267, 1992.

[21] J. Jensen, "Field: A program for simulating ultrasound systems," *Medical and Biological Engineering and Computing*, vol. 34, pp. 351–353, 1996.

[22] J. Wright, "Image formation in diagnostic ultrasound," *IEEE International Ultrasonic Symposium Short Course*, 1997.

[23] M. E. Anderson and G. E. Trahey, "A seminar on k -space applied to medical ultrasound," *Biomedical Engineering*, 2000.

[24] B. Brekke, H. Torp, and T. Bjåstad, "3D Tissue Doppler imaging with ultra high frame rate," *IEEE Ultrasonics Symposium, Proceedings*, pp. 717–720, 2011.

[25] S. Brekke, S. I. Rabben, A. Støylen, A. Haugen, G. U. Haugen, E. N. Steen, and H. Torp, "Volume stitching in three-dimensional echocardiography: distortion analysis and extension to real time.," *Ultrasound in Medicine & Biology*, vol. 33, pp. 782–96, May 2007.

# Chapter 5

# Coherent Plane Wave Compounding for Very High Frame Rate Ultrasonography of Rapidly Moving Targets

Bastien Dénarié[1], Thor Andreas Tangen[1], Ingvild Kinn Ekroll[1], Natale Rolim[1], Hans Torp[1], Tore Bjåstad[2] and and Lasse Løvstakken[1]
[1]MI-Lab, Department of Circulation and Medical Imaging, Faculty of Medicine, Norwegian University of Science and Technology (NTNU)
[2]GE Vingmed Ultrasound AS, Horten, Norway

Coherent plane wave compounding is a promising technique for achieving very high frame rate imaging without compromising image quality or penetration. However, this approach relies on the hypothesis that the imaged object is not moving during the compounded scan sequence, which is not the case in cardiovascular imaging. This work investigates the effect of tissue motion on retrospective transmit focusing in coherent compounded plane wave imaging (PWI). Two compound scan sequences were studied based on a linear and alternating sequence of tilted plane waves, with different timing characteristics.

Simulation studies revealed potentially severe degradations in the retrospective focusing process, where both radial and lateral resolution was reduced, lateral shifts of the imaged medium were introduced, and losses in SNR were inferred. For myocardial imaging, physiological tissue displacements were on the order of half a wavelength, leading to SNR losses up to 35 dB, and reductions of contrast by 40 dB. No significant difference was observed between the different tilt sequences.

A motion compensation technique based on cross-correlation was introduced, which significantly recovered the losses in SNR and contrast for physiological tissue velocities. Worst case losses in SNR and contrast were recovered by 35 dB and 27-35 dB respectively. The effects of motion were demonstrated *in vivo* when imaging a rat heart. Using PWI, very high frame rates up to 463 fps were achieved at high image quality, but a motion correction scheme was then required.

## 5.1 Introduction

Diagnostic ultrasound is associated with real-time imaging capabilities at high frame rates compared to other image modalities such as MR and CT. It has thus become the preferred modality for instance in cardiovascular applications where dynamic properties of myocardial contractions or blood flow may be associated with pathology. These capabilities have been established due to continuous technological developments from early analog to modern digital beamformers. Despite these advances, the current acquisition rate is still a limiting factor which compromises image quality, in particular for 3-D imaging, but also in general when combining both tissue and blood flow imaging in a duplex or triplex modality.

In recent years, several techniques have been proposed to further increase the acquisition rate in ultrasound imaging. Most approaches have been based on parallel receive beamforming (PRB), where several receive lines are beamformed in parallel for each transmitted pulse. This concept was first introduced for use in ultrafast cardiac imaging systems [1, 2] in the late 70's, where 20 lines could be formed in parallel to produced echographic images of the heart at 5000 frames per second; and was soon adapted for early 3-D imaging systems [3, 4]. Currently the computational resources available using standard multi-core CPU's or GPU's allows for full parallel beamforming of all image lines in real-time 2-D imaging. This concept of software beamforming offers a significant leap in flexibility for the development of new image reconstruction algorithms.

When combined with focused transmit beams, PRB is associated with image artifacts due to a misalignment of transmit and receive beams [5]. Although coherent interpolation techniques have been introduced to correct for these misalignments [5, 6], the maximum number of parallel receive beams is ultimately limited by the transmit beam width. A different transmit strategy is thus needed where a larger region of tissue is insonified in order to exploit a high degree of PRB. The two most investigated approaches are based on either defocused or unfocused transmit beams. Emitting broad pulses is however associated with a reduction in image contrast, resolution, and signal-to-noise ratio. In order to compensate it is has been proposed to coherently combine received low-resolution images to synthetically reproduce transmit focusing and aperture. This approach has in the literature been called synthetic (transmit) aperture [7, 8] or coherent plane wave compounding [9]. The latter should not be mistaken for incoherent image compounding used to reduce angle-dependent scattering and to smooth speckle noise [10].

In synthetic transmit aperture imaging (STAI) defocused pulses are emitted using small apertures, and a low-resolution image is formed for each transmit event [11, 12]. By subsequently emitting from different parts of the transducer, transmit focusing can be reconstructed by coherently adding a number of low-resolution images. Assuming a sliding window summation, the imaging frame rate is equal to the pulse repetition frequency, i.e. in the kHz range.

In plane wave imaging (PWI), an unfocused pulse is emitted over the full transducer aperture in order to insonify a broader field of view. Similar as for STAI, coherent summation of several plane waves transmitted at different angles has been proposed to

efficiently restore transmit focusing [1, 9]. Further, the use of more complex transmit pulse schemes were introduced to increase penetration and limit diffraction effects [13]. Compared to STAI, this approach emits more energy for each transmitted pulse, but is so far limited to linear arrays in order to achieve a full field of view. As for STAI, one image can be produced per emitted pulse, and very high frame rates can be achieved.

This very high frame rate capability offers new possibilities, such as the merging of the conventional color flow imaging with local pulsed-wave (PW) Doppler [14–16], elastography [17, 18], or ultrafast imaging of the myocardium [19].

Both STAI and PWI techniques are dependent on the coherent summation of several transmit events in order to produce B-mode images of quality comparable to that of using traditional focused beams. However, when the object under insonification moves between transmit events, perfect coherent summation is no longer achieved [20]. This susceptibility to movement restricts the number of transmit events which may be combined, and may infer significant image artifacts. Several approaches to limit this effect were proposed for STAI where compensation is made during beamforming given the estimated displacements of tissue or flow [21–23].

In this work the effects of object motion on image quality when using coherent compounding in plane wave imaging has been investigated in detail. Two different pulse sequences are evaluated for objects moving radially. Further, the possibility of limiting the number of plane wave transmit events to reduce motion susceptibility by increasing the angle increment is investigated. Finally, an algorithm is proposed to compensate for the movement during coherent summation in order to reduce image artifacts while retaining a high frame rate. Theoretical aspects and simulation models are used to investigate the effect of motion in detail. A relevant application where a high frame rate is needed and where object motion is a limiting factor is cardiovascular imaging in small-animal models. We present *in vivo* results to demonstrate the challenges in such settings, and the possibility to correct for motion artifacts.

## 5.2 Resolution of Coherent Plane Wave Compounding Systems

### 5.2.1 Plane wave imaging

Consider the transmitted sequence of $N$ plane waves with inclination

$$\alpha_n = \operatorname{asin}\left(n\lambda/L\right) \approx n\lambda/L\,, n = -(N-1)/2, .., (N-1)/2\,, \tag{5.1}$$

where $L$ is the size of the aperture, $\lambda$ is the transmitted pulse wavelength, and the approximation is valid for small inclinations. The beam profile at focal depth, $z = z_f$, for the monochromatic case can be written as [9],

$$p_c\left(x,t\right) = \sum_{n=-(N-1)/2}^{(N-1)/2} p_0 \exp\left\{j\left(2\pi x n/L - \omega t\right)\right\}\,. \tag{5.2}$$

This can be recognized as a geometric series and the sum can be written as

$$p_c\left(x,t\right) = p_0 \exp\left\{-j\omega t\right\} \frac{\sin\left(\frac{\pi x N}{L}\right)}{\sin\left(\frac{\pi x}{L}\right)} \exp\left(-j\frac{2\pi x}{2L}\right), \tag{5.3}$$

where $x$ is the distance from the imaging axis and $N$ is the number of angles in the sequence.

The number of angles to use in order to achieve equivalence with conventional imaging can be found by comparing the expressions for the beam profile in focus for the two methods. For conventional imaging, the beam profile in focus for the monochromatic case, using a linear array with pitch $\Delta x$, can be expressed as [24]

$$p\left(x, z_f, t\right) = p_0 \exp\left\{-j\omega t\right\} \frac{\sin\left(\frac{kxL}{2z_f}\right)}{\sin\left(\frac{kx\Delta x}{2z_f}\right)} \exp\left(-j\frac{kx\Delta x}{2z_f}\right), \tag{5.4}$$

where $k$ is the wave number $\omega/c$. To achieve equality between (5.3) and (5.4), the number of angles in the sequence must be

$$N = \frac{L}{F_{\#}\lambda}, \tag{5.5}$$

where $F_{\#} = z_f/L$ is the F-number.

Looking closer at the expression for the number of angles, (5.5), using an odd number of angles, the F-number can be expressed as

$$F_{\#} = \frac{L}{N\lambda} \approx \frac{1}{N\Delta\alpha} = \frac{1}{2\alpha_{max}} \frac{N-1}{N} \approx \frac{1}{2\alpha_{max}}. \tag{5.6}$$

Note that $N$ is the number of angles of the complete angle sequence, i.e. the sequence required to achieve equivalence.

### 5.2.2 Effects of Decimation

The F-number gives an indication of the beam width and thus the lateral resolution of the image. The expression in Equation (5.6) indicates that the resolution in the image is only a function of the maximum angle used and not the actual angle sequence. Thus, by decimating the angle sequence, but maintaining the maximum angle, one could achieve higher frame rate without losing resolution. The plane wave beam profile for the decimated angle sequence can be expressed as

$$p_c\left(x,t;D\right) = p_0 \frac{N}{D} \exp\left\{-j\omega t\right\} \frac{\sin\left(\frac{\pi x(N+(D-1))}{L}\right)}{\sin\left(\frac{\pi x D}{L}\right)}, \tag{5.7}$$

where $D$ is the decimation factor.

Though the beam width might be unaffected, decimation will introduce grating-lobes. For no decimation, *i.e.* D = 1, the denominator of the expression in (5.3) has

its first zero for the same value of $x$ as the numerator. For increasing values of $D$, the denominator will have its zeros at integer multiples of $x/D$, while the numerator will have its zeros at close to the same values of x as before. In Fig. 5.1, continuous wave (CW) beam profiles for different decimation factors are shown. Increasing the decimation factor introduce grating-lobes, increasingly closer to the main-lobe of the beam. The grating-lobes will not affect the beam width notably for decimation factors less than 8, but the contrast resolution will be affected.

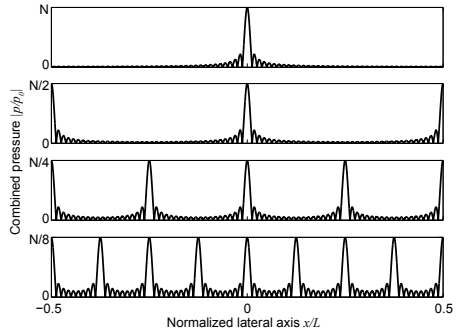


Figure 5.1: The combined pressure field $|p/p_0|$ using $N$ transmit angles plotted for decimation factors 1, 2, 4 and 8 as a function of $x/L$

## 5.3 Coherent Plane Wave Compounding in Presence of Motion

### 5.3.1 Effects of Motion

Since plane wave imaging generates the transmit focus synthetically by combining multiple plane wave transmissions coherently, the method is affected by motion of the object. If the scatterers move between each plane wave transmission, the plane waves will not be added coherently, thus possibly affecting the image quality. This is especially the case for radial velocities, i.e. velocities perpendicular to the surface of the transducer as illustrated in Fig. 5.2(a), where a small displacement of half a pulse period during the time required to acquire a frame will lead to destructive interferences in the compounding operation. In the case of lateral velocities, i.e. velocities parallel to the surface of the transducer, the displacements are expected to have a smaller influence on the image [20], since the point spread function acts as a spatial low-pass filter.

This phenomenon is illustrated for a single point scatterer in Fig. 5.2. In the absence of motion, the plane wave compounding algorithm will sum coherently the received echoes (here represented by their edge waves as presented in (b)) with a delay such as a synthetic focus is recreated on each point as in (c). In the presence of radial motion in the target as in (d), the wave fronts do not longer superpose at the desired

location, but instead refocus at two different locations with a lateral shift equal to:

$$\delta_{lat} = \frac{2 \cdot v_{rad}}{D \cdot \mathrm{PRF} \cdot \tan \Delta\alpha} = \frac{2 \cdot v_{rad}}{D \cdot \mathrm{PRF} \cdot \tan \frac{1}{NF_{\#}}}, \tag{5.8}$$

where $v_{rad}$ is the radial velocity, PRF is the pulse repetition frequency and $D$ is the decimation factor.

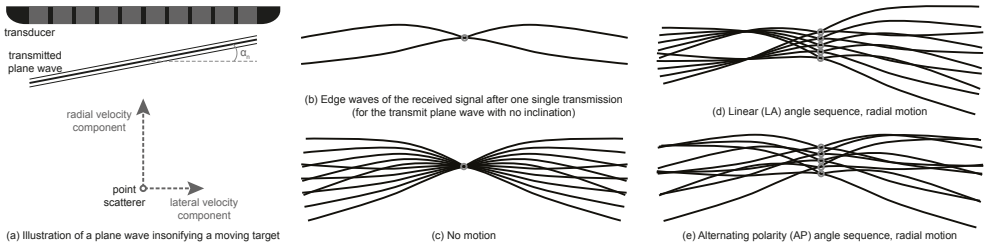


Figure 5.2: Superposition of the edge waves received for several plane wave transmissions in presence of a point scatterer moving upwards. The positions of the point scatterer at the time it is imaged by each plane wave are indicated with a gray circle.

As seen in Fig. 5.2 (d), the motion will affect both the lateral and radial resolution. Due to the motion, the different plane waves can in the worst case be added destructively, and the amplitude of the echo can be significantly reduced. This effect can give flickering in the gray scale images when the tissue velocities are varying with time, as it may be the case *in vivo* in *e.g.* the myocardium.

### 5.3.2 Reducing the Influence of Motion Using an Alternative Scan Sequencing

In order to reduce the influence of motion on the plane wave compounded images, different approaches can be followed:

- decimation of the angle sequence can be used to decrease the total time used for each compounded frame,
- the transmit sequence can be changed to be less sensitive to motion of the imaged object,
- the motion can be estimated and compensated during beamforming, as proposed in the following section.

Decimation of the angle sequence will result in a reduced displacement of the moving object during the acquisition of each frame. This can be expected to compensate the loss in image resolution due to motion, but the contrast resolution will be reduced. The authors believe there is a trade-off between the achieved frame rate and the obtained contrast that must be evaluated for each specific application.

Changing the transmit scan sequence to modify the impact of motion on the compounding may be realized using alternated polarity sequencing. This is done by transforming the classical sequence with a linear angle increment $[-\alpha_N, -\alpha_{N-1}, ..., -\alpha_1, 0, \alpha_1, ..., \alpha_{N-1}, \alpha_N]$ to a sequence where the transmit angles is alternatively positive and negative $[-\alpha_N, \alpha_N, -\alpha_{N-1}, \alpha_{N-1}, ..., -\alpha_1, \alpha_1, 0]$. Using an alternated polarity transmit sequence will not cancel the effect of motion, but will avoid the lateral shift of the focus observed with linear sequences as shown in 5.2 (e). In addition, this technique should lead to a contrast equivalent to the linear sequence, and therefore will reduce the influence of motion while keeping a high contrast. In the following, we shall use the abbreviations LA for sequencing with linearly increasing angles, and AP for alternated polarity sequencing.

### 5.3.3 Cross-correlation Based Motion Compensation

Correlation methods are widely used in ultrasonography for estimating the radial velocities of tissue and fluids in the observed field of view. In this study, we propose to adapt the cross-correlation method to estimate and correct for the motion observed between the low-resolution images formed for each plane wave acquisition, before compounding them to a high-resolution image.

Consider a group of scatterers moving at a given velocity with component $v_{rad}$ towards the transducer. The difference in the position of the scatterers at the time they are insonified by two successive plane waves is reflected as a time shift in the received beamformed signals. If motion is sufficiently small (less than a quarter of a wavelength), this time shift can be approximated to a phase shift in the received quadrature-demodulated (IQ) signals:

$$\angle x_{\alpha_{n+1},m} - \angle x_{\alpha_n,m} \approx \frac{4\pi \cdot f_0}{PRF} \cdot \frac{v_{rad}}{c}, \tag{5.9}$$

where $x_{\alpha_n,m}$ is the IQ signal received for the plane wave transmitted at an angle $\alpha_n$ and beamformed for the lateral line $m$, $f_0$ is the demodulation frequency, $c$ is the speed of sound, and PRF is the pulse repetition frequency of the system.

It is of interest to notice that the phase difference between two successive beams received in the same direction (5.9) may also be estimated locally by computing the phase angle of the cross-correlation $R^1_{n,m}$ between these two receive beams:

$$\angle R^1_{n,m} = \angle\left\langle x^\star_{\alpha_n,m} \cdot x_{\alpha_{n+1},m}\right\rangle \approx \angle x_{\alpha_{n+1},m} - \angle x_{\alpha_n,m}. \tag{5.10}$$

Motion in the field of view can henceforth directly be estimated in each point of the image from the angle of the phase estimate by combination of (5.9) and (5.10). This is valid as long as the radial displacement stays below a quarter of a wavelength of the demodulation frequency. In order to improve the cross-correlation estimates, it is necessary to apply smoothing locally as indicated in (5.10). In this study, it was chosen to apply a Gaussian sliding window on the computed cross-correlation, with a size corresponding to 1.5 wavelengths radially and 3 wavelengths laterally.

Taking note of this possibility to assess motion present in the imaging area, we can easily deduce a method for compensating for the effects of motion between successively

transmitted plane waves. The phase shift between the successively transmitted plane waves may be estimated from the beamformed IQ data before compounding. Once the velocities have been estimated, the low-resolution images can be compensated to ensure that they represent the object at the time corresponding to the central transmit event of the frame, i.e. 0.5/PRF.

One of the questions in implementing such a method is how the estimated displacement can be compensated for. If the estimated displacement to be corrected is less than a quarter of a wavelength, it has been shown that the correction could be simply modeled as a local phase shift of the IQ data [25]. In plane wave compounding applications such as explored in this study, 55 transmit events are used to form an image. This means that the velocity must be typically below $\mathrm{PRF} \cdot c/8 \cdot 27 \cdot f_0 \approx 7\,\mathrm{mm/s}$ in order to be corrected properly when using a PRF of 13 kHz along with a pulse center frequency of 13.3 MHz. This is of course not compatible with imaging of rapidly moving tissues such the myocardium. In such applications, the correction process must consist of both a phase rotation and a delay:

$$\tau_{n_0,m}(t) = \sum_{n=n_0}^{n=N/2} \frac{\angle R^1_{n,m}(t)}{2\pi \cdot f_0} \tag{5.11}$$

$$\hat{x}_{\alpha_n,m} = x_{\alpha_{n+1},m}\left(t + \tau_{n,m}(t)\right) \cdot e^{i \cdot 2\pi \cdot f_0 \cdot \tau_{n,m}(t)} \tag{5.12}$$

Another obstacle is that the difference in the diffraction patterns of the successive transmit events may also result in a phase shift of their cross-correlation [26]. The phase angle of the cross-correlation has thus two components: one dependent on the radial motion, and one dependent on the difference in transmit diffraction patterns. The latter is unfortunately varying with the propagating medium and cannot efficiently be estimated in forehand by for example simulations. In the areas with strong scattering, the velocity component is dominant in the phase angle of the cross-correlation. On the edges of these areas, however, the scatterers with a lower intensity will be overwhelmed by the side-lobes of the strongly scattering tissues, and the diffraction component will prevail in the cross-correlation angle. In order to ensure a good motion compensation of our plane wave compounded image, we need to isolate the component of the cross-correlation which relies on radial motion.

In this study, we assumed that the radial component of the velocities in the field of view could be considered as constant within the time required to acquire a frame. Using this assumption, we can extract the component of the cross-correlation corresponding to the radial motion by taking the average of the cross-correlation functions $R^1_{n,m}$ for all the pairs of successive transmit plane waves ($n \in [1; N-1]$). This process is subject to noise and the slowly varying part of the diffraction component of the cross-correlation phase angle. In order to improve the isolation of the velocity component further, we have decided to apply two thresholds before averaging:

- The first threshold $T$ will cancel out the phase of $R^1_{n,m}$ whenever the velocity it corresponds to does not represent a realistic velocity. Hence, after choosing the threshold velocity $v_T$ representing the maximal velocity that can be observed in

tissue for a specific application, the threshold operation can be defined to ensure that:

$$\angle R^1_{n,m} \quad < \quad T = \frac{4\pi \cdot f_0}{PRF} \cdot \frac{v_T}{c} \tag{5.13}$$

- The second threshold $T_{std}$ will cancel out the phase of $R^1_{n,m}$ whenever its standard deviation is larger than a fraction $p$ of $T$. The actual velocities of the tissue in the image can be considered as slowly varying between the successive transmits, and the variance of their cross-correlation will be lower in the areas where the tissue is located compared to areas where the diffraction component of the cross-correlation phase angle is dominant. Hence, we can apply the threshold:

$$\left( \frac{\sum_{n=1}^{N-1} \angle R^1_{n,m} - \overline{\angle R^1_m}}{N-2} \right)^{\frac{1}{2}} < T_{std} = p \cdot T \cdot \sqrt{D} \tag{5.14}$$

## 5.4 Methods

### 5.4.1 Experimental Setup

For the *in vivo* acquisitions, an Ultrasonix MDP (Ultrasonix, Richmond, BC, Canada) scanner with an Ultrasonix DAQ channel recording unit were used. The scanner can be programmed to transmit custom sequences and the DAQ unit is used to acquire channel data in parallel. A 128 elements, 15 MHz linear array with 50 % bandwidth and 100 µm pitch was used, suitable for rat imaging. Due to the limited transmit pulser sampling frequency of 80 MHz, the pulse center frequency was chosen to be 13.3 MHz, which was the closest possible to the probe center frequency, with a pulse length of one and a half periods. On transmit, a F-number of 2 was desired which according to eq. (5.5) yields 55 angles for the full angle sequence. Due to system power limitations when transmitting on all elements in phase, the imaging PRF was restricted to 13 kHz in our examples. The channel data was acquired at 80 MHz sampling rate.

The received channel data was beam formed using Hamming apodization and an expanding aperture with a F-number of 1.1. The beamformed RF images were IQ demodulated using a demodulation frequency of 13.3 MHz, and the low-resolution images where coherently compounded using a tapered-cosine window with 50% tapering. Finally, the envelopes of the high-resolution images were log compressed using a dynamic range of 70 dB to produce the final images.

The proposed motion compensation scheme was applied with the thresholds in (5.13) and (5.14) defined by the maximal expected velocity of tissue $v_T = 15$ cm/s, and $p = 50$ % which seemed to adapt well with the high level of variations in the phase angle estimates observed with the experimental equipment used in this study.

### 5.4.2 Simulation Setup

Simulations were conducted using Field II [27] in order to understand the effect of radial velocities on the observed plane wave compounding images, and evaluate the

Table 5.1: Simulated Velocities vs. Wavelength

| Radial velocity [cm/s] | Displacement between two transmits [wavelength] | Displacement per frame ($D = 1$) [wavelength] |
|---|---|---|
| 0 | 0 % | 0 % |
| 1 | 0.7 % | 36.0 % |
| 2 | 1.3 % | 71.9 % |
| 4 | 2.7 % | 143.8 % |
| 8 | 5.3 % | 287.6 % |
| 12 | 8.0 % | 431.4 % |

performance of our motion compensation method. The probe geometry, as well as the scan sequencing and the receive beamforming were chosen to match exactly the experimental setup described in 5.4.1.

In order to evaluate the effect of radial motion on the point spread function (PSF) of the coherent plane wave compounding process, a single point scatterer at depth 12 mm moving towards the transducer was first simulated.

Further, a tissue mimicking phantom was generated to evaluate the proposed motion compensation approach. The simulated phantom was a $5 \times 10$ mm rectangle composed of 20000 point scatterers with normally distributed amplitudes, centered at depth 12 mm from the probe, and where a 3.4 mm diameter cyst was extruded. One frame was simulated while the phantom was assigned a radial velocity corresponding to 0, 1, 2, 4, 8 or 12 cm/s towards the transducer. The simulated RF channel data was sampled at 80 MHz and white Gaussian noise was added with a mean amplitude corresponding to a -30 dB level in order to mimic the SNR of our experimental channel data before compounding.

As an indication for comparison with studies using different frequency ranges and PRF, Table 5.1 gives the equivalent radial displacement in percentage of the transmitted pulse wavelength for the velocities used in this study. The displacement is given both for a time corresponding to the pulse repetition time ($PRT = 1/PRF$) and the time between the first and last beams of a frame acquired with decimation factor 1 (*i.e.* $54 \cdot PRT$).

A difference in the application of the motion compensation algorithm compared to the *in vivo* experiments was that the noise level and the variations observed in the phase of the cross-correlations were lowered. Therefore, the threshold in (5.14) could be lowered using $p = 6.25\%$.

In the case of the tissue mimicking phantom, both the contrast and the SNR were evaluated using the mean intensity of the signal $s_{IQ}$ in three different square regions of size $1.5 \times 1.5$ mm. The cyst region ($H_c$), speckle region ($H_s$) and noise region ($H_n$)

were placed in the center of the image at depths 12 mm, 9 mm and 5 mm, respectively.

$$\mathrm{SNR} = 10 \cdot \log_{10} \frac{\left\langle |s_{IQ}(x,y)|^2 \right\rangle_{(x,y)\in H_s}}{\left\langle |s_{IQ}(x,y)|^2 \right\rangle_{(x,y)\in H_n}}, \tag{5.15}$$

$$\mathrm{contrast} = 10 \cdot \log_{10} \frac{\left\langle |s_{IQ}(x,y)|^2 \right\rangle_{(x,y)\in H_c}}{\left\langle |s_{IQ}(x,y)|^2 \right\rangle_{(x,y)\in H_s}}. \tag{5.16}$$

## 5.5 Results

### 5.5.1 Simulation Results

The transformation of the PSF of the coherent compounded sequence with varying radial velocities is presented in Fig. 5.3. As expected, we observe a general increase in side-lobe levels in presence of motion, while an additional lateral shift of the point position appears when using the linear transmit scheme.

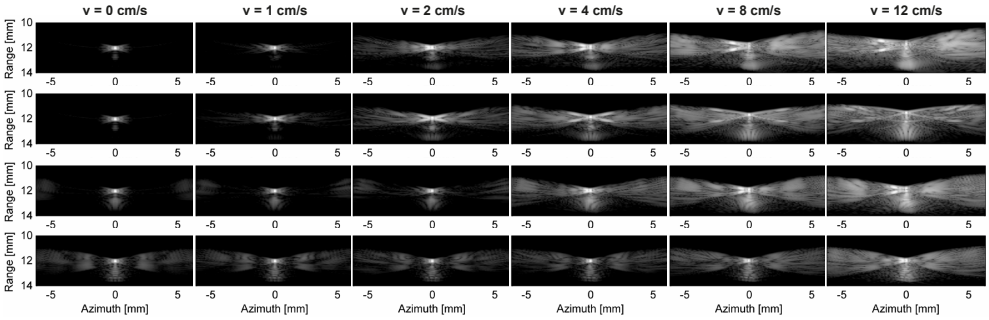


Figure 5.3: Evolution of the point spread function with varying radial velocities of the observed point scatterer (0, 1, 2, 4, 8 and 12 cm/s towards the probe). From top, first row: the linear transmit scheme without decimation. Second row: the alternated polarity scheme without decimation. Third and fourth rows: the linear transmit scheme with decimation factor respectively 2 and 5. Each point spread function is normalized in amplitude independently, with a dynamic range set to 80 dB for a better visualization of the grating-lobes.

Using the tissue mimicking phantom, the effect of radial motion on a typical plane wave compounding setup was simulated in the top row of Fig. 5.4, where the phantom moves towards the probe between each transmit event. On the bottom row, the motion compensated version of the same data is presented. We observe that radial velocities introduce a loss in intensity, as well as the addition of a *shadow* laterally shifted compared to the real location of the scatterers. The significance of the shift is increasing with increasing velocities.

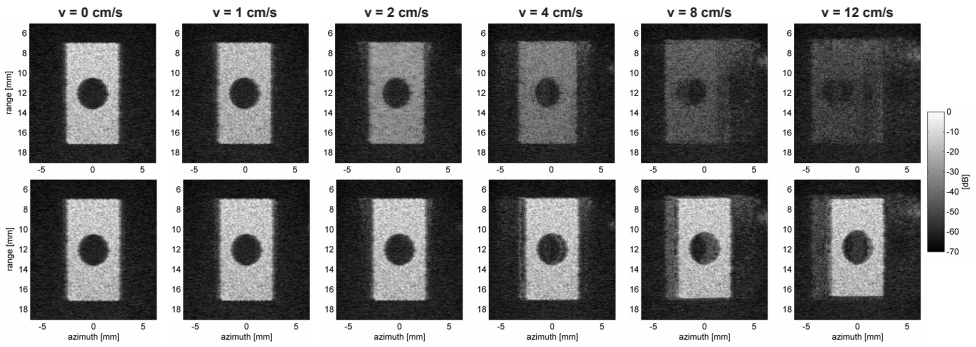


Figure 5.4: Images of a phantom moving radially towards the probe with velocity 0, 1, 2, 4, 8 and 12 cm/s towards the probe for the sequential transmit scanning scheme. Plane wave compounded images are on the top row, while the motion compensated plane wave compounded images are on the bottom row.

Using an alternated polarity transmit scanning scheme for the acquisition, as presented in Fig. 5.4 for both original and compensated plane wave compounded images, we notice that the laterally shifted shadow was replaced with an increase in the side-lobe levels. This phenomenon is critical for limited velocities (2 and 4 cm/s) while it becomes restrained for higher velocities (12 cm/s).

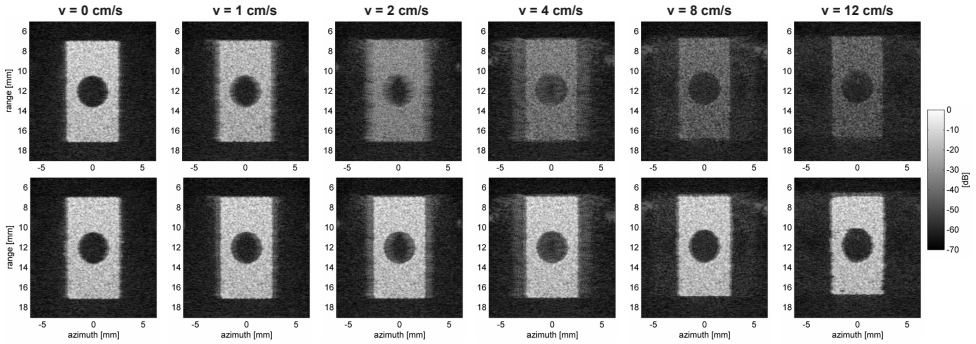


Figure 5.5: Images of a phantom moving radially towards the probe with velocity 0, 1, 2, 4, 8 and 12 cm/s towards the probe for the alternated polarity transmit scanning scheme. Plane wave compounded images are on the top row, while the motion compensated plane wave compounded images are on the bottom row.

The phantom was also simulated with a decimation factor of 2 for the sequential transmit order (i.e. 28 transmit plane waves instead of 55), as presented in Fig. 5.6. While the artifacts observed are similar to the one caused in the non-decimated version for half the velocities, the overall intensity in the speckle areas, and hence the SNR, is decreased. It was not observed any increase in the level of grating-lobes compared

to the non-decimated sequences.

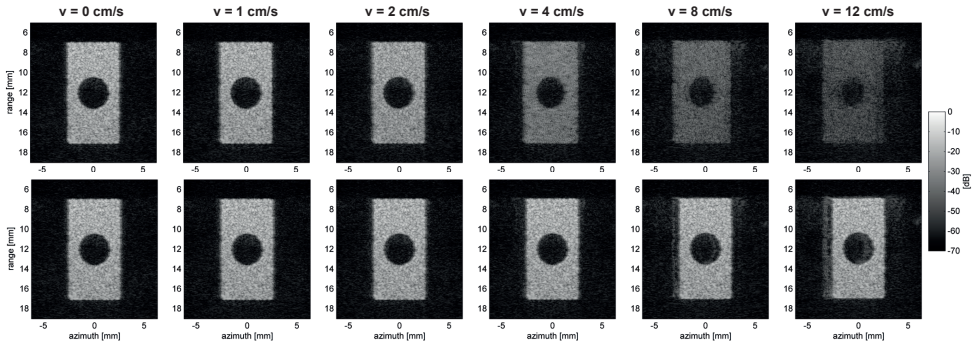


Figure 5.6: Images of a phantom moving radially towards the probe with velocity 0, 1, 2, 4, 8 and 12 cm/s towards the probe for the sequential transmit scanning scheme with decimation factor 2. Plane wave compounded images are on the top row, while the motion compensated plane wave compounded images are on the bottom row.

In order to visualize the effects of transmitting only a small number of plane waves, the phantom was generated in Fig. 5.7 with a decimation factor of 2 for the sequential transmit order (i.e. 28 transmit plane waves instead of 55). This sequence is the one which is the less influenced by radial motion, but also the one with the smallest SNR in absence of motion. Here, we do not observe the apparition of any shadow nor any strong grating-lobes, but motion reduces the intensity of the signal in the phantom.

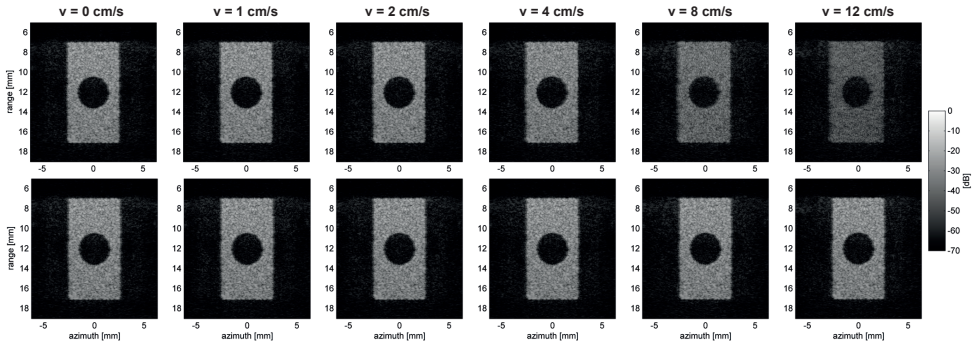


Figure 5.7: Images of a phantom moving radially towards the probe with velocity 0, 1, 2, 4, 8 and 12 cm/s towards the probe for the sequential transmit scanning scheme with decimation factor 5. Plane wave compounded images are on the top row, while the motion compensated plane wave compounded images are on the bottom row.

In both linear and alternated scanning schemes, we observed that the proposed motion compensation method succeeded in restoring the locations and amplitudes of

the point scatterers in their vast majority, while it does not manage to remove the shadow or higher side-lobes induced by motion.

The contrast between the cyst and the tissue of the simulated phantoms is presented in Fig. 5.8. We observe a significant loss in contrast with increasing radial velocities (from -45 dB to -7 dB) for both the sequential and the alternated transmit scheme. The motion compensation method presented in this article manages to keep the contrast level below -38 dB for all the velocity values. We note that the motion compensation performs better at low velocities (below 7 cm/s) with the sequential transmit scheme, whereas, at higher velocities, the alternating scheme provides better contrast.

The computed values of the signal-to-noise ratio for all the simulated phantoms are also presented in Fig. 5.9. Similarly to what was observed for the contrast, significant degradations of the SNR appear with increasing radial velocities (from 50 dB to 15 dB). In presence of motion, the highly decimated sequence (LA $D = 5$) provides the best contrast and SNR without any compensation scheme; but this advantage is lost when using the motion compensation technique or at small velocities (below 1 cm/s).

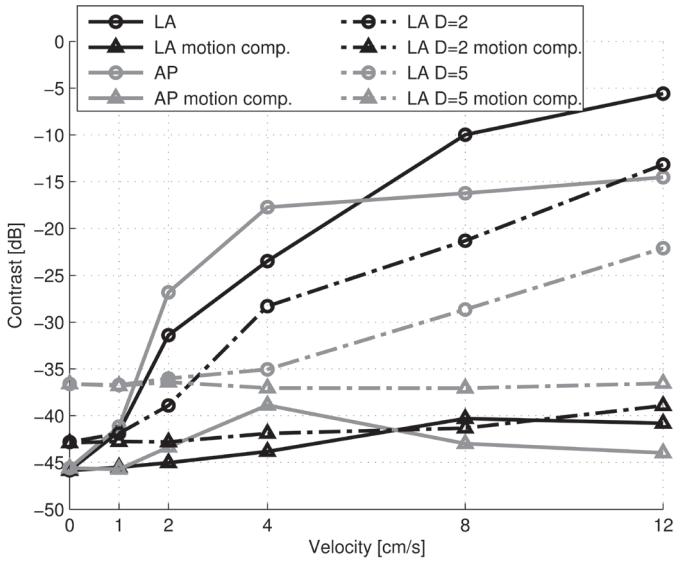


Figure 5.8: Evolution of the contrast in the phantom for different simulated radial velocities. Both the sequential transmit sequence (LA) and the alternated transmit sequence (AP) are presented, along with the values corresponding to their motion compensated version.

### 5.5.2 In vivo Results

Several hundred frames of channel data of a rat heart were acquired and processed into coherent plane wave compound images for the three studied situations: linear

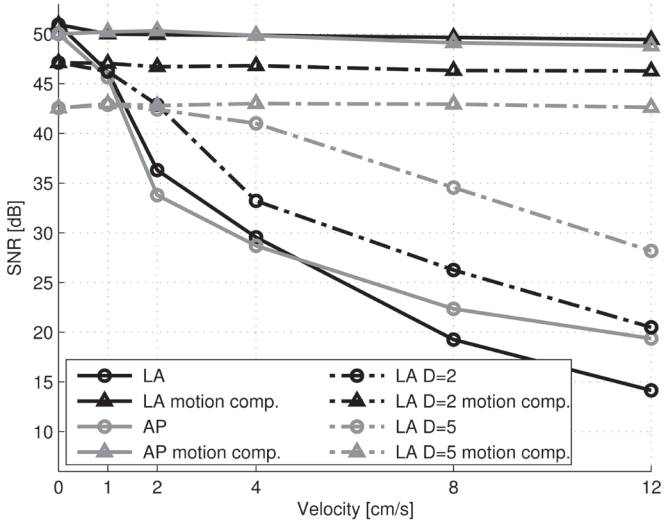


Figure 5.9: Evolution of the SNR for different simulated radial velocities. Both the sequential transmit sequence (LA) and the alternated transmit sequence (AP) are presented, along with the values corresponding to their motion compensated version.

transmit sequence without decimation, alternated polarity transmit sequence without decimation, and linear transmit sequence with decimation factor 2. An example frame without and with motion compensation are respectively presented for each setup in Fig 5.11, 5.12 and 5.13. Movies with up to 288 frames containing both the original and the motion compensated plane wave compounded images are also available as an attachment to this article (located at at http://folk.ntnu.no/denarie/thesis).

The physiology of the rat heart imaged in this study can be observed in the conventional B-mode image in Fig. 5.10. Due to the limited lateral size of the high-frequency transducer, the plane wave compounded images presented in this study cover only the upper portion of the left ventricle. The heart was beating at about 400 bpm, and the three frames selected in this article correspond the same time point in the cardiac cycle at end-systole.

In all three PWI scenarios studied, flickering can be observed in the compounded images in the areas presenting high radial velocities, such as in the myocardium tissue in the rightmost (apical) region of the images. Strong side-lobes and grating-lobes from the pericardium can be visualized on top the left atrium and mitral valve. The flickering is especially prominent in the LA setup without decimation. On the other hand, the level of noise due to side-lobes and grating-lobes is the lowest in this dataset. The motion compensation algorithm succeeds in recovering most of the tissue signal in the presence of motion. In addition, we observe more well-defined edges, as well as a slightly improved contrast in the near-field of the image. Lateral displacements were observed along the cavity, but no image degradations comparable to those caused by

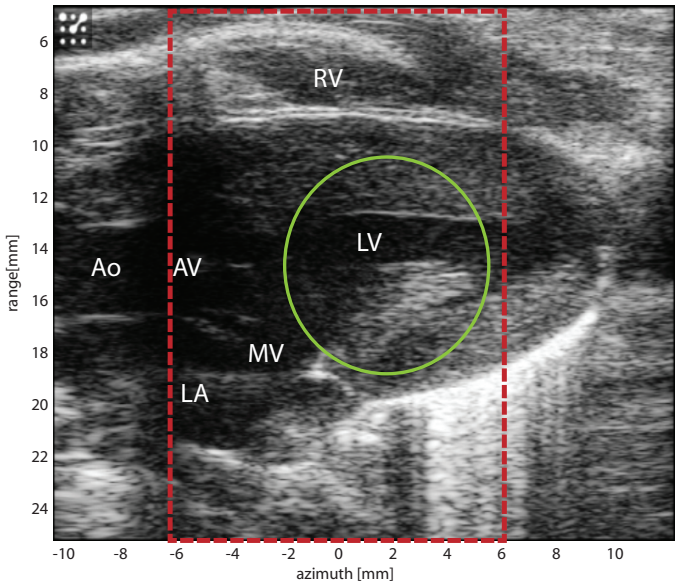


Figure 5.10: B-mode image of the parasternal long-axis view studied acquired with a conventional ultrasound scanner (Vevo 2100, with a 21MHz transducer). The physiology of the rat heart is detailed (LA = Left Atrium, LV = Left Ventricle, MV = Mitral Valve, AV = Aortic Valve, Ao = Aortic outlet, RV = Right Ventricle). The area covered by the plane wave compounding images is delimited by a dashed rectangle, and the area where the highest flickering is observed in the PWI examples is circled.

radial displacements were visualized.

The functioning of the motion compensation algorithm was illustrated for the linear transmit sequence without decimation in Fig. 5.14. Here, both the estimated velocities and the variance of these estimates are presented. Velocities with up to 8 cm/s were observed, leading to tissue displacements of up to about 3 times the wavelength of the transmitted pulse over one single frame. As expected, the variances are higher in the regions with a low scattering such as the blood pools, and close to the tissues with a strong scattering.

## 5.6 Discussion

In this work, we investigated the effects of radial motion on very high frame rate coherent plane wave compounding. Radial displacements of the imaged object larger than half a wavelength during the time necessary to acquire one frame were prone to noticeable image degradations. These degradations took the form of a loss of intensity of the imaged object, i.e. a lower SNR, as well as a loss in the focusing capability of the method, i.e. lateral shifting, grating-lobe formation, and hence a loss in resolution

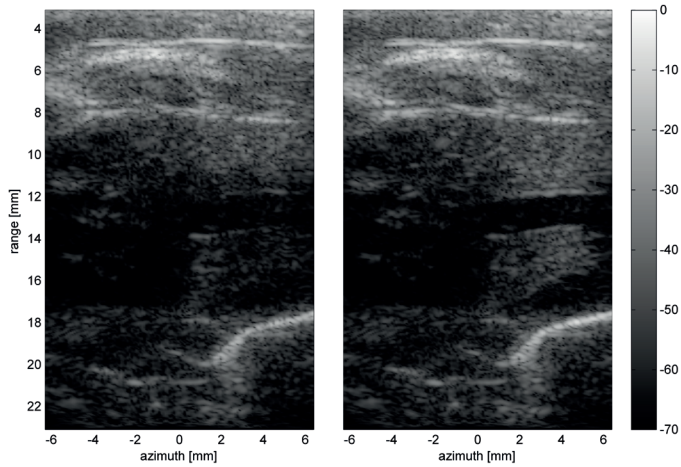


Figure 5.11: Parasternal long-axis view of a rat heart imaged using 55 planes waves transmitted sequentially without decimation, at a frame rate of 235.9 fps. On the left is the original compounded image, and on the right is the motion compensated image. A movie of 146 frames covering several heart cycles is available are located at http://folk.ntnu.no/denarie/thesis.

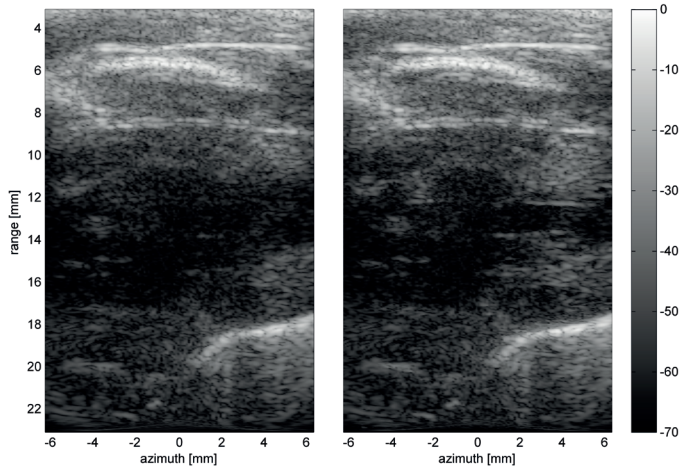


Figure 5.12: Parasternal long-axis view of a rat heart imaged using 55 planes waves transmitted in an alternated sequence without decimation, at a frame rate of 235.9 fps. On the left is the original compounded image, and on the right is the motion compensated image. A movie of 146 frames covering several heart cycles is available at http://folk.ntnu.no/denarie/thesis.

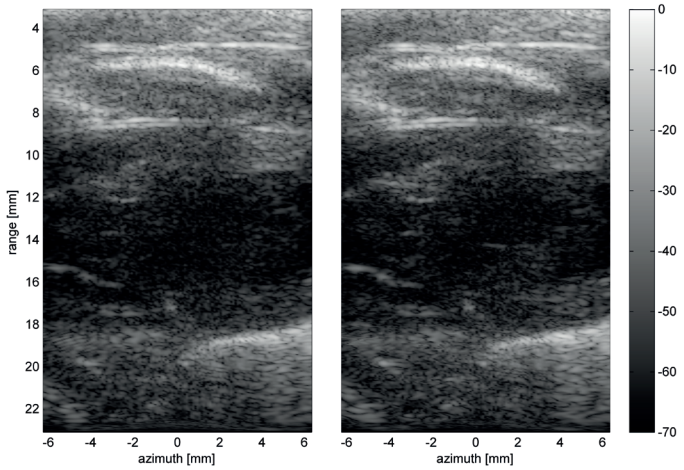


Figure 5.13: Parasternal long-axis view of a rat heart imaged using 55 planes waves transmitted sequentially with decimation factor 2, at a frame rate of 463.3 fps. On the left is the original compounded image, and on the right is the motion compensated image. A movie of 288 frames covering several heart cycles can be downloaded at http://folk.ntnu.no/denarie/thesis.

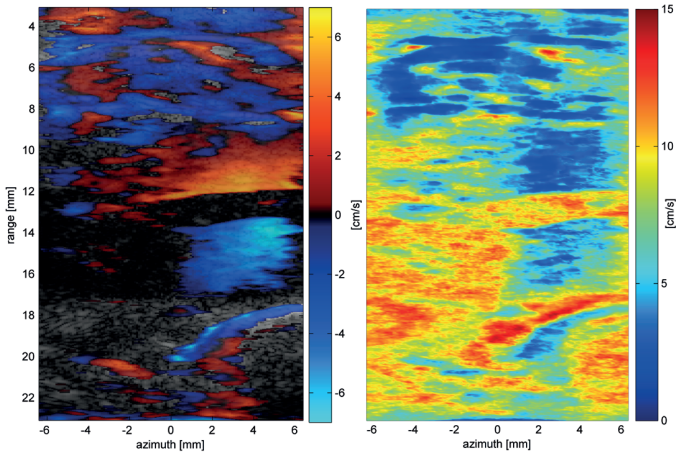


Figure 5.14: Example of information used by the motion compensation algorithm, for the data frame presented in Fig. 5.11. Left: Velocities estimated and used for correction, after the thresholding steps. Right: Standard deviation of the estimated velocity field, used for thresholding.

and contrast.

Ultrafast PWI was introduced as a method that ensured a very high frame rate while recreating the transmit focus at every position. The point spread functions presented in Fig. 5.3 show that this is not the case when significant radial motion is present in the medium. Notable degradations were observed in our examples as the total radial displacement over a compounded frame was more than half a wavelength, i.e. for the presented cases starting at $v = 2\,\mathrm{cm/s}$ for the non-decimated cases, and $v = 4\,\mathrm{cm/s}$ and $12\,\mathrm{cm/s}$ for sequences using decimation factor 2 and 5 respectively. For the linear angle transmit sequence (LA), we observed a lateral shift as described by (5.8), and a high increase in the level of side-lobes and grating-lobes. Using a decimated transmit sequence, the sensitivity to motion should be decreased since the overall displacement of the objects is divided by the decimation factor $D$, but we observe that additional grating-lobes are forming close to the location of the scatterer in the presence of motion, in addition to the already lower contrast and SNR caused by a lower number of combined transmits. Using an alternated polarity sequence, the energy contained in the PSF spreads out in both lateral directions in presence of motion. This did not result into any lateral shift, but a high loss of contrast may be expected. In both types of scan sequences, the radial resolution was also impacted.

Of maybe higher importance for the sonographer, the presence of radial motion will result in a loss of intensity of the imaged object, generating the impression of flickering of the image as the tissue is accelerating or decelerating. This phenomenon was confirmed by our phantom simulations presented in Fig. 5.4, 5.5, 5.6 and 5.7.

We proposed a correction algorithm with the aim of estimating the velocities in the imaged tissue and recreate the signal at the true point location. The results of our approach summarized by the SNR in Fig. 5.9 are highly promising, since the SNR after correction is approximately constant for all the simulated velocities, at the exception of the highest velocity, $12\,\mathrm{cm/s}$, where a loss of $4\,\mathrm{dB}$ is observed. However, our approach focused on recreating the signal at the correct location, and not on reducing the amount of grating-lobes and the shadows generated by motion outside of the moving tissues. This aspect of the correction scheme can be easily observed by the variation of the contrast in Fig. 5.8, where the correct amplitude of the signal in the cyst is perturbed by the lobes and shadows generated by motion. The origin of this approach was that the authors of this work wanted to obtain a correction method with a low computational cost, in the perspective of future implementation on a real-time scanner. In order to eliminate the remaining part of artifacts caused by motion, one could use more computationally intensive schemes. One may for example use a combination of cross-correlations estimated between transmit events that do not only have an adjacent direction, or estimate the velocities between successive frames [22, 28, 29].

In order to reduce the influence of motion, this work focused on two different approaches: decimating the transmit sequence and alternating the angle polarity of the transmit plane waves. The phantom simulations allow some conclusions to be drawn about the expected impact on *in vivo* acquisitions:

- When using the AP sequence, the laterally shifted shadow phenomenon that

appeared in presence of radial motion was removed. Instead, the energy spreads out laterally, generating high side-lobes that can even be higher than what is observed with the linear angle sequencing (see Fig. 5.4 and 5.5 for the velocities 2 to 4 cm/s). The motion compensation algorithm tends to be less stable as the time between two transmit beams with a single tilting angle increment is multiplied by 2, as can be seen in Fig. 5.5 for the highest velocity 12 cm/s.

- Decimating the transmit LA angle sequence by a factor 2 leads to a higher frame rate and therefore half the displacement observed within each frame. As expected, we observe that the shadow phenomenon is reduced. From theory, we would have expected the apparition of grating-lobes caused by the decimation. However, this phenomenon was not observed in our simulations. This may be caused by the fact that the phantom was a uniform speckle located in the center of the image, with a uniform vertical displacement, generating grating-lobes outside of the field of view. In addition, the general intensity is lowered due to the fact that we combine only half the number of transmit events, leading to a SNR reduced by $\sqrt{N_{D=1}/N_{D=2}} \simeq \sqrt{2} \simeq 3\,\text{dB}$ as also observed in Fig. 5.9. Here as well, the motion compensation algorithm is impacted by the fact that we must estimate the mean velocity using only half the number of correlation angles compared to the other sequences. This has been partly taken into account in the variance threshold (5.14), but we may nonetheless expect to have worse corrections *in vivo*.

- When decimating the transmit angle sequence further, as presented in Fig. 5.7, the distortions of the imaged object caused by radial motion tend to disappear. This is caused to the fact that the observed displacement within each frame is five times smaller than observed without decimation. In this case, the impact of motion is limited to a slight loss in the intensity of the signal in the tissue. Therefore, the loss in SNR and contrast caused by motion are the smallest using a highly decimated sequence. However, the highly decimated sequence suffers from a loss in SNR of $\sqrt{N_{D=1}/N_{D=5}} \simeq \sqrt{5} \simeq 7\,\text{dB}$ intrinsic to the decimation, and this sequence will provide the worst performances in the absence of motion or after the motion compensation algorithm, as seen in Fig. 5.9 and 5.8.

The *in vivo* applications of ultrafast coherent plane wave imaging on a parasternal long-axis view of a rat presented in this work illustrate in a clear way the problems caused by radial motion of the myocardium. In these examples, tissue velocities with up to 8 cm/s were observed, leading to displacements of up to about 3 times the wavelength of the transmitted pulse over one single frame. The frames selected in Fig. 5.11, 5.12 and 5.13 are representative for end-systole where the left ventricle relaxes and moves with a high velocity. In these frames, we observe a high loss of intensity in the myocardium, such that its borders are no longer visible. As expected from the simulations for the range of velocities observed in tissue, we obtain the best images after motion compensation for the linear transmit sequence without decimation. The alternating polarity sequence suffers from the spreading of the energy around the slowly moving tissue, forming grating-lobes that cannot be corrected for by our method, and

hence reducing the general contrast. The linear decimated sequence suffers from a lower SNR as well as less robust estimates of the velocities, due to the grating-lobes of decimation and the lower number of combined transmits. The decimated sequence ($D = 2$) results *in vivo* in the worst image quality, but with a frame rate twice as high.

Throughout this work, we have focused on how coherent plane wave compounding should be used in order to image rapidly moving structures like the heart. In our approach, we have used a large number of transmit events per frame in order to ensure a sufficiently high contrast required for the chosen *in vivo* application. However, it has been shown in previous studies that plane wave compounding would still present an advantage with a smaller number of transmit angles compared to conventional focused B-mode imaging [9]. Therefore, simulations with a decimation factor $D = 5$ were conducted. It clearly appears that in presence of high velocities and in the absence of algorithm correcting for the motion before compounding, a really small number of transmit angles should be preferred. On the other hand, we observed *in vivo* that a decimation of the transmit angle sequence will result in the formation of strong grating lobes that were not highlighted by the simulations. Previous work highlighted the trade-off between the number of transmit angles and the loss in SNR and contrast intrinsic to plane wave imaging. This work demonstrates the existence of a second trade-off between the number of transmit angles and the range of radial velocities that can be imaged without significant losses in SNR and contrast. This work also demonstrates the possibility of adding a motion compensation algorithm to recover the losses in SNR and contrast introduced by motion. While a highly decimated transmit sequence may be chosen to image large velocities, such as in Doppler applications, a large number of transmit combined with a motion compensation algorithm may be preferred for applications where a high image quality and the absence of grating lobes is necessary to have a high comprehension of the anatomy. Of course, applications such as plane wave Doppler would also benefit from a motion compensation scheme before compounding in order to maintain the same signal contrast and intensity throughout the whole range of velocities.

Another solution for keeping a small number of transmit events, without suffering from grating-lobes, would be to consider reducing the inclination between the transmit events, which in the meantime will result in an increased $F_{\#}$ according to (5.5). In this way, if we want to image an object with significant radial velocities, an additional trade-off must considered between the number of angles that can be discarded and how small $F_{\#}$ can be achieved while maintaining sufficiently low motion artifacts.

Because of technical limitations, the ultrasound system we used was restricted to a low PRF of about 13 kHz. This implies that the radial displacements observed in the *in vivo* datasets were greater than what could have been achieved with a better hardware, and that the motion artifacts were more pronounced. This does not mean, however, that the observations made here should be discarded, since the displacements observed with an optimal PRF would be similar to what is observed in the case with a decimation factor 2, where strong degradations caused by motion were observed.

It is of interest to further elaborate on how the motion compensation scheme we have presented in this article performs *in vivo*. The example velocity estimates and the corresponding standard deviations presented in Fig. 5.14 are one way to illustrate

this. We observe a high variance of the estimates in the cardiac cavities, where mainly side-lobes of the tissue are present. The highest variances are also observed close to really bright scatterers. In these areas, the signal is dominated by the mix of side-lobes from the tissue and grating-lobes generated by the motion of this tissue. The side-lobes are varying with the direction of the incident plane wave, and will result in different velocity estimates for the different transmit events, and hence a higher variance at these locations. Due to thresholding on the variance, no correction was applied, and the side-lobes and grating-lobes induced by motion are dominating the final image in these areas. The areas characterized by lower variances are the myocardium and the near field. In the myocardium along the left ventricle, high velocities are detected and corrected for as can be observed in the resulting compensated frame in Fig. 5.11. In the near-field, the method corrects the tissue displacements, but maybe as well the small imperfections of the delay model during the compounding operations, slightly improving the focusing and therefore the contrast in near-field as can be observed in the corresponding movie attached to this article.

Even though the proposed motion compensation scheme presented in this work performs well for the *in vivo* acquisitions, recovering the vanished myocardial tissues, it does not correct for some other artifacts that still negatively impact the plane wave images. The high level of side-lobes and grating-lobes introduced by motion is not corrected. Acceleration of the tissue has also been ignored when using the constant motion hypothesis within each frame. Even though there is no clear indication of image degradation caused by acceleration, we may suppose that an improved motion compensation scheme could take it into account, using e.g. a linearly varying velocity model. As expected from theory, the lateral motion was not seen to cause dramatic image degradations, confirming our approach of focusing on the impact of radial motion on the PWI. However, the presence of a combination of lateral and radial velocity components may be a limitation for the presented method. The cross-correlation based algorithm used in this study can only detect and compensate for the radial component of motion. High lateral or out-of-plane velocities may lead to wrong estimates of the radial velocities, even though this phenomenon was not clearly observed in the presented *in vivo* acquisitions .

## 5.7 Conclusion

In this work, we have presented how motion can influence coherent plane wave compounding techniques. Radial velocities will induce noticeable image degradations as soon as the observed displacement is larger than half a pulse wavelength per frame: the synthetic focusing mechanism of compounding is degraded, introducing grating-lobes, lateral shifting and radial spreading. In simulations, losses of SNR up to 35 dB and contrast up to 40 dB were observed. A motion compensation scheme was introduced, and the maximal losses in SNR and contrast were recovered by respectively 35 dB and 27-35 dB. The effects of radial motion were observed *in vivo* imaging a beating rat myocardium, where the necessity of a correction scheme such as presented in this work was demonstrated.

# References


[1] B. Delannoy, R. Torguet, C. Bruneel, E. Bridoux, J. M. Rouvaen, and H. LaSota, "Acoustical image reconstruction in parallel-processing analog electronic systems," *Journal of Applied Physics*, vol. 50, pp. 3153–3159, 1979.

[2] B. Delannoy, R. Torguet, C. Bruneel, and E. Bridoux, "Ultrafast electronical image reconstruction device," *Echocardiography*, vol. 1, pp. 1273–1282, 1984.

[3] D. P. Shattuck, M. D. Weinshenker, S. W. Smith, and O. T. von Ramm, "Explososcan: A parallel processing technique for high speed ultrasound imaging with linear phased arrays," *The Journal of the Acoustical Society of America*, vol. 75, pp. 1273–1282, 1984.

[4] O. T. V. Ramm, S. W. Smith, and H. G. P. Jr, "High-speed ultrasound volumetric imaging system. II. Parallelprocessing and image display," *IEEE Transactions on Ultrasonics, Ferroelectrics and Frequency Control*, vol. 38, no. 2, pp. 109–115, 1991.

[5] T. Hergum, T. Bjåstad, K. Kristoffersen, and H. Torp, "Parallel beamforming using synthetic transmit beams," *IEEE Transactions on Ultrasonics, Ferroelectrics and Frequency Control*, vol. 54, no. 2, pp. 271–280, 2007.

[6] T. Hergum, T. Bjåstad, L. Lovstakken, K. Kristoffersen, and H. Torp, "Reducing Color Flow Artifacts caused by Parallel Beamforming," *IEEE Transactions on Ultrasonics, Ferroelectrics and Frequency Control*, vol. 57, no. 4, pp. 830–838, 2010.

[7] S. I. Nikolov, J. Kortbek, and J. A. Jensen, "Practical applications of synthetic aperture imaging," *Proceedings of IEEE International Ultrasonics Symposium. IEEE*, 2010.

[8] J. Y. Lu, "Experimental study of high frame rate imaging with limited diffraction beams.," *IEEE Transactions on Ultrasonics, Ferroelectrics and Frequency Control*, vol. 45, pp. 84–97, Jan. 1998.

[9] G. Montaldo, M. Tanter, J. Bercoff, N. Benech, and M. Fink, "Coherent plane-wave compounding for very high frame rate ultrasonography and

transient elastography," *Ultrasonics, Ferroelectrics and Frequency Control, IEEE Transactions on*, vol. 56, no. 3, pp. 489–506, 2009.

[10] J. M. Hansen and J. A. Jensen, "Compounding in synthetic aperture imaging.," *IEEE Transactions on Ultrasonics, Ferroelectrics and Frequency Control*, vol. 59, pp. 2054–65, Sept. 2012.

[11] S. I. Nikolov and J. A. Jensen, "In-vivo synthetic aperture flow imaging in medical ultrasound," *IEEE Transactions on Ultrasonics, Ferroelectrics and Frequency Control*, vol. 50, no. 7, pp. 848–856, 2003.

[12] J. A. Jensen and S. I. Nikolov, "Directional synthetic aperture flow imaging," *IEEE Transactions on Ultrasonics, Ferroelectrics and Frequency Control*, vol. 51, no. 9, pp. 1107–1118, 2004.

[13] J. Lu, "2-D and 3-D high frame rate imaging with limited diffraction beams," *IEEE Transactions on Ultrasonics, Ferroelectrics and Frequency Control*, vol. 44, no. 4, pp. 839–856, 1997.

[14] J. A. Jensen, S. I. Nikolov, K. L. Gammelmark, and M. H. Pedersen, "Synthetic aperture ultrasound imaging.," *Ultrasonics*, vol. 44 Suppl 1, pp. e5–15, Dec. 2006.

[15] J. Udesen, F. Gran, K. L. Hansen, J. A. Jensen, C. Thomsen, and M. B. Nielsen, "High Frame-Rate Blood Vector Velocity Imaging Using Plane Waves: Simulations and Preliminary Experiments," *IEEE Transactions on Ultrasonics, Ferroelectrics and Frequency Control*, vol. 55, no. 8, pp. 1729–1743, 2008.

[16] J. Bercoff and G. Montaldo, "Ultrafast compound doppler imaging: providing full blood flow characterization," *IEEE Transactions on Ultrasonics, Ferroelectrics, and Frequency Control*, 2011.

[17] M. Tanter, J. Bercoff, L. Sandrin, and M. Fink, "Ultrafast compound imaging for 2-D motion vector estimation: application to transient elastography," *IEEE Transactions on Ultrasonics, Ferroelectrics and Frequency Control*, vol. 49, no. 10, pp. 1363–1374, 2002.

[18] S. Park, S. R. Aglyamov, and S. Y. Emelianov, "Elasticity imaging using conventional and high-frame rate ultrasound imaging: experimental study.," *IEEE Transactions on Ultrasonics, Ferroelectrics, and Frequency Control*, vol. 54, pp. 2246–56, Nov. 2007.

[19] B.-F. Osmanski, M. Pernot, G. Montaldo, A. Bel, E. Messas, and M. Tanter, "Ultrafast Doppler imaging of blood flow dynamics in the myocardium.," *IEEE transactions on medical imaging*, vol. 31, pp. 1661–8, Aug. 2012.

[20] J. Wang and J.-y. Lu, "Motion artifacts of extended high frame rate imaging.," *IEEE Transactions on Ultrasonics, Ferroelectrics and Frequency Control*, vol. 54, pp. 1303–15, July 2007.

[21] N. Oddershede and J. A. Jensen, "Effects Influencing Focusing in Synthetic Aperture Vector Flow Imaging," *IEEE Transactions on Ultrasonics, Ferroelectrics and Frequency Control*, vol. 54, pp. 1811–1825, Sept. 2007.

[22] B. Yiu, I. Tsang, and A. Yu, "A modified synthetic aperture imaging approach with axial motion compensation," *Ultrasonics Symposium*, pp. 1254–1257, 2008.

[23] K. S. Kim, J. S. Hwang, J. S. Jeong, and T. K. Song, "An efficient motion estimation and compensation method for ultrasound synthetic aperture imaging.," *Ultrasonic imaging*, vol. 24, pp. 81–99, Apr. 2002.

[24] B. Angelsen, *Ultrasound imaging*. Emantec Norway, 2000.

[25] B. Dénarié, H. Torp, G. Haugen, A. Sørnes, and T. Bjåstad, "Motion Compensated Synthetic Transmit Beam Technique for Real-time Echocardiography," in *IEEE Ultrasonics Symposium*, 2011.

[26] T. Bjåstad and H. Torp, "Single-pulse tissue doppler using synthetic transmit beams.," *IEEE Transactions on Ultrasonics, Ferroelectrics and Frequency Control*, vol. 56, pp. 2134–44, Oct. 2009.

[27] J. A. Jensen, "Field: A program for simulating ultrasound systems," *Medical and Biological Engineering and Computing*, vol. 34, pp. 351–353, 1996.

[28] K. Gammelmark, J. A. Jensen, and J. Dall, "Improving the Image Quality of Synthetic Transmit Aperture Ultrasound Images-Achieving Real-Time In-Vivo Imaging," *forskningsbasen.deff.dk*, 2004.

[29] M. Karaman, H. S. Bilge, and M. O'Donnell, "Adaptive multi-element synthetic aperture imaging with motion and phase aberration correction," *IEEE transactions on Ultrasonics, Ferroelectrics, and Frequency Control*, vol. 45, pp. 1077–87, Jan. 1998.